SENSING SLIP OF GRASPED BIOLOGICAL TISSUE IN MINIMALLY INVASIVE SURGERY

A DISSERTATION
SUBMITTED TO THE DEPARTMENT OF MECHANICAL ENGINEERING
AND THE COMMITTEE ON GRADUATE STUDIES
OF STANFORD UNIVERSITY
IN PARTIAL FULFILLMENT OF THE REQUIREMENTS
FOR THE DEGREE OF
DOCTOR OF PHILOSOPHY

Natalie Tran Burkhard
November 2018

I certify that I have read this dissertation and that, in my opinion, it is fully adequate in scope and quality as a dissertation for the degree of Doctor of Philosophy.

Mark Cutkosky, Primary Adviser

I certify that I have read this dissertation and that, in my opinion, it is fully adequate in scope and quality as a dissertation for the degree of Doctor of Philosophy.

Allison Okamura

I certify that I have read this dissertation and that, in my opinion, it is fully adequate in scope and quality as a dissertation for the degree of Doctor of Philosophy.

Ryan Steger

Approved for the Stanford University Committee on Graduate Studies.

Patricia J. Gumport, Vice Provost for Graduate Education

This signature page was generated electronically upon submission of this dissertation in electronic format. An original signed hard copy of the signature page is on file in University Archives.

Abstract

Minimally invasive surgery (MIS) is now broadly accepted as the standard of care for a number of surgical procedures, and robot-assisted surgery (RAS) has become increasingly prevalent over the last two decades [1]. RAS in particular holds great promise for improving surgeons' accuracy and dexterity over traditional laparoscopic surgery [2] due to enhanced vision and wristed instruments, among other factors. However, there is room for improvement: the loss of direct manual contact with the surgical site during MIS results in the absence of tactile information, so surgeons learn instead to interact with tissue based mainly on visual cues. Furthermore, unlike human hands, surgical graspers of all types (open hand-held tools, laparoscopic, RAS) have small dimensions which, if handled inappropriately, can cause high pressures and result in crushing or damaging tissue [3], [4]. Surgeons aim to grasp tissue lightly enough to avoid crushing it but with sufficient grasp force to prevent accidental tissue loss. Achieving this grasp balance is not straightforward because the amount of force that avoids tissue damage and grasp loss simultaneously is difficult to predict, and tissue damage is not always immediately visually apparent. Another important skill in MIS is maintaining situational awareness of all relevant anatomy and tools. Given the size and layout of many anatomies, a non-active tool may be outside of the surgeon's immediate focus or even be outside the endoscope's field of view, making the quality of grasp difficult to monitor. This thesis posits that the detection of tissue slip onset can provide useful information to address these concerns and improve grasping of biological tissue during MIS and uses a RAS platform for testing.

Although tissue slip negatively impacts grasping and manipulation tasks in surgery, it is a relatively unexplored topic in the literature across all surgical disciplines. Monitoring tissue motion between the jaws of MIS graspers has the potential to provide multiple benefits to surgeons. First, knowledge of when tissue slip occurs could enable surgeons to apply the minimum amount of grasp force to tissue and thus reduce overall the amount of

grasper-induced tissue damage they incur. The second anticipated benefit is that notifying surgeons of slip events in off-screen and/or non-active tools will provide otherwise unobservable information regarding that tool's tissue interaction and thereby reduce frustration, sudden loss of critical view, tissue tearing, and other negative consequences. The results of the first survey conducted on RAS surgeons' experiences with tissue slip support these ideas and are presented here.

This thesis introduces a novel slip sensor to provide information regarding tissue motion onset in RAS graspers. Sensing slip of wet, compliant objects during MIS is a challenge overcome by this novel anemometric slip sensor, which provides slip onset information *and* direction-dependent signals. A transient thermal simulation was developed to understand the sensor's working principles and provide guidelines for its design and use. The sensor is based on hot-wire anemometry: a heater establishes a thermal gradient in the grasped tissue, and four thermal probes monitor the gradient's movement. The results from validation experiments on two sensor prototypes establish the proof of concept and demonstrate the sensing method's robustness on porcine tissue *ex vivo* and *in vivo*. Finally, a user study illustrates the sensor's potential to inform human decision making and performance during a clinically-motivated task. This thesis is an important step towards safer and more efficient MIS.

Acknowledgments

I would like to thank my undergraduate mentors at Dartmouth College, **B. Stu Trembly** and **Doug Van Citters** (DVC), for investing in me when I was a relatively useless undergrad and giving me my first lessons in how to conduct well-founded research. Stu was one of the first people who made me feel like I belonged in engineering even when I struggled in his classes, and for that I am extremely grateful to him. I also love that I know what the 'B.' in his name stands for and that the rest of Thayer is too scared to ask. An engineering alumna told me that her most important advice for me was to find some way to work closely with DVC, and she was right. DVC was an amazing mentor to me during my senior thesis and capstone projects, and he was the one who told me that I should apply to Stanford for my PhD. I had not thought I would be a good candidate, but DVC convinced me that I was. From being in DVC's lab, I learned what a good lab culture can look and feel like, and I am lucky to have been able to work with him.

At Stanford, I have to thank **Tom Kenny** and **Matt Ohline** for stoking my love for mechatronics through the SumoBots competition in ME210. Until that class, anything that remotely resembled electrical engineering was very intimidating to me, and they did a great job making it fun, accessible, and exciting. This class changed my academic course in a way that no other class ever has. ME210 led me to take **Ed Carryer**'s intense ME218 series, which is hands-down the best course I have ever taken. I have never voluntarily gone without sleep for robots before or since that class.

I owe a lot to my labmates at the Biomimetics and Dexterous Manipulation Laboratory - **Hannah Stuart**, **Matt Estrada**, **Shiquan Wang**, **Alice Wu**, **Sam Frishman**, **Alex Gruebele**, and so many others for being my mentors, friends, idea-bouncers, stress-reducers, and intellectual advancers. Mark did a wonderful job cultivating a creative and inclusive workspace, and I am grateful to him for attracting great people like these. Hannah and Alice are the main reasons I joined the BDML – it was reassuring to join a lab with two

strong, sharp women that I admire now as much as I did then. Many thanks to **Allison Okamura**, **Maarten Lansberg**, and **Bruce Daniel** as well. As a third year PhD student, I was working on a (complete trainwreck of a) project, and Maarten was unfailingly supportive, generous, and validating to me, a student he barely knew, when I really felt like quitting. I had the pleasure of working with Bruce on a project my fourth year as a PhD student. Bruce is one of those incredibly intelligent, creative, curious people who finds fresh insights and enlivens discussions with ease. He has been a great mentor to me, and I was sad to leave that project because it meant ending a collaboration I enjoyed. Allison has been a constant throughout my grad school experience, and I've felt very lucky to have had the opportunity to take her classes and be mentored by her on grant applications and research projects. I loved working with her because she demands excellence in a way that makes you want to rise to the occasion, and she has this impossible capacity to mentor and engage with everyone she contacts. If you have the opportunity to work for or with her, do it!

At Intuitive Surgical, I did operate a one-woman parade but not without the help and support of many others who were incredibly generous with their time. Many, many thanks to **Jason Stamatelaky**, whose patience, technical skills, manufacturing intelligence, and ability to make creative build modifications helped make my prototypes functional and saved me countless hours. **Angie Fan** spent many hours helping me understand how to design a useful thermal simulation. **Alan Peterson** was always there for the hero save, whether to solve the problem I'd spent hours trying to debug or casually suggesting devastatingly simple yet impactful changes to my signal processing methods and/or circuitry. Thank you to **Asha Dektor** and **Jonathan Honibal** for spending time with me editing my surgeon survey and helping me obtain such valuable surgeon feedback. Many thanks to **Ashwin Suresh** and **Cliff Bargar** for helping me with software builds and robot debugging, as well as advice on how to get the information I needed from the da Vinci. Thanks also to **Dan Miller** for being my hangout buddy in the APD lab. Maybe someday we'll have a real sofa.

Thanks to the entire Clinical Development Engineering department at Intuitive – the CDEs were always more than willing to spend their time and brainpower helping me understand what surgeons need and want as well as their willingness to participate in my user study, even in its pilot infancy. Special shoutouts to **Barbara Kim**, **Chun Hua Zheng**, **Luke Reilly**, **Elizabeth Wicks**, and (interaction designer) **Sophia Hannaford** for their

help in making my user study great! Much gratitude also to **Laura Falkner**, **Olga Greenberg**, and **Brett McKenzie** (and double thanks to Chun Hua and Barbara) for being so accommodating and helping me get access to porcine models for my *in vivo* tests. Those would have been very, very difficult for me to get at Stanford.

My family has always been very supportive of the Ph.D. My dad and 5 of his 6 brothers all have one, so it's nice to join the club! My parents have both always encouraged academic excellence and instilled in me the confidence to succeed. Both my Gutierrez family and Burkhard family came to watch me defend, which meant a lot to me. The support of family is huge and the sum of many small interactions and emotions that are hard to list, but I couldn't have done this without that support. **Jose** had the luck (or misfortune) of living with me throughout this process, and I benefited from his checks on my sanity, his patient and loving open ears, and his belief that I'd make it out the other side.

Last but not least, my advisors! **Ryan** is basically the perfect boss. My thesis would not have been possible without him. He made up a role for me at Intuitive and shoved it through the Stanford and Intuitive bureaucracies, buying into the Natalie Thesis project for the next few years after knowing me for only a few months. To me, that level of investment with that little data was extremely reassuring and confidence-boosting, and to a PhD student on the verge of academic kamikaze, that meant the world to me. On my part, I signed up because the project sounded cool, but mainly I just wanted to keep working for Ryan. He's an amazing technical lead and seems to know at least a lot about everything, but also has the social EQ to not only avoid making you feel bad about it but push you to excel so you're worthy. Ryan is the kind of person who cares deeply about clicking with everyone on the team and invests in their long- and short-term goals as well as their leisure interests. Nothing but gratitude to Ryan, and thanks for teaching me that there's no We in PhD. Sorry I'm not sorry about the toilets.

I joined **Mark**'s lab early on, and apart from taking 218, this was the best academic decision I made in grad school. Mark is great!!! First, he has a lot of really, really good ideas. Thesis-making ideas. The idea to use Accoto's anemometric sensor on tissue was all Mark. I just built it. If Mark says to do something – run this experiment, make this prototype, read this paper, change your algorithm – *just do it.* If you don't, you'll regret it, and a year from now, you will eventually come to the conclusion that you should do what Mark recommended you do a year ago... womp womp. Second, nothing fazes the man: Mark has caught me crying in my office no fewer than 3 times (dynamics quals, a NIH

research grant, and that trainwreck project), has seen me with essentially a shaved head and the largest nose ring ever made, and listened while I told him I was setting up a risky industry-funded multi-year internship to finish my PhD with Intuitive, yet he barely batted an eye (and never mentioned the crying). Amazing. Third, he attracts really great people to his lab, inquisitive intelligent friendly reflective people. Mark cares about lab culture, inclusion, and diversity. Few engineering labs led by men consistently have as many women in it as his does. Finally, and mostly, Mark lets you learn however you need to learn, except he won't hold your hand, and that's very important. Mark wants you to explore and play and fail and discover, and it's all okay and safe because you're in the BDML. Thank you, Mark.

Contents

List of Tables

List of Figures

Chapter 1

Introduction

1.1 Motivation

Robot-assisted surgery (RAS) using the *da Vinci* ® Surgical System has become increasingly prevalent over the last decade [1] and holds great promise for improving surgeons' accuracy and dexterity [2]. Although traditional laparoscopy is also minimally invasive, robotic systems offer better ergonomics [3], [4], improved visualization, more degrees of freedom, and reduced tremor effects [5]. In both laparoscopic surgery and RAS, the loss of direct manual contact with the surgical site results in the absence of tactile information when compared with open surgery. Surgeons instead learn to interact with tissue based mainly on visual cues. Unlike human hands, which have large sensorized surfaces, surgical graspers have small dimensions which can cause high pressures and result in crushing or damaging tissue [6], [7].

Surgeons aim to grasp tissue lightly enough to avoid crushing it, but with sufficient grasp force to prevent accidental tissue loss. Achieving this grasp balance is challenging because the amount of force that avoids tissue damage and grasp loss simultaneously relies on many situational factors, including tissue type and health, grasper type, grasp angle, grasp history, and more. Some tissue slip is permissible provided that enough tissue remains in the jaws to prevent loss or damage to grasped biological tissue. Correct handling of surgical instruments and tissues can minimize tissue damage and accelerate healing, and improvements to this interaction are needed. A study of manual laparoscopic colectomy reports a success rate of only 63% of grasping actions with 7% of failures attributed to tissue slip, of which half resulted in trauma [8]. Surgeons consider grasping forceps to be

one of the most dangerous instruments in laparoscopy [8]. The goal of any surgeon is to carry out the desired procedure while minimally disturbing healthy tissue. This thesis posits that helping surgeons achieve atraumatic, reliable grasping is best served by sensing slip onset directly, rather than estimating it from visual and/or force cues.

An important skill in minimally invasive surgery (MIS) is maintaining situational awareness of all relevant anatomy and tools. The *da Vinci Xi* surgical system [9] allows surgeons to use three tools and an endoscope, but no more than two of these are under direct manual control at any time. MIS surgeons are taught to keep active tools in view but at times elect to use a non-active tool to provide traction on tissue and maintain exposure (see Chapter 2). Given the size and layout of many anatomies, this non-active tool may be outside of the surgeon's immediate focus or even be off-screen. This can occur in large intestine work and in cholecystectomies, among other procedures. Consequences of slip at the third arm can include lengthened procedure time, tissue tearing, and loss of critical view.

Although tissue slip negatively impacts these grasping and manipulation tasks in surgery, it is a relatively unexplored topic in the literature across all surgical disciplines. The work in this thesis is motivated by the idea that monitoring tissue motion between the jaws of MIS graspers has the potential to provide multiple benefits to surgeons. First, knowledge of when tissue slip will occur will enable surgeons to apply the minimum amount of grasp force required to retain tissue, thus reducing grasper-induced tissue damage. The second anticipated benefit is that notifying surgeons of slip events in off-screen tools and/or tools that are not under direct manual control (non-active) will provide otherwise unobservable information regarding that tool's tissue interaction and thereby reduce frustration, sudden loss of critical view, tissue tearing, etc.

This thesis is based on the hypothesis that it would be desirable to detect slip – particularly as RAS systems become increasingly semi-autonomous with one or more tools not under direct manual control. In the future, robotic surgery may incorporate shared autonomy or automation of low-level surgical tasks. This will require more information regarding their interaction with biological materials and a heightened ability to communicate that information with the human user. To that end, testing the utility of supplying feedback to a tool that is not controlled by the human user can provide important insights.

1.2 Contributions

This dissertation makes the following contributions in the field of minimally invasive surgery, surgical robotics, and sensing:

- a survey of 112 RAS surgeons on their experiences with tissue slip in RAS. Prior to this work, no such study existed. The results of this survey provide a useful foundation and motivation for the work presented here and for further studies investigating tool/tissue interactions in RAS and MIS.
- a novel slip sensor for detecting slip of biological tissue *in vivo*. This device is the first known slip sensor intended for sensing slip of biological tissue that has been integrated into a MIS instrument that can fit through a standard laparoscopic cannula and is driveable by a RAS system. The sensor is capable of detecting slip of a variety of *ex vivo* tissues in $\leq 2.1\,\text{mm}$ and *in vivo* tissues in $\leq 3\,\text{mm}$.
- a simulation that informs the design and optimization of the presented thermal-based slip sensor. This simulation provides a useful thermal model that captures the effects of component materials, dimensions, spacing, heater temperature, grasped tissue properties, etc. The model also enables useful predictions of sensor behavior within the range of thermal conditions one would anticipate encountering *in vivo*.
- an evaluation of providing tissue slip feedback in a user study. This study showed that with slip feedback participants drop tissue less and are more aware of impending tissue slip and grasp loss. Participants report feeling more confident, relaxed, and task-focused when slip feedback is present than without it; all participants reported liking the feedback and preferring its presence to its absence during the user study. An evaluation of workload via self-assessment on the Surgeon Workload Index (SURG-TLX) showed that participants experienced significantly decreased mental and temporal demands and situational stress.

1.3 Thesis Outline

The remainder of this dissertation is laid out as follows. **Chapter 2: Motivations for slip prevention** establishes the foundation for this work, beginning with motivations for researching tissue slip in minimally invasive surgery. To strengthen the arguments presented, the chapter also contains the methods and results of a survey of RAS surgeons to establish

the clinical motivation for this work and is a broad exploration of their experiences with slip in RAS. Need-finding is an important step in any research. A discussion of when and why tissue slip in RAS is an important problem worth exploring follows.

Chapter 3: Identifying and measuring slip begins with a mathematical definition of slip. The chapter ends with a summary of the prior art in this area (of which there exists relatively little that is directly relevant to the present application). This chapter also introduces the concept of thermal slip sensing as a promising solution for detecting motion of soft, wet tissue in a surgical grasper.

Having selected a promising slip sensing technology, **Chapter 4: Thermal modeling and simulation** discusses a series of transient thermal simulations developed using ANSYS 19.0 to understand the working principles of the sensor. Specifically, I sought to explore the effects of tissue thickness and water content on the thermal gradient and the time constant associated with achieving the steepest local thermal gradient. This information helps provide an understanding of whether the sensor may be expected to function under the variety of conditions it may encounter *in vivo*. The details of the sensor design and performance depend on the results of thermal modeling. The main objective was to determine whether the sensor was likely to function under the range of conditions one would expect to encounter *in vivo* and provide guidelines for designing production-level sensors based on slip sensing requirements. Material in this chapter draws on:

- ©2018 IEEE. Reprinted with permission, from Burkhard, Natalie, et al. [10]

Chapter 5: Slip sensor prototypes presents two distinct rounds of prototyping. The first round's purpose was to establish foundational data that validates the working principle of the sensor. The second round of prototyping demonstrates greater adherence to the application requirements, ultimately producing a sensor integrated with a modified RAS tool, driveable by a da Vinci Surgical System. Further developments to facilitate sensor use during realistic tissue manipulation are also presented. The chapter concludes with a description of sensor validation on *in vivo* porcine tissue to demonstrate robustness to perfusion. Material in this chapter draws on:

- ©2017 IEEE. Reprinted with permission, from Burkhard, Natalie, et al. [11]
- ©2018 IEEE. Reprinted with permission, from Burkhard, Natalie, et al. [10]

Chapter 6: User study presents a study conducted to evaluate whether experienced users would benefit from slip detection and feedback during RAS procedures. This study

demonstrated the slip sensor's utility in helping inform human decision-making and relieve cognitive load and stress during a grasping and manipulation task.

Chapter 7: Conclusions summarizes this dissertation and recommends future studies based upon the presented work, as well as guidelines for implementing the presented slip sensor into several common RAS graspers.

Chapter 2

Motivations for Slip Prevention

2.1 Slip in MIS

Grasping and manipulation of tissue is an important task in MIS: it enables tasks like dissecting, moving, stabilizing, suturing, elevating, and exposing tissue [12]. Preventing tissue slip from a grasper in MIS is a well-motivated goal because slip is an undesirable, accidental, and often surprising event that disrupts surgeons' workflow. The goal of this work is to enable efficient and atraumatic grasping. Although slip of a grasped object can occur in any RAS instrument, the focus here is on instruments specifically intended for grasping tissue. The following discussion thus excludes staplers, needle holders, scissors, hooks/spatulas, clip appliers, etc. The concerns presented here are supported by interviews with 3 expert RAS surgeons and 2 clinical development engineers (CDEs) from Intuitive Surgical, Inc. and review of 15 RAS videos from relevant procedures (splenectomies, cholecystectomies, Nissen fundoplications, colectomies, etc.). CDEs are a special role at Intuitive; they have extensive knowledge of anatomy, physiology, and surgery and help define and validate the clinical risks and requirements for in Intuitive's product development process.

What if tissue slip never occurred – what would that *really* do for surgeons? There are two sides to the answer that are concerned with (1) the repercussions of slip and (2) with the behaviors surgeons adopt to avoid slip. The following discussion motivates the survey on tissue slip conducted on 112 RAS surgeons (presented in Section 2.2), the results of which bolster the arguments presented here.

2.1.1 The repercussions of slip

When slip, or accidental tissue loss, occurs, there are an array of possible consequences. First, surgeons report that tearing often accompanies slip. At the very least, this creates another defect that the surgeon must fix, which extends the length of the case and can add to the surgeon's frustration. However, tears may not be so benign; they can have many secondary effects: sepsis, serious infections, leak of infectious fluid, and/or spread of cancerous cells. If the tear causes bleeding, that can make the tissue even more difficult to grasp, and it can occlude the surgeon's view and make the operation more difficult. Furthermore, vessels retract when torn, making anastomosis more challenging. Some tears can even be irreparable. If tissue slips onto an active electrocautery tool, all of the aforementioned consequences are even more dire and significantly lengthen procedure time. Wasting time in the operating room (OR) drives up procedural costs quickly; the OR costs on average $37 per minute [13].

Slips may also disrupt a surgeon's workflow because they force the procedure to halt, causing frustration and wasting time. This disruption may be as minor as requiring the surgeon to re-grasp the tissue or as major as having to delve back into the body cavity and find the desired anatomy all over again, wasting minutes. For example, when retracting the bowel back into the body cavity during an inguinal hernia repair, the bowel's tendency is to fall back into the hernia. Loss of grasp can result in starting the task over. Loss of a critical view can take substantial time to recover, and if the slip causes bleeding, that recovery will be even more difficult due to view occlusion.

Tissue slip also reduces surgeons' confidence in their tools, which can increase the opportunities for errors and complications. Many surgeons already switch between multiple grasper types with different maximum forces to optimize their grasping, but this can be expensive and time consuming. Other surgeons report that they usually try not to grasp fragile tissue, relying instead on sweeping it aside with the instruments' shafts.

2.1.2 Behaviors intended to avoid slip

Many surgeon behaviors can reduce the chance that slip occurs; for example, ensuring that applied traction is not excessive. However, the most direct way they can prevent tissue slip is by modulating their grasp force. However, balancing grasp force to simultaneously be high enough to prevent tissue slip *and* low enough to avoid causing tissue damage is

difficult, particularly when relying on visual information alone (See Section 1.1 for more details). Tissue damage is not always readily apparent and may take minutes to hours to develop [7], at which point it is too late to prevent.

In open surgery, surgeons may grasp and manipulate tissue with their hands, relying on large surface areas and friction. However, in laparoscopic and robot-assisted surgery, surgeons must use short, stiff, sharp (to enhance grip [8]) jaws with small grasping areas that must pinch to obtain the same result, often resulting in a high-pressure interaction [6]. This can cause tissue trauma and serious clinical consequences [12], [14], [15] and therefore requires care, skill, and cognitive load from the surgeon. However, insufficient force may result in tissue slip and procedure delay [8]. Balancing these competing goals is especially difficult when handling delicate tissue that is easily crushed or damaged, like small bowel [16]. D'Alessio et al. [17] found that grasp control is more efficient when based on slip-related signals than signals related to exerted finger force. If surgeons knew the minimum grasp force they could apply to avoid slip, perhaps they could more confidently manipulate tissue with lower forces and/or use a single grasping instrument. It is the ultimate long-term vision for this project to realize an autonomous grasper that offloads this task from the surgeon altogether, grasping with the minimum grasp force necessary to avoid slip.

One aspect that makes applying safe grasp forces so difficult is that incurred tissue damage is not always immediately apparent. Tissue damage is defined as any disruption of normal tissue function and may include cell death, inflammation, and vascular damage [7]. Acute responses to injury are difficult to observe until long (minutes–hours) after the fact [12]. Most tissue damage during MIS occurs at the site of grasping due to the higher stress concentration there [18]. Although some observable changes may occur (color changes [7], oxygen saturation levels [19], etc.), these signify that damage has already occurred rather than presenting a preventable situation.

In any surgery – open, laparoscopic, or robot-assisted – it is the goal of surgeons to minimally disturb healthy tissue while performing their intervention. To mitigate the issue of applying the appropriate amount of grasp force, surgeons select task-specific graspers and modulate the grasper jaws to provide enough force to prevent slip, but not so much that damage occurs. However, the maximum force with which one can atraumatically manipulate tissue and maintain grasp stability varies by tissue type [7], [12], jaw geometry [8], and other situational factors. Realistically, implementation would be technically complex and require empirical tuning. A study of manual laparoscopic colectomy reports a success rate

of only 63% of grasping actions with 7% of failures attributed to tissue slip, of which half resulted in trauma [8]. Surgeons consider the grasping forceps one of the most dangerous instruments [8]. Histological evidence shows that excessive forces on tissues applied through graspers/retractors can obstruct the blood supply and lead to localized necrosis [19].

Grasper-induced injuries often occur during tissue retraction [20], [21] and may result in perforation or hemorrhage [14], [22]. Furthermore, increased grasp duration leads to increased tissue damage [12]. Whether the surgery conducted is open, laparoscopic, or robot-assisted, tissue injury can be difficult to detect promptly and can lead to disastrous complications like sepsis and serious infection. Even for less immediately severe injuries, negative effects may propagate due to interrupted blood supply and crushed tissue and from secondary consequences like inflammation, coagulation, cell death, and ischemia-reperfusion injury [23]–[25]. Injury risk is higher in MIS than in open surgery, with a 2-4% risk of injury to the bile duct, bowel, vascular structures [21], [26]. Grasping injuries may result in scar tissue formation, bleeding, adhesions, and loss of bowel motility [23], [27]. Laparoscopy-induced bowel injury has a 3.6% mortality rate [28], and other reports include bladder [29], gallbladder [30], and splenic [31] injuries.

In summary, although surgeons can select process-specific graspers and attempt to modulate their grasp force to avoid incurring damage or accidental tissue loss, it is a difficult balance to maintain, and the consequences of grasper-induced tissue damage can be high. A slip sensor would permit use of the minimum grasp force necessary to prevent slip and lessen the cognitive load associated with this secondary task. Given this background, acquiring qualitative data regarding surgeons' opinion on tissue slip was deemed a valuable endeavor.

2.2 Surgeon opinions on slip in RAS

2.2.1 Methods

Prior to this survey, there was no information publicly available regarding slip of biological tissue, particularly during RAS. To improve tissue-tool interactions in RAS, it is crucial to understand the needs of the surgeons who perform them. A survey was prepared and distributed to understand the importance of tissue slip. Electronic invitations were sent to 983 surgeons who opted in to receive surveys from Intuitive between May 23–June 1, 2018 and offered a $15 honorarium.

The survey was estimated to take 15 minutes to complete and consisted of 19 questions

(see Table 2.2). The three main sections of the survey sought to understand (1) the clinical importance and occurrence of slip, (2) specific surgeon experiences and responses to tissue slip, and (3) preferences for receiving slip feedback. Identifying information was removed before analysis, which was conducted in MATLAB 2017b (MathWorks) using frequency distribution tests. Optional comments were free-text reflective format and designed to allow participants to elaborate on multiple choice answers.

2.2.2 Survey Results

112 (11%) of the 983 surgeons responded; see Table 2.1 for participant demographics. The surgeons were analyzed as a single population. It was not meaningful to check for differences between surgeon specialties because over half of the subgroups had only 1-4 members. Respondents gave informed consent to Intuitive to be solicited for surveys; only surgeons within the Intuitive database were contacted. Information regarding age or level of experience were not obtained. When applicable, results are reported as the mean value ± one standard deviation.

Table 2.1 – Surveyed RAS surgeon demographics

Specialties	
Cardiac	2 (2%)
ENT	1 (1%)
GEN: Bariatric	3 (3%)
GEN: Colorectal	13 (12%)
General Surgeon	26 (23%)
Gynecology	38 (34%)
Gynecology/Oncology	4 (4%)
Thoracic	3 (3%)
Urogynecology	4 (4%)
Urology	18 (16%)
Gender	
Male	83 (74%)
Female	29 (26%)

In question #1, surgeons ranked the mean clinical importance of tissue slip comparable to that of tissue crushing or tearing (6.0 ± 0.4 vs. 5.6 ± 0.5 and 5.8 ± 0.6 out of 10). A score of 6 corresponds to a delay in procedure without requiring conversion or causing harm to the

Table 2.2 – Survey questions administered to RAS surgeons

Introduction

Question	*Response*
(1) Rate the clinical importances of crushing, tearing, and slipping of tissue.	Rate each from 0 (negligible) to 10 (catastrophic)
(2) How often does slip happen during a typical RAS case?	[Never; 1-2 times; 3-5 times; >5 times]

RAS experiences with tissue slip

Answer questions #3-17 w.r.t. your experience with each of these situations: tissue slip during (A) retraction; (B) establishment of a critical view; and (C) handling of fragile tissue. E.g., #3 has #3A, 3B, and 3C.

Question	*Response*
(3-5) How often does it occur? Describe a case, procedure or situation where it occurred.	Rate from 0 (never) to 10 (always); optional comment
(6-8) How would you rate its clinical risk? Explain your rating.	Rate from 0 (negligible) to 10 (catastrophic); optional comment
(9-11) How annoying or frustrating is it?	Rate from 0 (not at all) to 10 (extremely)
(12-14) What is your typical response to it?	[N/A; Grasp with different part of jaw; Grasp at different angle; Re-grasp exactly as before; Select new instrument; Other]
(15-17) What is the average time it takes to recover the operating pose or critical view prior to the slip event?	[N/A; 5 s; 30 s; 1 min; 1-5 min; > 5 min]

Tissue slip feedback modality preferences

Question	*Response*
(18) Imagine you can receive feedback regarding slip of grasped tissue from a tool you ***are*** actively controlling.	Rank these feedback modalities from most (1) to least (6) preferred. • Auditory (beep, warning sound) • Visual (overlaid on tool) • Visual (on screen edge) • Haptic (vibration) • Haptic (resistance/force) • None (prefer to ignore)
(19) Imagine you can receive feedback regarding slip of grasped tissue from a tool you ***are not*** actively controlling.	

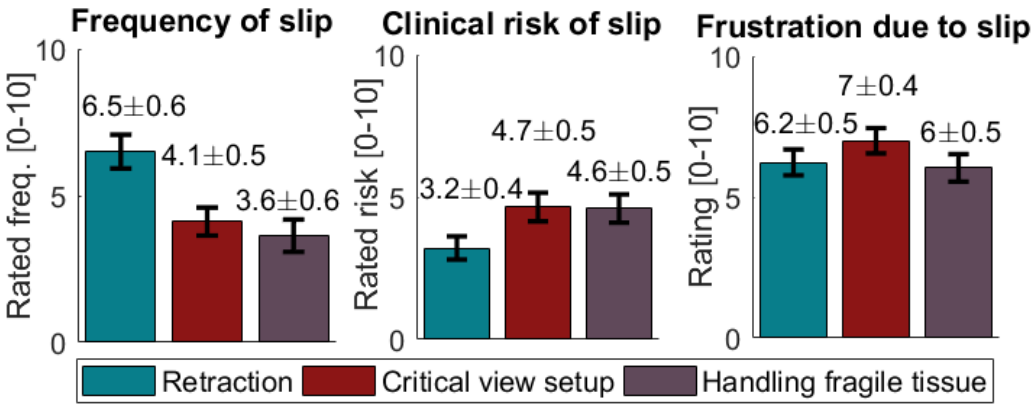

Figure 2.1 – Questions #3-11: Rated frequency of slip, risk of slip, and frustration due to slip during RAS retraction, set up of critical view, and handling of fragile tissue ($\mu + 1\sigma$ shown). For rated (clinical) risk, see Table 2.3 for rating description. Although the rated clinical risk of slip is overall low (the chosen category describes no harm to the patient), frustration and frequency of slip are significant.

patient or user. For a full description, see Table 2.3 for Severity Evaluation Criteria which was derived from an Intuitive Surgical, Inc. protocol based on [32]. For the number of slip events in a typical RAS procedure, 4% reported slip never occurring, while 41% reported 1-2 times, 34% reported 3-5 times, and 21% reported > 5 times.

The responses for questions #3-11 are summarized in Fig. 2.1; #12-17 are in Fig. 2.2. Surgeons reported tissue slip occurring more frequently during retraction (6.5 ± 0.6) than during critical view setup or while handling fragile tissue (4.1 ± 0.5 and 3.6 ± 0.6, respectively), but frustration and rated clinical risk (see Table 2.3) across the three categories did not differ significantly. Clinical risk of slip was overall deemed low with no harm to the patient or user. Surgeons described slip occurring more often on anatomies that consist of bulky stiff tissue (e.g., the vaginal cuff), during high-tension tasks (e.g., hernia repair, Nissen fundoplications), and during procedures where surgeons choose to retract tissues out of the field of view (e.g., lower anterior resection, cholecystectomy). Fragile tissues with high consequences for tears (e.g., small bowel, blood vessels) due to slip were of the greatest concern to surgeons, however. Surgeons are loath to grasp and re-grasp fragile tissues with high consequences for tears (e.g., small bowel, blood vessels) due to slip. Experience and care are required to apply just the right amount of tension to fragile tissue.

Surgeons tended to describe slip as annoying, frustrating, and time-wasting. However,

Table 2.3 – Severity Evaluation Criteria

Ranking	Qualitative Approach - Degree of Severity	
1	Negligible	Failure will not have a perceptible effect on the performance of the product or procedure. The user or patient will not notice the failure or be harmed.
2	Insignificant	User is only minimally affected by the failure. No harm to the user or patient.
3	Insignificant	Failure will cause user to notice only a minor nuisance or negative impact on the product. No harm to the user or patient.
4	Minor	Failure causes significant dissatisfaction or nuisance for the user, no medical intervention is required to resolve, no harm to the user or patient.
5	Moderate	Failure causes noticeable negative impact on the product or system performance product is operable at reduced performance level. No system re-start required. No harm to the patient or user.
6	Moderate	Failure causes acceptable delay to procedure as defined in the products clinical requirement documents, but procedure can be completed without conversion. No harm to the patient or user.
7	Moderately Significant	Failure causes product to be inoperable. Product enters fail-safe mode. Alternate surgical approach may be required, with no harm to the patient or user.
8	Significant	Failure requires no or minor surgical or clinical intervention and results in easily reversible harm to the patient or user. No permanent damage or serious injury occurs.
9	Extremely Significant	Failure requires significant surgical or clinical intervention to prevent serious injury, permanent damage to a body structure, or death to the patient or user.
10	Hazardous	Failure causes serious injury, permanent damage to a body structure, or death to the patient or user.

when slip does occur and bleeding or tearing results, significant time and effort is required to fix it and is highly desirable to avoid. Because time in the operating room costs $20-$46 per minute [13], the cost of a single slip event can range from $1.60 to $230, and surgeons report slip occurring twice or more during a typical RAS case.

Most surgeons reported responding to slip by changing the angle of their grasp. However, when handling fragile tissue, surgeons were more likely to either change nothing about their grasp or to change the tool completely than during retraction or view setup. Most surgeons reported requiring 5-30 s to recover their prior operating pose as a result of tissue slip, although a non-negligible percentage reported spending a minute or more (Fig. 2.2). The longest recovery times were reported during handling fragile tissue; surgeons reported working more slowly to limit tissue tearing, damage, and bleeding.

Surgeons were asked to rank in order of (hypothetical) preference how they would like to receive feedback for slip of biological tissue during RAS. Surgeons' responses differed greatly when considering receiving feedback on a tool they were actively controlling as opposed to a non-active instrument. However, whether the tool was actively controlled or not, surgeons overwhelmingly reported that they would prefer to receive some kind of feedback as opposed to nothing: $> 70\%$ of respondents listed ignoring slip as the least preferred option for active and non-active tools. Reported feedback preferences for slip in an actively controlled tool showed no clearly superior feedback modality. However, for providing slip in a non-active tool, surgeons strongly favored receiving auditory cues as their top preference (48%), followed by visual displays either on the screen edge or on the tool (15% and 16%, respectively). Logically, for the *non-active tool*, users did not prefer receiving haptic feedback (as either vibrations or resistive forces, $< 8\%$ for each) because their hands would already be engaged with active tools.

The overall results showed that slip is both a frustrating and common occurrence. Surgeons tend to work with three tools and switch among them, keeping two under active manual control and the focus of their visual attention, while the non-active tool continues to passively hold tissue. Although slip at the active tools can result in bleeding, tearing, or loss of exposure, slip at the non-active arm is particularly problematic because the same consequences apply but occur outside the surgeon's focus area. This finding motivates the three-tool user study detailed in Chapter 6. The results from this survey also motivated the design of the state machines implemented in Sections 5.3.5 and 6.2, which were made to only tell surgeons about slip when it is likely that slip is important.

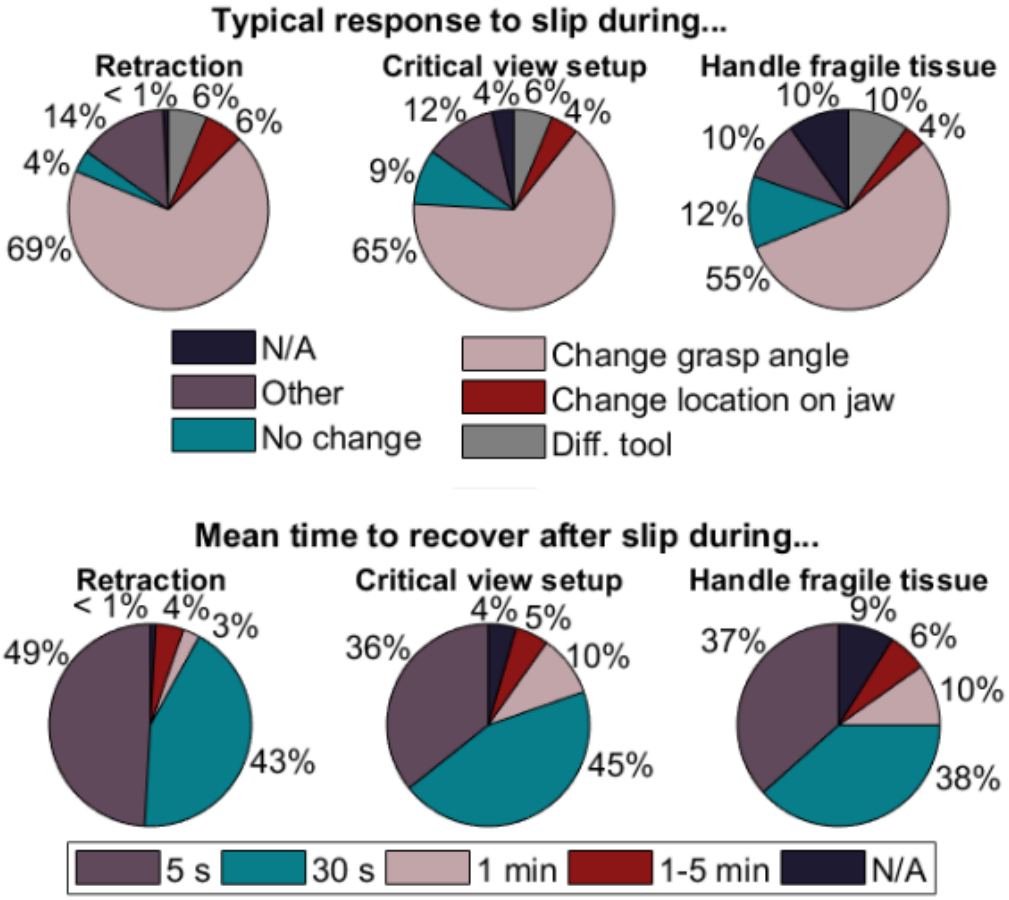

Figure 2.2 – *Top:* Questions #12-14: Typical responses to slip during RAS retraction, set up of critical view, and handling of fragile tissue. *Bottom:* Questions #15-17: Mean time to recover prior operating pose during RAS retraction, set up of critical view, and handling of fragile tissue.

2.2.3 Discussion

In general, surgeons perceive slip predominantly as a frustrating, annoying waste of time. Several surgeons mentioned that their frustration can lead to additional problems or conversion to open or laparoscopic surgery. However, many surgeons acknowledged that slip is as clinically important as tearing or crushing tissue. In the open comments section, surgeons indicated this was due to their perception of tissue slip: both crushing and tearing were described as avoidable events that were the direct cause of an action they understood. Tissue slip, meanwhile, was described as an *unavoidable*, unpredictable event that had no relation to their actions, and it was often accompanied by tissue tearing anyway. Thus, surgeons felt that although tearing and crushing had immediate negative consequences that outweighed those of slip, slip was deemed of equal importance because it was outside their power to control it.

Surgeons also reported that slip may also have serious consequences for the patient, particularly if the grasped tissue is fragile or if slip is accompanied by tearing, tissue damage, and/or bleeding. Common across all specialties was the fear that slip on or near a blood vessel would cause bleeding and retraction of the vessels, making them more difficult to access and repair.

Anatomies that are the most challenging include the colon, gallbladder, bladder, prostate, and vessels, and procedures where slip was reported to happen include vaginal cuff closure and hernia sac dissection. The vaginal cuff is a very thick, stiff tissue that must be grasped quite hard to hold the cuff edges together for suturing, and the tissue tends to spring out from tools' grasp. Similarly, a majority of the general surgeons mentioned slip during retraction of the hernia sac during hernia repair or of the gallbladder during cholecystectomies. Nearly all urologists mentioned retracting the prostate. Colorectal, urologic, gynecologic, and general surgeons all agreed that slip occurred often during retraction/elevation of the colon and/or rectum due to its being off-screen and the tissue's fragile nature. Because surgeons tend to grasp fragile, easily crushed tissue more lightly, slip happens more often.

Overall, the results of the survey indicated that notifying surgeons of slip onset would likely provide clinical benefit, and the vast majority of surgeons would prefer to receive some form of slip feedback than none at all. Slip is perceived as an unpredictable and disruptive event that typically does not result in disastrous consequences but may still have negative effects for the patient. In summary, this chapter has presented a sound motivation for exploring methods and technologies to prevent and/or detect slip of grasped biological

tissue in minimally invasive surgery.

Chapter 3

Identifying and Measuring Slip

3.1 Slip definition

Having determined in Chapter 2 that slip of grasped, biological tissue during MIS is a well-motivated problem, this chapter presents a definition of slip as well as a discussion of prior slip sensing technologies concerning their applicability to MIS. Slip sensing has been an important topic in robotic manipulation since at least the 1990s [33] and has similarly been the subject of investigation into human mechanoreception and manipulation [34]. However, most analyses of slip for robotic grasping assume that the grasped object is rigid, or at least stiff in comparison to human or robotic fingertips. With this assumption, slip can be a rotation, a translation, or some combination thereof, and it may be described equivalently as an instantaneous rotation about some center of rotation (CoR) in the plane of the tool jaw.

The picture becomes more complicated when the grasped object is highly deformable. Given a grasper in contact with biological tissue, one can measure the motions of several particles on the surface to obtain a measurement of motion and deformation. In general, local tissue movement can arise from any combination of *motion* (translation and rotation) and *deformation* (dilation, extension, and shear) [35] (see Fig. 3.1).

This deformation of tissue may thus be described as an affine deformation, which is composed of a linear transformation (containing rotation, shear, extension, and/or compression) and a rigid body translation [37]:

$$\vec{x}(\vec{X}, t) = \boldsymbol{F}(t) \cdot \vec{X} + \vec{c}(t) \tag{3.1}$$

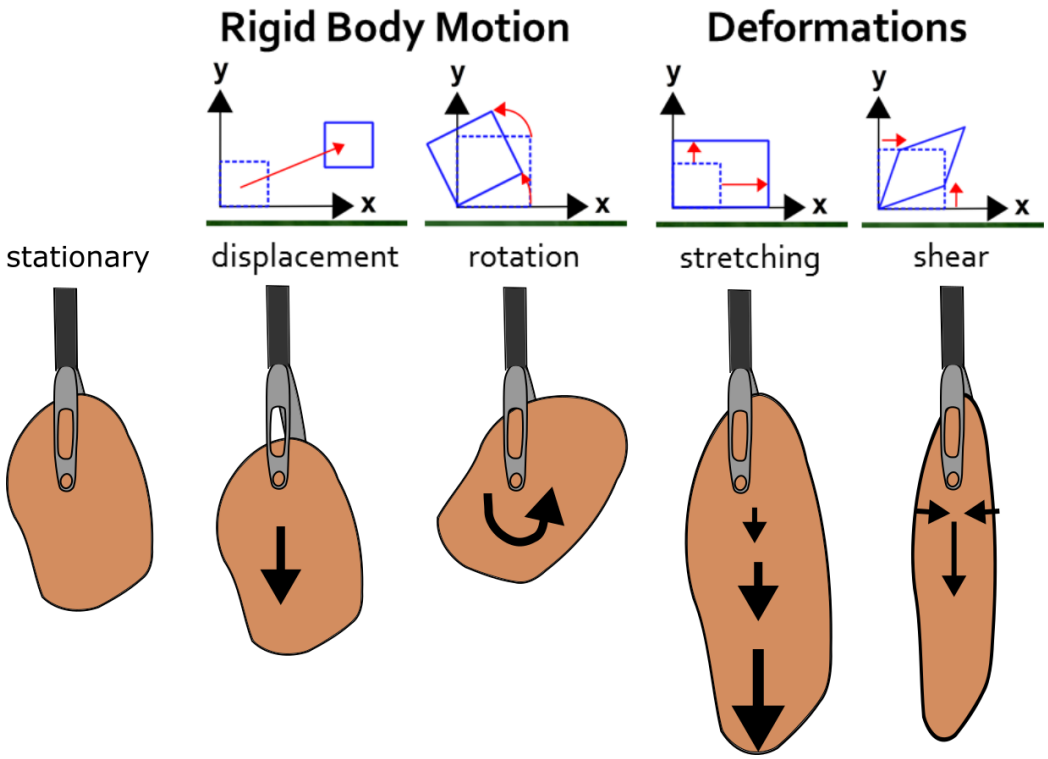

Figure 3.1 – The components of general deformation of a body. Images in top row reprinted with permission from Bob McGinty [36]. Supplemental artwork added to relate to MIS grasper. Top view of MIS grasper shown, holding tissue in a plane (no gravity effects).

where $\vec{x}$ is the position of a point in the deformed configuration, $\vec{X}$ is the position of that point in the reference configuration, t is a time parameter, $\boldsymbol{F}$ is the linear transformation, and $\vec{c}$ is the translation. Note that neither $\vec{c}$ nor $\boldsymbol{F}$ varies with position $\vec{X}$. Rigid body motion is a special case of the affine deformation that does not involve shear, extension, or compression – only translation and/or rotation. In this case, $\boldsymbol{F}$ is proper orthogonal to permit rotations but no reflections:

$$\boldsymbol{F}^T\boldsymbol{F} = \boldsymbol{F}\boldsymbol{F}^T = \boldsymbol{I} \tag{3.2}$$

$$det(\boldsymbol{F}) = 1 \tag{3.3}$$

For the purposes of this thesis, I define slip as consisting only of the rigid-body component of tissue motion. Deformations (e.g. Poisson radial expansion as a grasper squeezes

soft tissue) are not of concern as they do not immediately lead to grasp failure. Rather, stretch may be a precursor to slip or may even occur simultaneously, but in and of itself, stretch alone will not lead to loss of grasped tissue. This does not mean that stretch is unimportant; in Section 7.2, a recommendation for future work includes exploring the relationship between tissue stretch and slip to infer information regarding incipient, rather than total, slip. In the present case, the goal is to simply identify the net displacement of the tissue and reject the deformation and rotation components of motion.

As will be discussed later in Section 3.2, it is possible to obtain estimates of $\vec{x}$ and $\vec{X}$ by using a video camera to track markers or particles on the surface of a thin piece of tissue. This allows approximation of the coordinate mapping between adjacent frames, which gives us $\boldsymbol{F}$. Using polar decomposition, it is possible to then separate $\boldsymbol{F}$, the general deformation gradient, into a rotation matrix and a deformation matrix [36]. Standard vision or MATLAB software enables extraction of the rigid body translation and rotation components using various approaches; [36] contains a page on polar decomposition. Section 5.3.6 describes use of such an image-based method that served as a ground truth for slip measurement.

In the present case, translation matters when it results in accidental grasp loss. Deformation, expansion, contraction, etc. are not of interest here because they do not signal impending loss of grasp. Furthermore, the sensing approach presented here (see Section 3.3) provides only a single 2D vector of motion at a single point in the plane. Thus, extraction of only the rigid body translation component of motion is required because the sensor can only measure net translation; rotations are precluded by the symmetry assumption.

3.2 Slip Sensing Prior Art

As noted above, rigid-body slip is a relative displacement between two surfaces. Robotic slip sensors (see Fig. 3.2) are intended to detect impending motion (incipient or micro slip), or the very beginning of motion (macro or total slip onset). Incipient slip precedes total slip [38]. The majority of the work below was developed with robotic graspers in mind. Much of the prior art in this area focuses on robotic manipulation and tactile exploration; these slip sensors are thoroughly reviewed in [38] and [39].

Displacement-based slip sensors detect motion between two surfaces and may rely on mechanical parts joined to magnetic or optical transducers (see Fig. 3.3a). Early sensors in this category used rollers with encoders to detect motion [40]. Sensors with interstitial

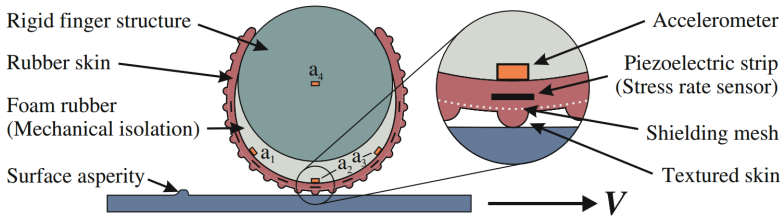

Figure 3.2 – Vibration transducer for slip sensing. Cross-section of robotic skin with accelerometers mounted to the skin and isolated from the finger by a compliant layer. Piezoelectric strips in the skin provide localized dynamic responses to changes in skin stress. Image reprinted from ©2016 Springer Science & Bus Media [39].

spaces or moving parts do not work well in a MIS setting because they tend to accumulate impurities and may adversely affect grasp stability. They are therefore are difficult to clean, would pose sterilization issues, and may not function correctly when interacting with the fluids and tissues in the body cavity. Other sensors compare CMOS sensor-acquired image sequences which are analyzed to obtain slip speed and direction. Such a technique is used in Section 5.3.6 to obtain a ground truth for slip. These types of sensors present computational challenges for rapid motion analysis and packaging challenges for integration into the jaws of a surgical instrument and may be inaccurate if the tissue is bloody. The GelSlim Sensor presented by Donlon et al. [41] has nearly the appropriate package and capabilities, although any silicone or gel skin in contact with the body cavity will need to be disposable (see Fig. 3.3b). If the computational cost and size issues could be overcome, this sensing method would have very high reliability and redundancy [42] and perhaps serve additional sensing purposes; e.g. monitoring tissue health or perfusion.

Other sensors — including thick film PZT cantilevers, PVDF film transducers, accelerometers [43], [44] (see Fig. 3.4a), and acoustic emissions detectors [45] — detect the high frequency ($> 100\,\text{Hz}$) stick-slip microvibrations that tend to signal incipient slip between contacting dry surfaces with Coulomb friction [34]. In dry rigid body slip, stick-slip vibrations tend to signal incipient slip [34], [38], [39]. However, sensing slip of wet, deformable objects (like biological tissue) poses additional challenges because wet slip lacks (or severely attenuates) these vibrations. Brown et al. [46] added brass ridges to the jaw's contact surface and detected slip by monitoring pressure changes with PVDF (see Fig. 3.4b), but their results stated that even with this mechanical amplification and alteration to the jaws, false positives were common. This rough addition to the grasping surface of instrument

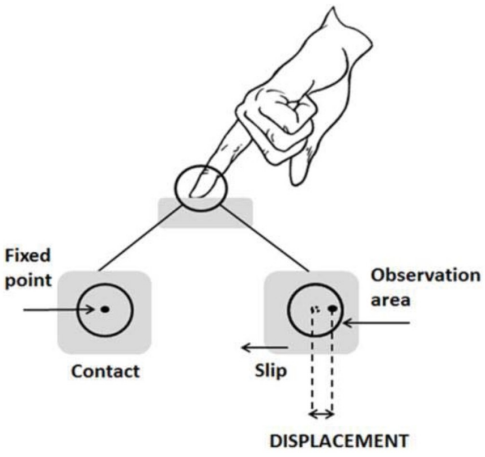

(a) Displacement-based slip sensor. Image reprinted from ©2013 IEEE [38].

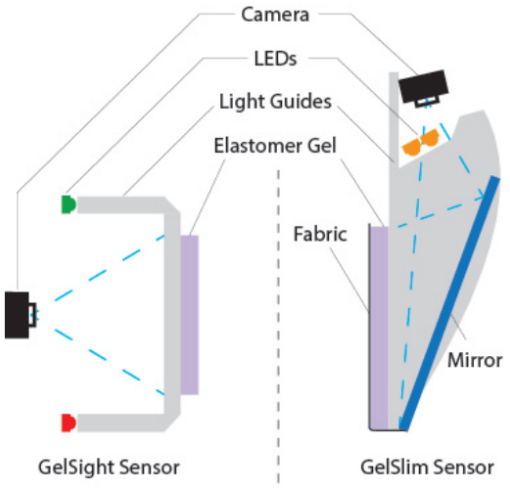

(b) Optical-based tactile sensor. GelSlim at right approaches the size constraints for MIS. Image reprinted from ©2018 IEEE [41].

Figure 3.3 – Displacement-based sensors.

jaws would likely cause additional tissue damage.

Force transducers for slip sensing often sense changes in pressure distribution or surface deformations; e.g. using dielectric elastomers to relate pressure changes to resistances [47] or to capacitances [48]. Many variations on this idea exist and utilize micromachined structures, sensing for instance changes in stress [33] or changes in thickness [48] as a compliant layer contacts a surface. These designs often present miniaturization challenges and high likelihood of incurring false positives and negatives due to the compliance and relaxation of biological tissue. Furthermore, the nature of conforming contact may cause changes in pressure distribution without slip occurring, but slip may also occur without accompanying force changes: biological tissue creeps and relaxes. Designs that seek to estimate the grip force required to balance the shear force or to detect the transition between static and dynamic friction are ill-suited to this application: the friction coefficient between the tissue and grasper jaw is difficult to estimate and changes with time, trauma, tissue type and other physiological factors. Stoll and Dupont [16] presented an approach that requires tangential grasp force measurement and differentiating relaxation and friction forces (see Fig. 3.5). However, this method may require modifications to the grasping surface to amplify friction forces and may be inaccurate if pressure concentrations are present.

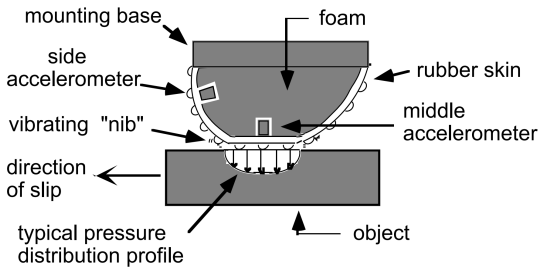

(a) Incipient slip sensor used to modulate grasp force to prevent grasped objects from slipping. Image reprinted from ©1993 IEEE [43].

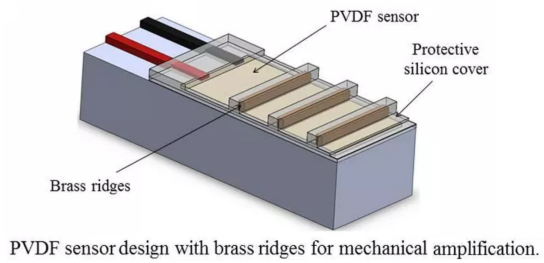

(b) PVDF-based tissue slip sensor. Brass ridges cause tissue to exhibit stick-slip vibrations characteristic of slip in dry, rigid-body scenarios. Image reprinted from ©SAGES 2012 Abstract Archive [46].

Figure 3.4 – Microvibration transducers

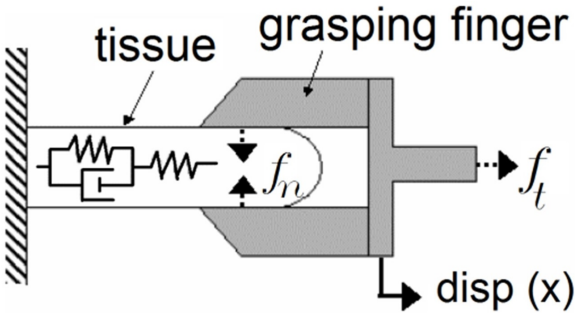

Figure 3.5 – Force-based tissue slip sensor. Image reprinted from ©2006 IEEE [16].

Many other groups have sought to use force sensing to otherwise inform the tool-tissue interaction in MIS. Prasad et al. [49] sought to quantify the intra-abdominal forces that laparoscopic instruments experience during MIS and designed a sleeve instrumented with strain gages to sense forces during tissue retraction. Horeman et al. [50] designed a sensor to measure suture tension both inside a closed incision and while pulling it. A goal of the work was to provide a method of quantifying how much tension is safe to apply to sutures on different tissues. Perri et al. [51] devised a method with capacitive-based pressure sensors to obtain an active pressure map of the contact surface of organs to locate tumors during MIS. This information can provide some information that can help surgeons assess tissue health or inform their approach for various procedures. However, as revealed by the results in Fig. 5.5 (shown in Section 5.2), force sensing by itself is insufficient to achieve reliable, atraumatic grasping. Therefore, the goal is to instead sense slip directly, perhaps ultimately

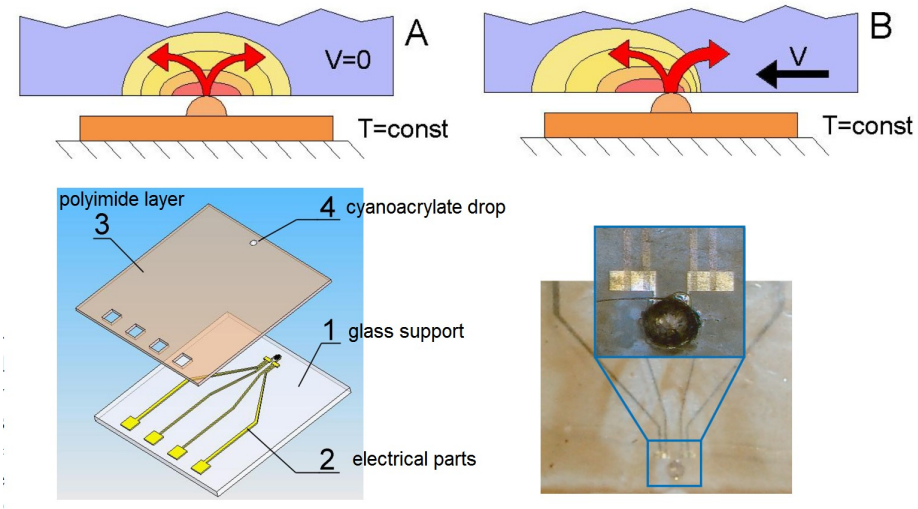

Figure 3.6 – Thermal-based slip sensor. Images reprinted from ©2007 IEEE [52].

in combination with force sensing.

Another class of slip sensors senses temperature changes associated with mechanical slip [52], [53]. Based on hot-wire anemometry, these sensors use a thermal probe to maintain a heater at near-constant temperature via bang-bang current control. When slip occurs, a convective heat transfer term is introduced to the simple conduction problem, and the current required to maintain a constant temperature increases; the slip sensor monitors this change (see Fig. 3.6). Although robust to vibrations and surface roughness of grasped objects, acknowledged drawbacks of this design are its inabilities to differentiate between making/breaking contact and slip or to sense slip direction. The sensor presented here is inspired by this work. However, our design relies on detecting movement of a spatial temperature gradient rather than changes in heating power, which can enable sensing directionality of motion.

3.3 A novel anemometric slip sensor for MIS

Sensing slip in MIS requires solutions to be capable of sensing slip of wet, compliant objects and have the potential for integration into MIS or RAS end effectors, e.g. Intuitive Surgical's da Vinci EndoWrist® instruments. Integration into the end effector imposes significant packaging constraints. Slip is most easily sensed near the event of interest, so the sensor must fit into the grasper jaws or at least pass through the bore of a standard laparoscopic

trocar. Furthermore, to facilitate surgeon acceptance, our technology must only minimally change the nature of the grasper jaws.

Drawing on the ideas of [52], [53], the following sensing strategy was proposed (see Figure 3.7). In **A**, a top view of the slip sensor is shown. Four thermistors (labeled N, S, E, and W for ease of reference) surround a central heating element, providing spatial information regarding the thermal distribution in the plane of the sensor. **B** shows a cross-sectional view through E and W.

When tissue comes in contact with the jaw, heat is conducted from the heating element into the tissue, forming a thermal gradient $T(x, y, t)$ in it. This thermal energy is then conductively transferred to the thermistors (mainly through the grasped object, by design) when stationary ①. As in [52], [53], we approximate this heat transfer problem as:

$$\frac{\partial T}{\partial t} = \kappa \nabla^2 T - v \cdot \nabla T + \dot{q}(x, y) \tag{3.4}$$

where $\dot{q}(x, y)$ $[\frac{W}{s}]$ is the heat source, κ $[m^2/s]$ is the thermal diffusivity of the grasped tissue, and $v \cdot \nabla T$ is the convection term that models the slip of the tissue against the sensor; this term is zero if no motion is present. When the object slips ②, E senses a temperature increase above baseline while W senses a decrease. N and S remain near baseline.

Thus, if tissue moves over a thermistor, there will be a signal in proportion to the change in temperature. As noted in Section 3.1, local tissue movement can arise from any combination of *motion* (translation and rotation) and *deformation* (dilation, extension, and shear) [35]. For slip sensing, we are interested in translation. With a single sensor we cannot entirely separate the effects of motion and deformation because distinguishing them requires multiple points of measurement and a sense of scale: a microscale slip may be part of a macroscale slip *or* stretch, and motion may have both rigid and deformation components. However, we can construct signals that respond primarily to translation in the $\hat{x}$ and $\hat{y}$ directions, respectively.

For a translation, assuming an approximately symmetric heating zone, the thermistor in the leading direction should experience an increase in temperature while the thermistor in the trailing direction should experience a temperature decrease. Therefore, we define slip signals as:

$$\dot{S}_x = \frac{\partial}{\partial t}(T_E - T_W), \quad \dot{S}_y = \frac{\partial}{\partial t}(T_N - T_S) \tag{3.5}$$

in the $\hat{x}$ and in the $\hat{y}$ directions, respectively. Time derivatives are used to avoid reliance

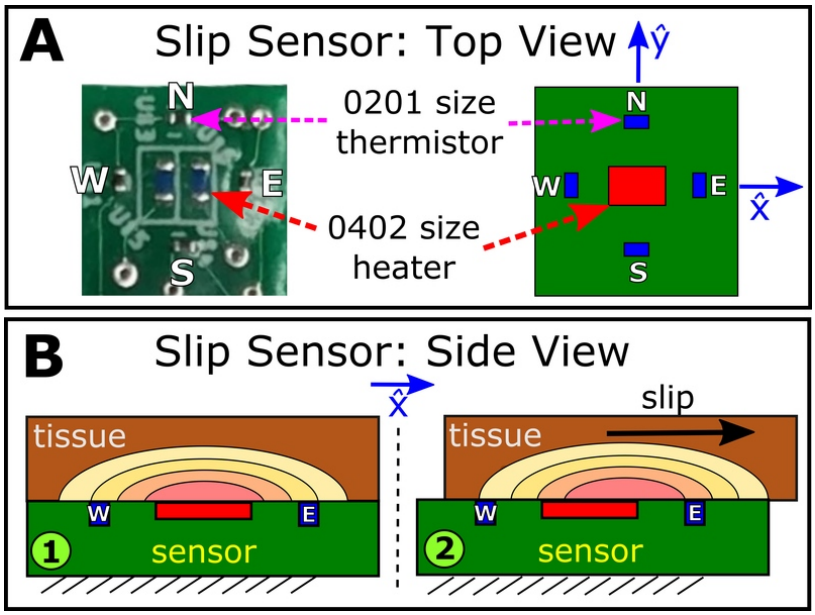

Figure 3.7 – **A**: Slip sensor top view with labeled N, S, E, and W thermistors. Component sizes are 0201 and 0402[1], as labeled. **B**: Cross-sectional view through E-W plane. Heater emits thermal energy conductively transferred to the thermistors (mainly through the grasped object) when stationary ①. When the object slips ②, E senses a temperature increase above baseline while W senses a decrease. N and S remain near baseline. Figure adapted from [11].

on magnitude. These signals ($\dot{S}_x$, $\dot{S}_y$) may also be combined as

$$\dot{S}_{mag^2} = |\dot{S}_x|^2 + |\dot{S}_y|^2 \tag{3.6}$$

to produce an onset-specific signal that indicates slip magnitude only for a higher signal-to-noise ratio than the direction-specific signals. Note that dilation (as may occur when increasing the grasp force on a piece of tissue so that it expands radially) will produce no signal because the thermistors' temperatures will decrease together. A pure rotation will also produce no signal, due to symmetry.

The signals $\dot{S}_x$ and $\dot{S}_y$ (and $\dot{S}_{mag^2}$) are imperfectly correlated with slip and should not be interpreted as exact measures of the amount of slip that has occurred. The temperatures measured at each thermistor also depend on the history of heating and tissue movement and on the overall conduction and convection at the boundaries. These issues are examined in detail in Chapter 4. This sensing strategy is also not robust to uneven contact or release of

[1] 0201 = 0.6 mm×0.3 mm; 0402 = 1.0 mm×0.5 mm

tissue, which causes unpredictable changes in the four sensed temperatures and can mimic slip. Therefore, as discussed in Section 6.2, software and sensor fusion with the *da Vinci Xi* is required to reject these false positives generated during tissue grasp and release during tests with human subjects. Despite these limitations, for realistic grasping scenarios, $\dot{S}_x$ and $\dot{S}_y$ provide a useful single-point indicator of slip occurrence and direction.

Using an array of such sensors, a topic for future work, would enable estimation of the tissue's planar motion and deformation over the grasper jaw (see Fig. 3.8). Note that each heater has its own cluster of thermistors around it rather than allowing a thermistor to sense two neighboring thermal gradients. This is so thermistors do not experience crosstalk. As will be discussed in Section 4.3.3, this is because for the given sensor components and desired slip sensitivity of 2-3 mm, the thermistors must lie within 1.5-2.5 mm of the heater to achieve high sensitivity to tissue motion, given a heating power of 45 mW. In addition, heaters must reside further than 6 mm away from one another to avoid crosstalk. Therefore, given the currently used components, each thermistor should only respond to one heater's local thermal gradient. If a more sophisticated thermistor differencing method were employed, perhaps this would not be an issue.

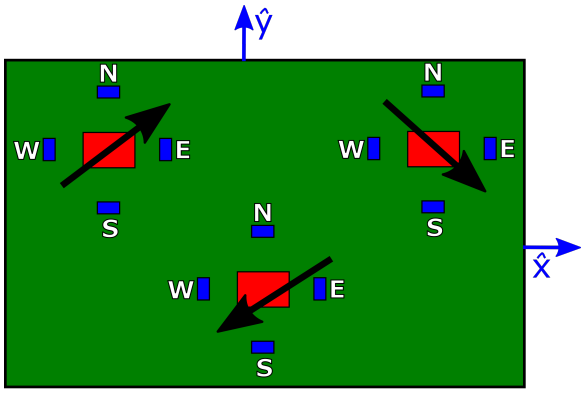

Figure 3.8 – Hypothetical sensor array. Each sensor produces at its center a 2D vector that describes slip magnitude and direction. Given three such sensors in a plane, an estimation of how tissue is moving overall may be obtained. Here, the tissue is undergoing a pure rotation, which would not have been evident given a single sensor or even two, given that tissue can deform.

The design shown in Fig. 3.7 is well-suited to sensing biological tissue slip: by collecting redundant measures of temperature, we can monitor a critical parameter tied to tissue damage. The sensor design is inherently robust; varying moisture content and tissue thickness

are rejected common mode events. Furthermore, neither tissue stiffness nor viscosity substantially affects slip measurements. As long as the tissue contacts the entire sensor, even grasp force does not affect the measurement. Although this thought experiment provides hope that this slip sensing method may have applicability in MIS, it is important to understand the working principles of the sensor with respect to its intended environment and let these principles inform prototype design decisions. Therefore, the next section delves into a thermal model and simulation of this anemometric slip sensing approach.

Chapter 4

Thermal Modeling and Simulation

4.1 Purpose

The information that follows was largely published in [10]. The thermal sensor was developed through a series of prototypes, as described in Sections 5.2 and 5.3. In this chapter we present the thermal model and analysis that guided the design evolution. Among the questions that we sought to answer through modeling were the following:
Dimensions and Guidelines

- What trends and design guidelines characterize the slip sensing approach?
- How do thermal properties of the tissue affect results?
  - Initial temperature
  - Thermal mass
  - Thermal conductivity
  - Tissue moisture content
- What dimensions (e.g. distance between heater and sensors) will provide sufficient sensitivity to slip?
- How would use of 3 (rather than 4) thermistors affect slip sensing?
- What is the minimum spacing required to avoid crosstalk and performance degradation if multiple heaters are used?
- To what depth does the heating penetrate in the tissue?

Practical Use

- What is the minimum time a stable grasp must be maintained to avoid false positives?

- What is the minimum heat required?
- Does pulsing the heater help avoid saturation?
- How quickly do thermal changes occur in our system, and what are the ramifications regarding sample rate, resolution, and performance?
- Given realistic time constants and components, how fast a slip can we detect?

4.2 Thermal model

A simple thermal model provides an idealized representation of the slip sensor interacting with tissue and is useful for understanding some of the main effects. We assume the tissue is a uniform, homogeneous half-space in contact with the flat sensor. The sensor has a central heating element that provides direct Joule heating and one or more temperature sensing elements some distance away along the boundary of the half-space. It is possible for heat to be conducted through the sensor structure as well as through tissue.

When tissue contacts the sensor, heat is conducted into it, forming a thermal gradient $T(x, y, t)$ local to the heater. As in [53], this heat transfer problem is approximated as:

$$\frac{\partial T}{\partial t} = \alpha \nabla^2 T + \dot{q}(x, y) - v \cdot \nabla T \tag{4.1}$$

where $\alpha = k/(c_p \rho)$ is the thermal diffusivity [m^2/s] of the grasped tissue, and k, c_p, and ρ are respectively the thermal conductivity [W/(m·K)], specific heat [J/(kg·K)], and density [kg/m^3]. The term $\dot{q}(x, y)$ is the electrically controlled heat source, and $v \cdot \nabla T$ is a convection term that represents tissue slip against the sensor and is zero if no motion occurs. This partial differential equation results in radially symmetric solutions about the heater, assuming uniform tissue and infinite boundaries. The heater is approximated as a point boundary condition because it maintains a constant temperature. One could also imagine using a cooling element rather than a heater; we elected to use the latter because cooling elements (thermoelectric coolers, for example) require a heat sink for dissipation and typically are larger than heaters.

Before drawing further conclusions from this thermal model, Pennes' Bioheat Transfer Equation [54] should also be considered, as it is a useful and standard model for predicting temperature distributions in living tissues:

$$\nabla \cdot k \nabla T + q_p + q_m - W c_b (T - T_a) = \rho c_p \frac{\partial T}{\partial t} \tag{4.2}$$

As Huang et al. describes in [54], T [°C] is the local tissue temperature, T_a [°C] is the arterial temperature, c_b [J/(kg ·°C)] is the blood specific heat, c_p [J/(kg ·°C)] is the tissue specific heat, W [kg/(m^3· s)] is the local tissue-blood perfusion rate, k [W/(m ·°C)] is the tissue thermal conductivity, ρ [kg/m^3] is the tissue density, q_p [W/m^3] is the energy deposition rate, and q_m [W/m^3] is the metabolism, which is typically far smaller than q_p and is assumed to be homogeneously distributed through the tissue of interest. This equation describes how blood at temperature T_a entering tissue through capillaries exchanges heat with the surrounding tissue at temperature T. This thermal energy exchange between the blood and tissue is proportional to the density, specific heat, and perfusion rate of blood through the tissue. At the scale of the slip sensor and the small heated volume it generates in the tissue (see Section 4.3.3), the effects of these terms are far smaller than the effects of tissue slip ($v \cdot \nabla T$) and are not highly variable in time or space during the time period associated with detecting slip. The results presented in Section 5.4.2 support these conclusions.

A few design insights arise immediately from this simple thermal model. First, the slip signals measured at each temperature sensor are represented by the time derivative of temperature, $\frac{\partial T}{\partial t}$. To obtain directional slip information we will compute $\frac{\partial}{\partial t}(T_i - T_j)$ using two sites on either side of the heater. To obtain a strong signal, we want the term $v \cdot \nabla T$ to dominate over heat diffusion and conduction $[\alpha \nabla^2 T + \dot{q}(x, y)]$. This could represent a limiting factor in highly perfused tissue. In addition, the slip signal will be larger when the slip velocity, v, is comparatively large and when the thermal gradient ∇T is comparatively large (i.e., when the temperature profile varies sharply in the vicinity of the sensor). Thus the sensor is more sensitive to faster slips. The sensor's noise floor may also be considered a rough estimate of the (idealized) minimum slip velocity that this sensor could be expected to sense, assuming no other issues.

Sensor performance is also affected by the amount of heat conducted to the sensing elements (thermistors) through the sensor substrate as compared to through the tissue; the latter aids performance while the former limits it. It is therefore advantageous for the encasing material between the heater and thermistors to have low thermal conductivity and for the components to be as exposed as possible to the tissue (while eliminating electrical conduction).

After building a slip sensor PCB prototype, it became apparent that the amount of copper residing in the layers underneath the sensing portion of the board substantially affected performance: too much copper resulted in parasitic heat conduction, reducing the

sensitivity to convective effects (tissue slip). Thus, limiting trace widths and vias in the sensing region was important for PCB design, as discussed in Section 5.3.2.

There is also a design tradeoff associated with the spacing of the thermistors with respect to the heater. Sensitivity to tissue motion relies on the thermistors residing within the steepest part of the thermal gradient, but not so near that internal substrate isolation is poor. The thermal properties of the materials used for the sensor substrate and the grasped material dictate this balance. As an aside, one must also consider in practical terms what slip distance it is useful to detect: it is worth sacrificing sensitivity to slips $< 0.5\,\mathrm{mm}$ if one prioritizes detection of 1-2 mm slips.

These initial findings dictated many of the design choices for the prototypes. However, a numerical thermal analysis was deemed necessary to examine these issues more carefully.

4.2.1 Conduction

This section considers the system to consist of the slip sensor, embedded in an instrument jaw, grasping biological tissue. The main source of heat transfer in our system is conduction; convection and radiation are both relatively insignificant [54] unless slip occurs, which is represented here as a convection term. Conduction transfers heat through direct molecular collisions (e.g. physical contact) across a stationary solid or fluid medium. The governing equation is Fourier's Law of conduction:

$$Q = -kA\frac{dU}{dx} \tag{4.3}$$

where Q is the heat flow rate [W], k is the thermal conductivity of the body material [W/(m K)], A is the cross-sectional area normal to the direction of heat flow [m^2], and dU/dx is the temperature gradient in the direction of heat flow [K/m].

The constant k is a transport property and indicates the rate at which heat energy is transferred through the medium via conduction. The thermal conductivity of various biological tissues have been measured; bone, fat, and skin have lower thermal conductivities compared with most other organs and tissues ($< 0.3\,\mathrm{W/(m\,K)}$ vs. $0.5\,\mathrm{W/(m\,K)}$, respectively) [55].

In the sensor prototypes presented in Chapter 5, conduction paths exist within the sensing PCB, between the PCB and its substrate (the instrument jaw), and between the sensing PCB and the grasped tissue. Limiting heat transfer in the first path and facilitating

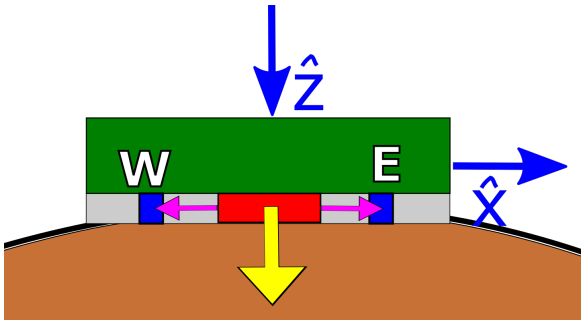

Figure 4.1 – Main conduction paths in the anemometric slip sensor. It is desirable to limit the internal conduction paths (pink arrows) by sealing the electrical components with a thermal insulator (grey region). It is also desirable to maximize the conduction path from the heater to the tissue (yellow arrow), so the thermistors and heater are placed as superficially as possible (as opposed to embedded).

it in the last two is desirable for sensor performance (see Fig. 4.1). If the first path is highly conductive, then the signal-to-noise ratio (SNR) will decrease because the thermistors will saturate, sensing the accumulation of heat in the PCB which will mask the relatively small (tenths of a degree Celsius) temperature changes that occur during slip.

4.2.2 Convection

Convection is the diffusion of energy due to random molecular motion and bulk motion (e.g. advection) between a surface and a moving fluid. The effects are highly dependent on the boundary layer conditions. The governing equation is Newton's Law of cooling:

$$Q = hA(T_a - T_b) \tag{4.4}$$

where Q is the heat transferred [W], h is the heat transfer coefficient [W/(m^{2}K)], A is the heat-transfer area [m^2], T_a is the surface temperature, and T_b is the moving fluid's temperature. Here, convective effects affect the rate of heat transfer from our system of interest into the environment, and thus tissue slip is estimated as a convective term. Although a physically imperfect representation, it provides useful insights as a modeling expression. Faster tissue slips result in larger convective terms and a larger slip signal.

4.3 Thermal Simulation

A numerical simulation was created to understand the general underlying trends behind the slip sensing method proposed and to investigate the effects of changes in geometry and materials. A transient thermal simulation was thus developed in ANSYS and tuned according to matching benchtop experiments until results over 5 min matched and were robust to finer meshing and time steps.

4.3.1 Simulation setup

Transient thermal simulations were developed using ANSYS 19.0 to explore the effects of tissue thickness and water content on the thermal gradient and its development. The slip sensing PCB was modeled in SolidWorks by exporting each PCB layer from Eagle (AutoDesk). In Eagle, the desired layers were displayed and exported as a DXF file. This provided precise trace, via, and component locations as an importable sketch. Each trace width was then manually added in each layer's sketch and extruded. The components were manually added and positioned according to the traces and pads in the PCB assembly. Materials were added based on the components' datasheets; the thermistors were approximated as nickel and the heating resistors as aluminum. This model was then imported into ANSYS via SpaceClaim.

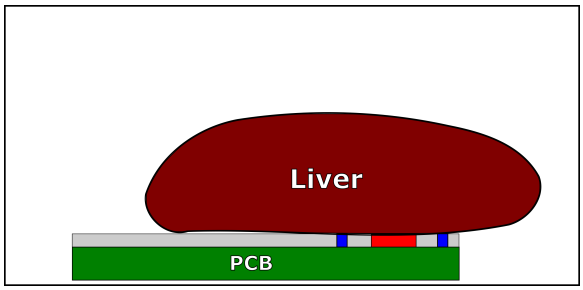

Figure 4.2 – Benchtop test setup for ANSYS simulation validation. Liver rests atop slip sensing PCB under a plastic box to limit convective effects.

The transient simulation was tuned using a benchtop test run at two heating powers (see Fig. 4.2 for setup and Fig. 4.3 for results). The slip sensor was placed in a loosely covered tray to limit convection, and a 5 mm thick piece of liver tissue (at room temperature) covered the sensor. Liver was chosen because it is an organ with a standard thermal conductivity (0.5 W/(m K)) as is the case for most biological tissues) that is easy to obtain, relatively

uniform, and easy to slice into test specimens. The heater was powered at 45 mW or 25 mW and run for 5 minutes. Constant current heating was used here rather than PID control of the heater (as used in Section 5.3 to maintain a constant temperature) because it was simpler to simulate a volume heat source rather than a time-varying temperature. In addition, this model would help inform the worst case effects of the heater. Two thermistor probes were adhered to the board aligned with $\hat{y}$ (out of the page in Fig. 4.1); one over the heater and another 4 mm away. The transient response of these probes and the N and S thermistors were used to tune the simulation's thermal loads (Fig. 4.3 shows results; Fig. 4.9 shows probe locations on a PCB).

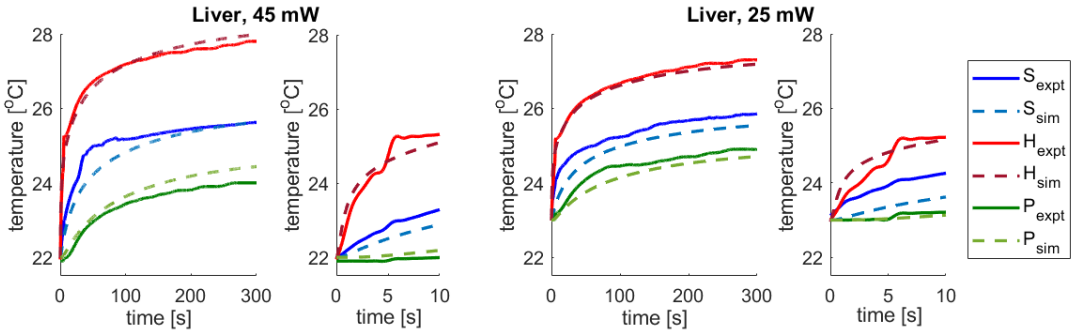

Figure 4.3 – Tuning data from experiment (solid lines) and simulation (dashed lines). Temperatures were collected from probes adhered along the PCB on the heater (H), 4 mm along the $\hat{y}$, and over the S thermistor. Close-ups of the overall tuning data at the onset of heat conduction are shown.

Figures 4.8A and B show the components modeled in simulation: the FR4 PCB substrate and its first layer of copper traces (vias extend to the PCB base); the thermistors, resistors, and their epoxy covering; and the tissue (modeled as liver, bone, water, or air with thermal properties from [56]). FR4 is a composite material made of woven fiberglass cloth with a flame resistant epoxy resin binder. This set of modeled parts was determined through trial and error as the minimum amount of detail required to obtain a useful model. Observations of poorer (discarded) board designs helped inform initial decision making on this point as well; original designs had substantial copper in the board layers underneath the slip sensor, which reduced their performance because the traces would accumulate heat. This finding signified that traces and copper would be important to model. The heater power and initial conditions reflected the experimental values and were excluded from tuning.

Table 4.1 – Materials used in ANSYS simulation

Material	**Density** [**kg m^{-3}**]	**Thermal Conductivity** [**W m^{-1} C^{-1}**]	**Specific heat** [**J kg^{-1} C^{-1}**]
Copper [57]	8933	400	385
Epoxy	1290	0.15	1535
FR4	1840	1	1535
Nickel [57]	8900	90	444
Aluminum [57]	3720	26	790
Tissue [56]	1050	0.5	3500

The convective loads and bulk thermal properties of the FR4 PCB substrate (a combination of FR4 and copper) were tuned to match the experimental results while maintaining realistic values. The mesh was then increased and the time step decreased to confirm the insensitivity of the results.

4.3.2 Simulation conditions

The details of the transient thermal simulation run in ANSYS 19.0 are described here for replication by the interested reader. If a section in ANSYS is not mentioned (e.g., 'Named Selections,' it means that no modifications were made to that section from the ANSYS-defined defaults.

Geometry

The components in the model are copper, the PCB, two heating resistors, 4 thermistors, the epoxy layer, and the tissue. See Figure 4.4 for all parts that are not simple rectangular boxes. All are boss extrudes except the epoxy and PCB, which are both cavities. The PCB's cavity is made by subtracting the copper from a boss extrude, and the epoxy's cavity is formed by subtracting the heating resistors and thermistors from a boss extrude.

Table 4.1 contains the Engineering Data used to supply the material properties. The PCB was assigned the material called FR-4 below which has material properties chosen to reflect a combination of glass-reinforced epoxy laminate and copper. The thermal conductivity of Loctite 435 is not released in the public domain by Henkel Corporation, so a typical value for epoxy was used. Based on information from the components' datasheets, the thermistors were assigned Nickel and the heating resistors Aluminum.

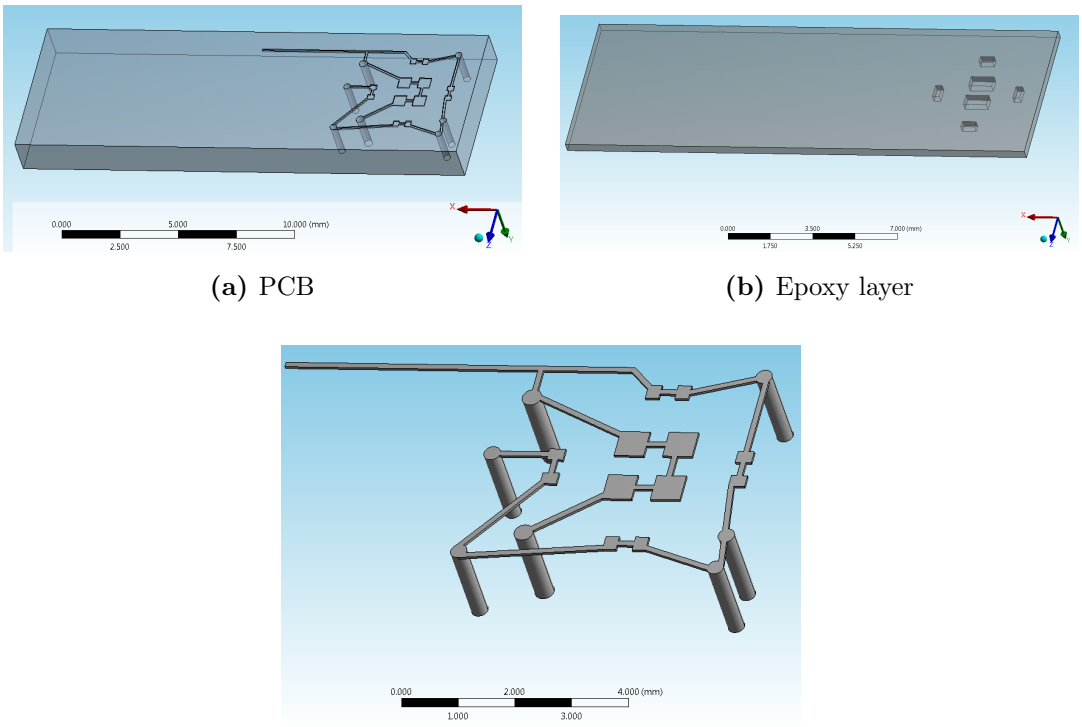

(a) PCB

(b) Epoxy layer

(c) Copper traces

Figure 4.4 – Part geometries in ANSYS simulation.

Coordinate Systems

ANSYS requires coordinate systems to lie anywhere that setting a probe to track solution quantities, e.g. temperature, is desired. The coordinate systems were thus set between the heating resistors, one at the center of each thermistor, and 7 additional ones along the N-S axis at 0.8, 1.0, 1.2, 1.4, 1.6, 2.1, and 3.6 mm from the center of the heating resistors. Figure 4.5 shows the PCB, the copper traces, and electrical components within their epoxy layer and where the coordinate systems are located with respect to them.

Connections

All of the connections between parts were 'Bonded' type. Bonded-type contact between two faces uses a multi-point constraint formulation that internally adds constraint equations to artificially tie the displacements between the contacting surfaces and results in an efficient solution. In the present case, nothing should move but rather expand or contract due to

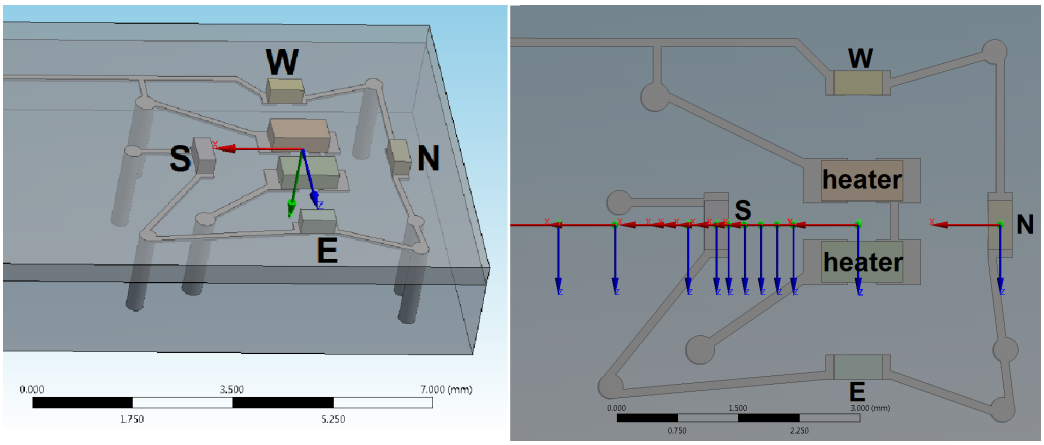

Figure 4.5 – Simulation coordinate systems along the N-S axis at 0.8, 1.0, 1.2, 1.4, 1.6, 2.1, and 3.6 mm from the center of the heating resistors. Additional coordinate systems are located at ± 1.75 mm from the heater on the N and S thermistors.

thermal loading.

Mesh

The mesh contained 385,143 nodes and 268,300 elements. Under **Defaults**, the overall mesh Relevance was set to 20. Under **Sizing**, the Adaptive Size Function was used with a Medium Relevance Center, a Slow Transition, and a Coarse Span Angle Center. Under **Quality**, Medium Smoothing was used. These are all rather coarse settings because mesh controls were used to obtain fine meshing in the main area of interest, near the heaters. Instead, the emphasis was on obtaining overall good quality of mesh elements (see Fig. 4.6). Element quality was chosen as the desired metric.

The Element Quality option provides a composite quality metric that ranges between 0 and 1. This metric is based on the ratio of the volume to the sum of the square of the edge lengths for 2D quad/tri elements, or the square root of the cube of the sum of the square of the edge lengths for 3D elements. A value of 1 indicates a perfect cube or square while a value of 0 indicates that the element has a zero or negative volume. As seen in Fig. 4.6, the quality of most elements is better than 0.7, which is very good. However, element quality is just one feature of a mesh and is a relative judgment.

Five additional mesh controls were used. First, a Patch Conforming Method was applied to all 10 bodies in the simulation to specify tetrahedrons as the meshing method. Second,

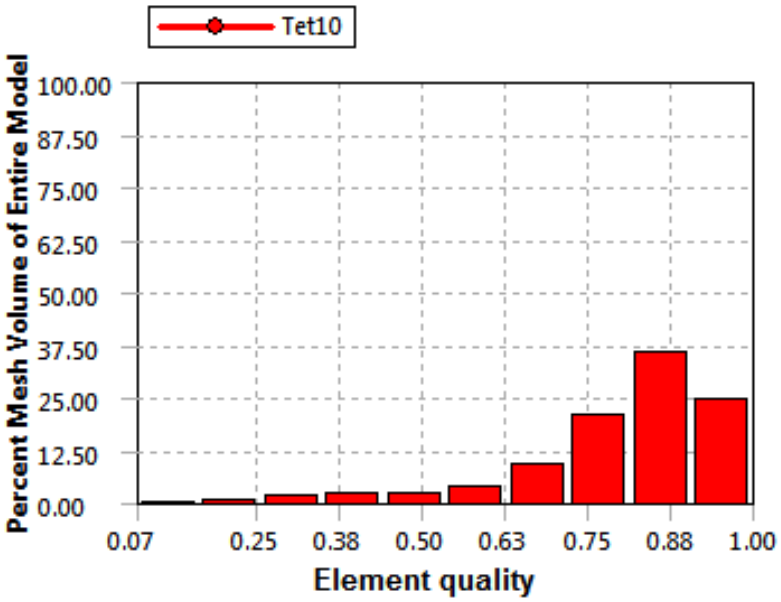

Figure 4.6 – Simulation mesh metrics. It is desirable to have a higher element metric. The metric chosen here is 'Element Quality,' which relates elements' edge lengths to their volume. As a rule of thumb, values above 0.7 are very good or excellent, but quality is a relative metric.

Edge Sizing was applied to the edges of the Copper body that specified the trace thickness. Each edge was required to have at least two divisions for more accurate heat transfer without drastically increasing the number of mesh elements. Third, Face Sizing was applied to the contacting faces of the tissue and epoxy bodies. The elements on these faces were forced to have elements of size 1.25 mm. Fourth, the overlapped contact area between the contacting faces of the tissue and epoxy bodies had a Contact Sizing mesh control where elements were forced to have a 0.25 mm size. Lastly, Body Sizing was applied with the Sphere of Influence type. The sphere was centered between the heating resistors, had a radius of 2.5 mm, and enforced an element size of 0.2 mm. This mesh control was the most stringent because it was where the most important thermal effects occurred. See Fig. 4.7 for section view of the overall mesh. The number of mesh elements was increased by 20% and results over a 10 s simulation compared to ensure independence of results from mesh refinement.

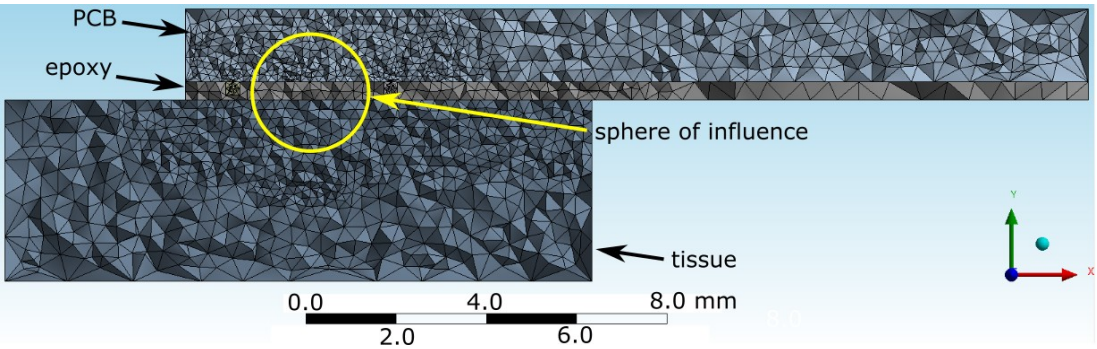

Figure 4.7 – Simulation mesh, section view. Finer mesh elements are used near the region of interest – at the heater and thermistors' contact interface with the epoxy and tissue.

Initial Temperature

The default initial temperature of all bodies unless specified or overridden in subsequent settings was set at 22°C to match the settings of the benchtop experiment. A simulation was run with *in vivo* conditions to confirm that the results had the same trends at different temperature magnitudes (e.g., everything experienced the same temperature difference).

Analysis Settings

The analysis was divided into three analysis steps to allow for fine time steps early in the simulation and coarser ones later because the most important thermal effects that affect stability occur early on. The details are tabulated in Table 4.2. All used Auto Time Stepping, where the time step size is automatically determined in response to the analysis's current state. Concurrently, loads are adapted as well. Given the current and past analysis conditions, the algorithm determines the next time increment, which is largely predictive. The second feature of the algorithm determines whether or not to reduce the present time step size and redo it with a smaller one based on whether proper convergence is achieved or not anticipated. Time steps were decreased by a factor of 10 to check robustness of the simulation results to the time step size over 40 s of the transient simulation. 40 s was chosen because the simulation results had reached steady-state in that amount of time.

Thermal Loads

Four thermal loads were applied in this simulation. Convection was tuned until the simulation matched the benchtop experiments and checked to ensure it did not exceed 75 $\mathrm{W/(m^2K)}$

Table 4.2 – Time step (TS) settings for thermal simulation

Step	End time [s]	Initial TS [s]	Min TS [s]	Max TS [s]
1	5	1E-5	1E-7	0.01
2	10	Carry Over	1E-5	469746650.1
3	300	Carry Over	1E-3	0.2

because typical values for convection in a laboratory environment should be between 2-50 $\mathrm{W/(m^2K)}$. However, higher values up to 75 $\mathrm{W/(m^2K)}$ were deemed permissible because convection was also being used to model heat transfer to the unmodeled parts of the benchtop experiment. Convection at a constant 50 $\mathrm{W/(m^2K)}$ was applied to the 5 faces of the tissue body that were not contacting the epoxy body; this represented the airflow on the surface of the tissue as well as the effects of conduction within the unmodeled portion of the tissue (the entire slab of liver tissue was not modeled to facilitate faster solve times). Convection at a constant 40 $\mathrm{W/(m^2K)}$ was also applied to the sides of the PCB and epoxy layers not in contact with the tissue. This modeled the heat transfer due to ambient airflow. To model the heat transfer that flowed between the PCB and the table it was resting on, convection at a constant 10 $\mathrm{W/(m^2K)}$ was applied to the bottom of the PCB. Ambient temperature for all convective thermal loads was set at 22°C.

Internal heat generation was applied to the two heating resistor volumes with a magnitude of 0.1 $\mathrm{W/mm^3}$ which equated to 45 mW. This was changed as described in the following sections to explore the effects of lower heating powers.

4.3.3 Simulation results

Results from the simulation are shown in Figures 4.8 and 4.9 and Table 4.3. The heat-affected zone, defined here as the volume that experiences a temperature increase of ≥ 3°C within 5 minutes of constant contact, is 10.4 $\mathrm{mm^3}$ (smaller than a mini M&M). Outside this volume, which extends just over 1 mm into the tissue, the sensor's heater has little effect. Fundamentally, the sensitivity of the slip sensor depends on detecting this superficial thermal gradient that it generates.

One purpose of the simulation was to model how the steepness of the local thermal gradient changes over time (Fig. 4.9). Of course, the thermal time constant associated with achieving the steepest thermal gradient from the heater to each thermistor will differ based on thermal contact conditions. However, from these benchtop tests and simulations

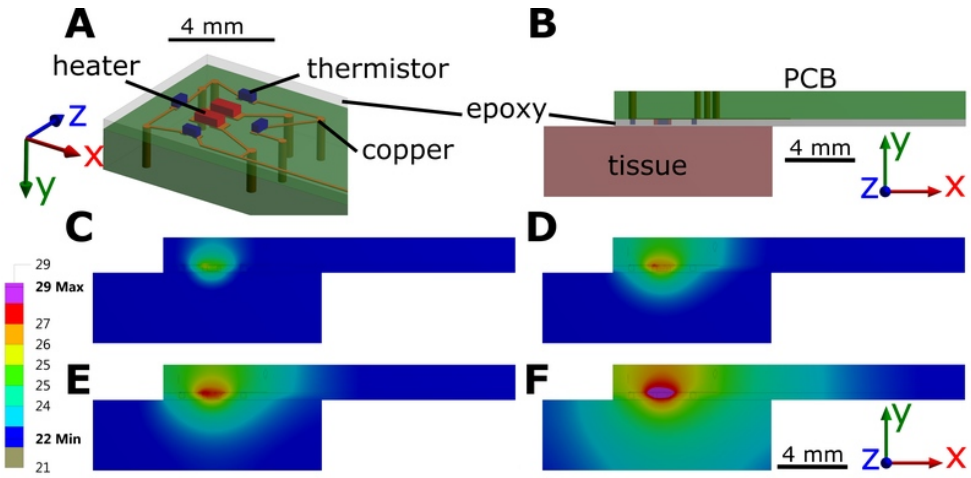

Figure 4.8 – Transient thermal simulation of room temperature tissue resting on the slip sensor. **A** shows the PCB with the tissue hidden to expose copper traces, heaters, thermistors, and epoxy. **B** is a semi-transparent side view of the tested model. **C**-**F** show the temperature profile on a bisecting section view at 5 s, 30 s, 1 min, and 5 min, respectively.

(see Section 4.3.1), one may conclude that higher heating power ultimately results in a steeper thermal gradient (for better slip sensitivity), but lower heating power reaches a (lower) steady-state gradient more quickly (Table 4.3). The experiments were conducted with room temperature tissue rather than at *in vivo* body temperature, but the general trends are still characteristic of the sensor's interaction with tissue. Experimentally, the thermistors have $\pm 0.05°\text{C}$ of noise, so these thermal gradients have a signal-to-noise ratio of $\geq 15:1$ if tissue slips by ≥ 1 mm or more, which is more than sufficient for our purposes.

This simulation also describes qualitatively how changes in the sensor's environment would affect performance. The geometry and thermal parameters of the tissue were altered to reflect thick (10 mm), thin (2 mm), very moist (water), and very dry (bone or fat) tissue. Changing the grasped object's moisture content was represented as a change in thermal conductivity. As in Table 4.3 and Fig. 4.9, the heating power is the single most important determining factor of the resultant steady-state local thermal gradient, regardless of tissue moisture content or thickness. When the PCB is in contact with objects of low thermal conductivity (e.g., air, or to a lesser degree, bone or fat), it maintains a steeper maximum thermal gradient.

Figure 4.10 shows the difference in local thermal gradients that develop after 20 s of contact on tissues of widely differing thermal conductivities. Biological tissue that is commonly

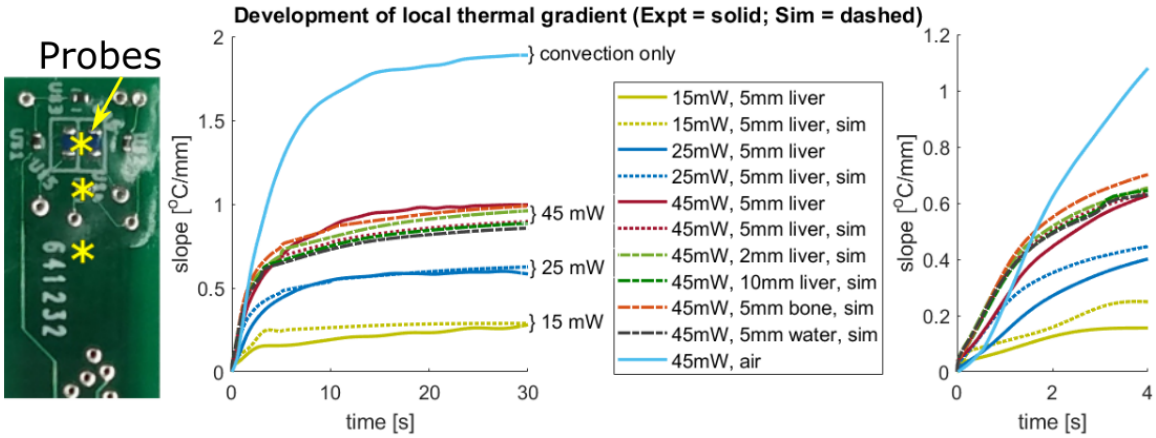

Figure 4.9 – Local thermal gradient vs. time. Linear estimate of the thermal gradient slope from experiment and simulation through the heater, S, and the probe. See yellow asterisks on PCB for probe locations used to estimate linear slope local to the heater. The plot shows the how the slope changes over time for each condition. Higher heating power results in steeper thermal gradients that take more time to develop. Heating power mainly dictates the local slope, regardless of tissue thickness, thermal conductivity $[0.2 - 0.5\,\mathrm{W/(m\,K)}]$, or moisture content. Steepest gradient occurs when only in contact with air because convective losses are far less than conductive ones. The inset at right shows a zoomed-in portion of the plot at the beginning of heat conduction.

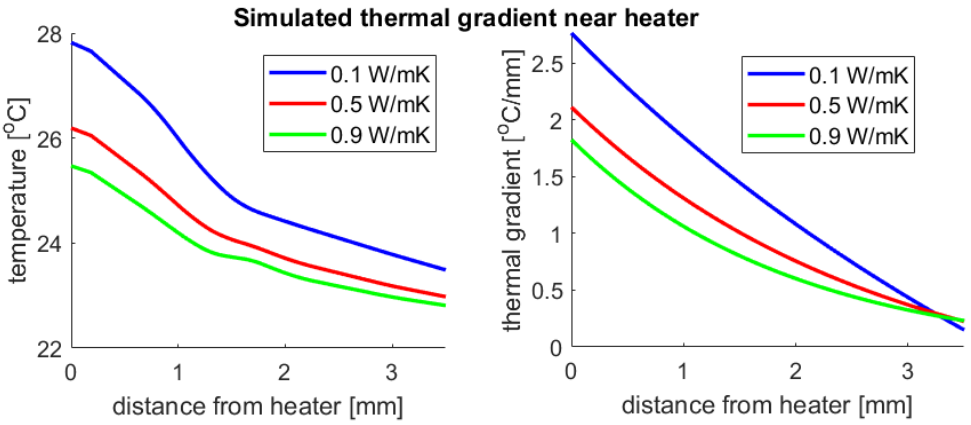

Figure 4.10 – The plots show local temperatures and thermal gradients that form within 30 s of contact for a variety of tissue thermal conductivities at 45 mW heating power. The simulations used very extreme thermal conductivities (bone and fat are at least 0.19 W/(m K), and water is at most 0.6 W/(m K)) to better express the trend: a steeper local thermal gradient is achieved for tissues with lower thermal conductivities, so the sensor is more sensitive on tissue that is less thermally conductive.

grasped and retracted in MIS and/or RAS does not have thermal conductivities that range outside [0.19-0.6], but displaying the results for the [0.1-0.9] range illustrates the main point nicely. Tissues with lower thermal conductivities have steeper local thermal gradients, and thus the presented slip sensor is more sensitive to their motion. Tissue commonly grasped in the body is typically in the 0.2-0.5 W/(m K) range.

Table 4.3 – Steady-state (S.S.) thermal gradient development for various simulated contact conditions

	Tissue			***Time to reach...***	
Power	**Thickness**	**Model**	**Max slope**	**S.S.**	**50% S.S.**
15 mW	5 mm	Liver	-0.3 °C/mm	31.7 s	1.8 s
25 mW	5 mm	Liver	-0.5 °C/mm	32.3 s	1.8 s
45 mW	5 mm	Water	-0.8 °C/mm	31.1 s	1.7 s
45 mW	2 mm	Liver	-0.9 °C/mm	36.9 s	1.9 s
45 mW	5 mm	Liver	-0.9 °C/mm	29.6 s	1.7 s
45 mW	10 mm	Liver	-0.9 °C/mm	35.8 s	1.9 s
45 mW	5 mm	Fat	-1.0 °C/mm	36.0 s	1.8 s
45 mW	0 mm	Air	-1.9 °C/mm	20.3 s	3.5 s

The plot in Fig. 4.10 also lets us comment on the minimum distance needed between

two heaters at 45 mW: at 3 mm away, the local thermal gradient is approximately zero. Users report wanting to know about slips in the 2-3 mm range. Therefore, as long as the second heater is at least 3 mm away (for a zero thermal gradient) plus another 3 mm away (for when tissue slips) from all of the first heater's thermistors, there will be no crosstalk or performance degradation.

A final takeaway from Table 4.3 is that the sensor requires very little time to achieve an acceptable thermal gradient; 2 s will suffice to achieve useful slip sensitivity to 1 mm slips, and 1 s will suffice if sensitivity to larger (say, $\geq$ 2 mm slips) slips is tolerable. This information was used to help determine the "reliable grasp" wait time for use in the slip detection algorithm used in Sections 5.3.6 and 6.2.

4.4 Overview of sensor principles

4.4.1 Component spacing

In general, the slip sensor relies on sensing changes in temperature related to changes in the tissue's planar displacement. Thus, better performance is achieved when the sensor can establish a steeper thermal gradient about its central heating element. This occurs when the sensor is in contact with an object with lower thermal conductivity or its heating power is higher.

To sense slip, the sensor must be in contact with a solid object that retains heat enough to establish a temperature gradient. It cannot sense on a gas or pure fluid but can sense slip of a solid object that retains fluid (as long as the barrier thickness is $>$ 1 mm, because that is the depth to which our sensor generates its thermal gradient). In other words, the sensor needs consistent contact with an object; grasping a soaked sponge will incur many false positives because the fluid is not retained in the sponge very well. However, it can sense slip of biological tissue because typical RAS grasping results in expulsion of the fluid boundary layer, resulting in a wet and compliant object that allows for consistent contact across the sensing region. The thermistors ought to reside quite near the sensor's surface to limit the effects of internal substrate conduction and sense instead the superficial temperature changes at the grasping surface.

The optimal spacing between the heater and thermistors relies on both physically determined phenomena and on the user's desired optimal sensing range. There is a distance away from the heater that the thermistors must reside to avoid thermal saturation from within

the substrate. In the limit, with the thermistors located infinitely far from the heater, the thermal gradient that the heater generates will not affect the thermistors (unless its heating power is also quite high, which would be unsafe), and the tissue would have to slip infinitely far and fast for the thermistors to recognize that any movement occurred. At the other extreme, the heater and thermistors would be overlaid, and the thermistors would always sense the temperature of the heater. This layout would result in very poor sensitivity to slip: a moving object in contact with the sensor would have almost no effect on the sensed temperatures, which would be dominated by internal conduction. Thus, physically, a balance exists between the conduction possible through the grasped object and through the sensor. A good slip sensor design would require low thermal conductivity through the sensor substrate, lower than that through the grasped object.

As mentioned above, the user's desired slip sensitivity matters as well when determining optimal thermistor-to-heater layout distance. As found experimentally in Chapter 6, it is often desirable to have high sensitivity to slow slips of 2 mm displacement. High sensitivity means, from the sensor's perspective, that the difference of the opposed thermistor pair (in the direction of slip) is maximized when the desired amount of slip occurs. Unfortunately, knowing the difference exactly is only possible if one intends to grasp only objects of specific, known, unchanging thermal properties, because those thermal properties determine the precise shape of the local thermal gradient that forms. However, for the range of thermal properties one experiences *in vivo*, the simulation can provide guidelines that cover normal operating conditions in RAS. Assuming 45 mW heating power and typical tissue (0.5 W/(m K)), the steepest thermal gradient lies within 2 mm of the heater. If a 2 mm slip happened instantaneously, then the thermistor should be located 2 mm for maximum signal. However, most slips in RAS tend to happen rather slowly: tissue stretches and creeps first, then catastrophically slips later. This means that the thermal gradient will be less steep in practice as the slip progresses because heat in the tissue will dissipate. Therefore, to catch slow 2 mm slips, locating thermistors at around 1-1.5 mm away from the heater is better. If the user wanted to know about very small slips, say 0.5 mm, the same ideas apply. The sensor would need to be located within 2 mm of the heater, but within 0.5-1 mm of the heater would be optimal.

The ideas expressed above apply to the components modeled in the above simulation and used in the prototypes discussed in Section 5. From the manufacturer's datasheet, the thermistors have ± 0.05°C noise. The DAQ used in this work, the Arduino Due, has an

analog to digital converter with 12 bits of resolution over 0-3.3 V, so it is accurate to 0.8 mV. Based on the thermistor conversion used (see Section 5.3.3), 0.05°C equates to 6Ω or 3 mV, for which the DAQ has sufficient resolution to express (4 counts). Thus, improving the thermistor to have lower noise would enable use of lower heating, more relaxed spacing of components, etc. because it would be capable of sensing shifts in a lower thermal gradient.

Use of three thermistors at 120° spacing rather than four at 90° spacing would also work, although the computation of the directional slip signals and the overall slip indication variable would change. The temperature signals would have vector components, and the $\hat{x}$ and $\hat{y}$ components would be extracted for use (e.g., in Equations 3.5 and 3.6). The signal to noise ratio would not be worsened in this case because it is still possible to construct two unit vectors in the plane to describe the slip, given 3 points. The use of four thermistors simplifies the interpretation of their signals in terms of slip along and transverse to the grasper jaw. Additional thermistors would provide some redundancy and could be averaged to reduce noise, but unless an additional heater (located far enough away to avoid crosstalk, at least 6 mm for the given components) was employed, there would be no additional directional information.

4.4.2 Thermal time constants and heating considerations

Another implication of the desire for a steep thermal gradient is that more heating power is better, particularly when the grasped object has a comparatively high thermal conductivity. Higher heating power results in a steeper steady-state thermal gradient and a higher temperature directly over the heater. In RAS, the heating power is limited by the competing requirement for a safe thermal interaction with living biological tissue. For these reasons, the amount of current permitted to pass through the heating resistors is controlled to not exceed the safe temperature threshold as stated by [58]. Section 5.3.4 discusses this constraint further.

As discussed in Section 4.3.3, the heating power applied is the main factor determining how quickly the local thermal gradient is established and how steep a gradient one can achieve. Although for heating powers in the range of 15-45 mW it requires approximately 30 s to achieve the maximum thermal gradient, it only takes a 2-3 s to reach a gradient half as steep. Our sensor has ±0.05°C of noise, and a reasonable desired detectable slip amount is 2 mm. Thus, if we wish to operate at, say, 10 times our noise floor, then we need a gradient of $\geq$ 0.25°C/mm to be sure we could detect it – easily achievable within

1 s of grasping if using a heating power of 45 mW. With the implementation presented in Section 6.2 where slip detection is not permitted while the tool is actively used, this 1 s interval occurs naturally; else, a 1 s delay (as implemented in Section 5.3) is useful. In any case, because the act of grasping typically results in a signal that mimics slip (if contact with the sensor is made unevenly), it is wise to wait 1 s after grasping before starting slip detection to reject the resultant false positive. This strategy is employed in both the freeform grasping tests in Section 5.3.6 and during the user study in Section 6.2.

In simulation, there was no downside to applying maximum heating power over long periods of time (5 minutes) – the maximum local thermal gradient was also the steady-state value. In other words, saturation did not appear to be an issue, so pulsing the heater was not deemed necessary. However, in practice, tissue and other water-saturated materials may experience desiccation if heated for extended periods, and these are not results the simulation was built to predict or describe. On a separate note, because the tissue thermal properties are not estimated or measured in real time, it is difficult to tune the PID controller to maintain the heater safely below the 43°C limit with zero overshoot. Thus, pulsing the heater (75% duty cycle at 0.25 Hz) was implemented once the temperature control signal is within 3°C of the target temperature to ensure overshoot never occurs, and control reverts back to PID control otherwise (see Fig. 4.11).

For a typical 2 mm slip at 45 mW heating power on tissue with thermal conductivity of 0.5 W/(m K), the expected temperature change is approximately 1.6°C if it happens instantaneously. The difficulties in slip sensing occur at both ends of the slip speed spectrum. If the slip is extremely fast, faster than the thermistors can register the movement of the heated patch moving past one or two thermistors, there is a chance that the paired thermistors will never sense different temperatures, and it will appear as if slip never occurred. If tissue could instantaneously slip 8 mm, this would be the case (the thermal gradient is nearly 0 at 4 mm; 8 mm would ensure both thermistors see the cold patch at once). However, surgeons do not tend to manipulate tissue in such aggressive ways that would cause this kind of slip to occur. Of greater practical concern are very slow slips.

If the slip is sufficiently slow, the rate of heating and cooling of the tissue can potentially present no appreciable temperature difference across the heater as the tissue moves. This is most likely to occur if the slip occurs in a slow, stop-start fashion, with slight movements so the temperature change in the direction of slip is very small. After each very small slip the heater has time to reheat a new patch. This effect would be especially problematic if

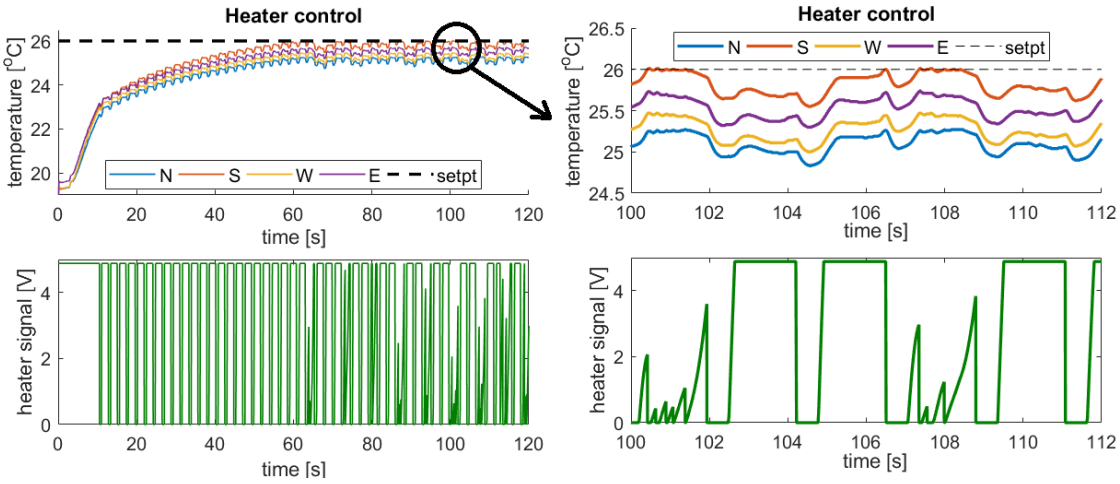

Figure 4.11 – Heater control over time. PID setpoint was 26°C. Gain scheduling is in effect: initially, the maximum heater signal (5 V) is applied to quickly approach the temperature setpoint. Once the hottest thermistor is within 3°C of the setpoint, the controller switches to a combination of PID control and pulse width modulation. Regardless of the heater signal value, it is set and held at zero for 500 ms every 2 s, which prevents overshoot in most situations tested experimentally. This is by no means optimal. For the other 1.5 s, PID control determines the heat control signal.

the thermistors were located beyond 2 mm from the heater where the thermal temperature gradient is small. The most direct fix would be to use higher-performance thermistors.

4.4.3 Concluding remarks

The presented simulation and results support the use of the simulated design in MIS. Based on the model, it appears that sensor's characteristics are sufficient to provide tissue motion information within 1-3 s of consistent contact with biological tissue and that the sensor should perform approximately equally well under all conditions expected *in vivo*. The next chapter, Chapter 5, presents prototypes that benefit from this modeling effort.

Chapter 5

Slip Sensor Prototypes and Validation

5.1 Application-specific requirements

Slip is defined here as the net displacement of tissue because it is important when it results in accidental loss of grasp. The goal is to detect tissue translation in $< 3\,\text{mm}$, which is less than typical standard grasper jaw widths ($4.7 - 5.3\,\text{mm}$ for the *da Vinci* ® Tip Up, Fenestrated Bipolar Forceps, ProGrasp, and Cadiere instruments), on a variety of tissue types, and with a range of slip onset speeds. This requirement motivates Section 5.3.6.

Any proposed solution must be capable of detecting slip of wet, compliant objects (biological tissue). See Section 3.2 for a description of the prior art in the slip sensing space. The majority of prior art is inapplicable to the present application because tissue slip lacks the stick-slip vibrations that tend to signal dry scenario *incipient slip*. Thus, as described in Section 3.2, a thermal-based slip sensing method was chosen. Solutions must have the potential for integration into RAS end effectors, e.g. Intuitive Surgical's resposable (reusable and disposable) da Vinci EndoWrist® instruments. This imposes significant packaging and robustness constraints. Slip is most easily sensed near the event of interest, so the sensor must pass through the bore of a standard laparoscopic trocar. Furthermore, to facilitate surgeon acceptance, it is advisable to minimally change the profile, geometry, and envelope of the grasper jaws.

Finally, slip detection must function during typical RAS grasping processes; e.g., applying traction and counter-traction with 2 tools. To avoid cognitively overloading surgeons,

which can hinder rather than facilitate them [59], slip information should only be provided when relevant. This means that slip detection should not occur during every grasping action but rather only when the intent of the surgeon is to maintain that grasp for a sustained period of time.

A description of the two rounds of prototypes follows. The first round of prototypes sought to prove the concept of the slip sensor by generating foundational data through a highly idealized, constrained experimental setup. The prototypes thus did not adhere strictly to the application requirements although the path toward that goal existed. The second round of prototypes sought to demonstrate that the slip sensor could function under human-controlled grasping, which required much stricter adherence to the application requirements, including integration into a RAS tool. For each round of prototypes, many iterations on the slip sensor PCBs, adapters, and assembly parts were required, resulting in rounds of iterative prototyping.

5.2 Round 1 of Prototypes: Benchtop version

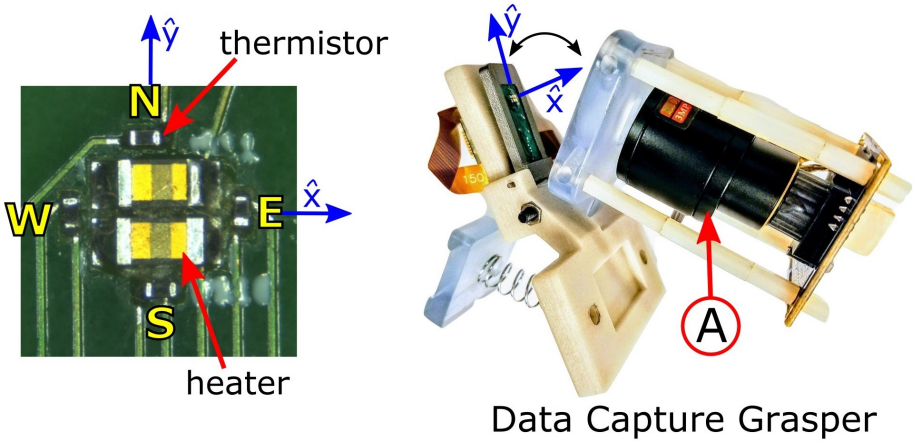

Figure 5.1 – Benchtop version of slip sensor. *Left*: Close-up of slip sensing PCB's sensor area. Two heating resistors are in series with four thermistors arranged around them in a compass layout. *Right*: Data capture grasper used in validation experiments. Grasper is spring-loaded to enable a range of grasping forces. The slip sensor PCB has a load cell underneath it to capture these grasp forces. The other jaw contains an optically clear window to allow a camera Ⓐ to capture tissue motion between the grasper's jaws.

The following section is largely based on [11], which describes the first published prototype and validation experiments, performed on a benchtop setup meant to mimic a (large) grasper that served as a proof-of-concept to gather foundational data and determine whether this sensing scheme was worth pursuing. Figure 5.1 shows the system used to achieve these goals. The left image shows a close-up of the the prototype slip sensor PCB used for data collection. The right image shows the experimental platform, a 3D-printed grasper with a spring-loaded clamp. The grasping region was enlarged to allow for video capture via a camera Ⓐ as a ground truth for motion analysis.

5.2.1 Description

The sensor design is consistent with that described in Section 3.3. Four thermistors surround a heating element, all embedded in a heat-sinking grasper jaw. The slip sensor has a surface area of 3.5x3.5 mm^2; the overall PCB is 7x26 mm^2. The thermistors' resistances are converted to voltages with transimpedance circuits. Temperature is calculated from resistance using the Steinhart-Hart equation as recommended in the thermistors' datasheet:

$$\frac{1}{T} = A + B[ln(R)] + C[ln(R)]^3 \tag{5.1}$$

where $A = -2.2 \times 10^{-3}$, $B = 7.9 \times 10^{-4}$, and $C = -2.2 \times 10^{-6}$ (fit against a thermocouple in a water bath and checked against manufacturer-provided calibration data). Opposing pairs of thermistors (N-S, W-E) are fed into instrumentation amplifiers to amplify their differences; see Section 3.3. The signals used here to detect slip onset were the direction-dependent signals from Equation 3.5 alone, not combined as in Equation 3.6. The sensor's signal is proportional to temperature changes, which occur if tissue moves over a thermistor.

This slip sensor design is better suited to sensing slip of wet, compliant materials than that presented by Accoto et al. [53] for a few reasons. They used the amount of current (e.g., heating current required to maintain a temperature setpoint) supplied to their heater as their slip signal, but this only works if the sensor has time to reach thermal steady state and the object is cooler than the sensor. Because the sensor must work quickly (grasping actions occur much more frequently than the time scale of thermal equilibrium, which can be 15-60 s for the presented sensor depending on the temperature setpoint), this signal is inapplicable to the present application. Second, each of the slip sensors provides a vector of tissue motion and rejects rotation and stretching of tissue. Furthermore, an array of at

least 3 of these sensors (as shown in Fig. 3.8) would allow an estimation of overall tissue motion, which could be used to help guide surgeons to a grasp that better supports tissue if it starts to slip.

The heater (a pair of 49.9Ω Vishay Thin Film resistors in series, PCAN0603E49R9BST5) is resistively heated at a constant 110 mW; heater modulation was not implemented until Section 5.3. This heating power was selected after preliminary tests to determine the maximum heating power that does not exceed the 43°C limit for direct tissue contact safety [58] over 10 minutes of continuous on-time. To create a smooth contact interface, the resistors and thermistors are coated up to the level of the tallest component (0.5 mm) in Loctite 435™(Henkel Corporation), a colorless, toughened, ethyl-based instant adhesive selected for its low thermal conductivity and manufacturability (UV cure).

5.2.2 Validation experiments

Figures 5.2 and 5.4 illustrate the benchtop experimental setup made to imitate a MIS grasper. A DAQ (Sensoray826, Sensoray) reads the analog output from 4 thermistors, the thermistor pair differences, their derivatives ($\dot{S}_y$, $\dot{S}_x$), and a single-axis button-type 15 N load cell (FSS015WNGX, Honeywell; 2.4 mV/(V/N)) into a custom C++ program. The heating circuit maintains constant maximum power (110 mW) to establish the steepest thermal gradient possible for the best chance of demonstrating the proof of concept. Section 5.3 discusses the safe implementation changes made after these experiments. The load cell was centered below the slip sensor to obtain grip force.

Video was recorded at 60 fps with 1280 x 720 pixels resolution using an ELP-USBFHD01M-L21 camera (Ailipu Technology Co., Ltd) calibrated with the MATLAB Camera Calibration toolbox. This camera was cheap, around $50, but was prone to premature death after a week or two of heavy use and is thus not recommended. Videos were used to perform digital image correlation (DIC) to estimate displacements at the contact interface and ensure slip (rather than stretch) occurred during testing (see Fig. 5.3). DIC is a common non-contact technique for measuring material displacement and deformation based on the comparison of two images acquired at different states, before and after motion. Here, DIC was performed in MATLAB using Ncorr, an open source 2D-DIC MATLAB software [60]. To aid DIC analysis, grasped objects were stained with randomly placed dots of black food coloring. The grasped object was displaced using a custom-built system based on a monocarrier (MCM03015P02K, NSK Global), a linear slide (6709K301 and 6709k120, McMaster-Carr),

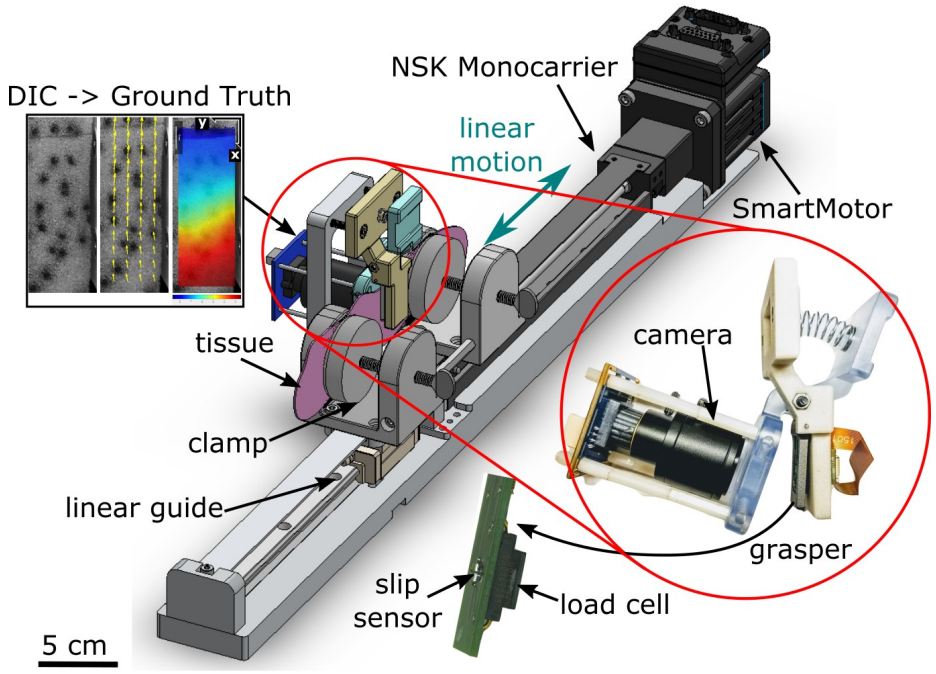

Figure 5.2 – Experiment setup for commanding slip trajectories and measuring slip. **Right inset** shows the grasper; the jaw-mounted camera obtains video of the planar tissue deformation. On the underside of the slip sensor board, a load cell collects grasp force. **Left inset** depicts DIC analysis on speckled foam. Left image is the reference image. Middle image is taken 0.5s later; the vector field of Lagrangian displacements with respect to the reference image is overlaid. Right image shows a Ncorr colormap output of the x displacements; color gradient shows increasing displacement from bottom to top, implying stretch (see Fig. 5.3 for detail).

and a SmartMotor (Moog Animatics). Accuracy of Ncorr and the SmartMotor system were validated using a laser displacement sensor (LK-H082, Keyence); displacements agreed within 0.5% of desired motion.

Figure 5.2 shows the experiment setup for commanding slip trajectories and measuring slip. **Right inset** shows the grasper; the jaw-mounted camera obtains video of the planar tissue deformation. On the underside of the slip sensor board, a load cell collects grasp force. **Left inset** depicts DIC analysis on speckled foam. Left image is the 'reference' image. Middle image is taken 0.5 s later; the vector field of Lagrangian displacements with respect to the reference image is overlaid. Right image shows a Ncorr colormap output of the x displacements; color gradient shows increasing displacement from bottom to top, implying stretch.

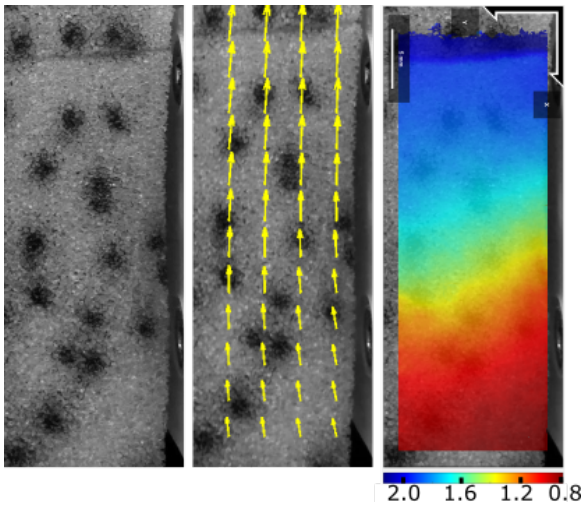

Figure 5.3 – Enlarged from inset of Fig. 5.2. Left image shows some pink foam, dotted with a sharpie, in its undeformed state. Middle image shows the displacement arrows Ncorr generates when comparing pixel motion from the undeformed configuration to the deformed one (in the background). Image at right shows a displacement colormap.

Tests were conducted to test the effectiveness of the sensor and the feasibility of the concept. The slip sensor was mounted in one jaw of a rigidly-mounted 3D-printed grasper. A force sensor under the slip sensor allows precise selection of the grip force prior to each trial; 0.5 N was chosen experimentally because it allowed tissue to move with nearly rigid body motion between the grasper jaws without catching or tearing. The other grasper jaw contains an optically clear window to allow video capture of the grasped tissue for motion analysis. Thin samples of tissue (slices of turkey bacon) were used to obtain accurate planar deformation estimates. Tissue is held in two clamps mounted on a passive linear guide carriage and a linearly actuated carriage. The passive carriage is linked rigidly to the other carriage to mimic tissue slip through the grasper. Rigid-body motion of the tissue is enforced by imposing slip trajectories with the SmartMotor and checking homogeneity of motion using DIC analysis, which was also used to calculate net tissue displacement.

5.2.3 Results and Conclusions

The results from tests comparing two speeds of slip in the $+\hat{x}$ direction are shown in Figure 5.5. Results from 10 trials each of fast ($0.61\,\mathrm{mm/s^2}$) and slow ($0.12\,\mathrm{mm/s^2}$) slip of room temperature tissue slipping through the grasper in $+\hat{x}$ for 3 mm (*row 3*); mean and

Figure 5.4 – Benchtop experiment setup for prototype slip sensor validation, shown holding slice of liver tissue. Data used in publication reflects experiments on turkey bacon, rather than liver as shown here.

standard deviations are shown. Grip force was set at 0.5 N for all trials (*row 2*). Row 1 shows the slip signals; there is clearly a $\dot{S}_x$ response but no $\dot{S}_y$ response. The dashed black line denotes a significant deviation ($\mu + 3\sigma$; $\mu = 2.504, \sigma = 6.4 \times 10^{-3}$) above baseline slip signal levels, or the level at which we can identify slip. Minimum detectable slip levels ranged from 0.7-0.9 mm. Grip force was set at a relatively low value (0.5 N) to allow nearly rigid-body motion with minimal stretch (confirmed with DIC). Fluctuations in grip force associated with slip were present but with a poor signal-to-noise ratio. As expected, $\dot{S}_x$ changes repeatably in response to slip while $\dot{S}_y$ remains approximately unchanged.

Figure 5.6 presents results from tests where the acceleration (velocity ramp rate of the controlled stage) of slip was varied. $\dot{S}_x$ vs. slip displacement were collected for 5 different slip accelerations; mean and standard deviations are shown. As shown in the inset, the rate of change of slip signal with slip distance is independent of the acceleration. For faster slip, the tissue moves faster than it is locally heated, so the signal continues to grow. For slower slip, convection is less, so the slip signal reaches a lower maximum. As in Fig. 5.5, the dashed black line denotes ($\mu + 3\sigma$) above baseline slip signal. Minimum detectable slip ranges from 0.87-1.4 mm. The rate of change of slip signal with slip distance is the same regardless of the acceleration. We hypothesize that for faster slip, the tissue moves faster than it is locally heated, so the signal continues to grow. For slower slip, convection is

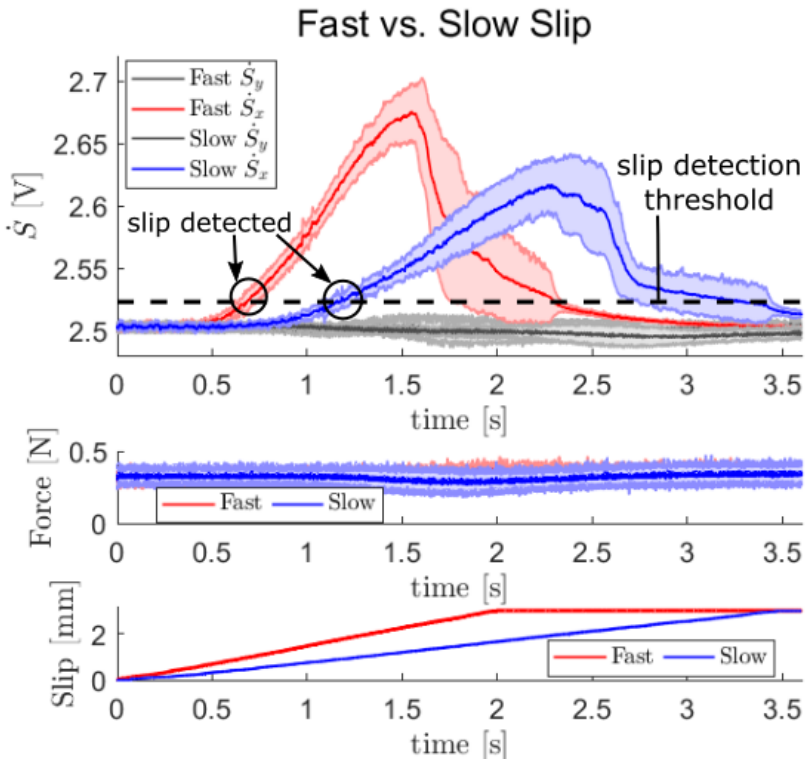

Figure 5.5 – Results from 10 trials each of fast ($0.61\,\mathrm{mm}/s^2$) and slow ($0.12\,\mathrm{mm}/s^2$) slip of room temperature tissue slipping through the grasper in $+\hat{x}$ for 3 mm (*row 3*); mean and standard deviations are shown. Grip force was set at 0.5 N for all trials (*row 2*). Row 1 shows the slip signals; there is clearly a $\dot{S}_x$ response but no $\dot{S}_y$ response. The dashed black line denotes a significant deviation ($\mu + 3 * \sigma$; $\mu = 2.504, \sigma = 6.4 * 10^{-3}$) above baseline slip signal levels, or the level at which we can identify slip. Minimum detectable slip levels ranged from 0.7-0.9 mm.

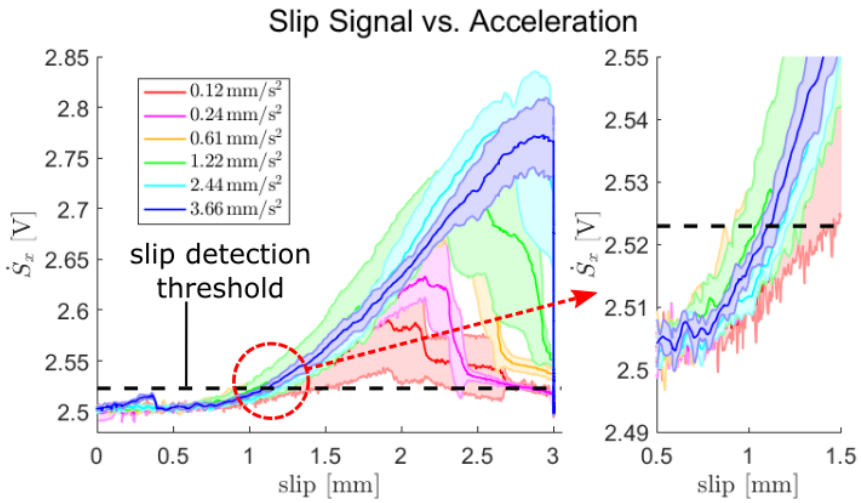

Figure 5.6 – $\dot{S}_x$ vs. slip displacement at different accelerations. 5 trials were conducted for each acceleration; mean and standard deviations are shown. *Inset*: the rate of change of slip signal with slip distance is independent of the acceleration. For faster slip, the tissue moves faster than it is locally heated, so the signal continues to grow. For slower slip, convection is less, so the slip signal reaches a lower maximum. As in fig. 5.5, the dashed black line denotes $(\mu + 3\sigma)$ above baseline slip signal. Minimum detectable slip ranges from 0.87-1.4 mm.

less, so the slip signal reaches a lower maximum. We anticipate that this result will be consistent with higher speeds up until some maximum where the tissue is moving so fast that the sensors cannot obtain a measurement.

During slip, the difference between opposed pairs of thermistors increases at a rate independent of slip speed or acceleration. Faster slips are accompanied by larger maximum slip signals because the tissue is moving faster than heat can be conducted through it. Grip force fluctuations do occur during slip, but the variations have a poor signal-to-noise ratio and are visually poor indicators of slip.

There are some error sources on the hardware side. The signals rely on resistance measurements, so any asymmetry in the signal conditioning circuits (performance variations, manual potentiometers, component value tolerances) and amplifier nonidealities contribute to error. Furthermore, although the nichrome heating resistors were selected for their low temperature dependence, a value of zero is not achievable so the heating power does vary with temperature.

The tested tissue was near room temperature $(24 - 29°C)$ which is much cooler than the heating element $(> 35°C)$. Tissue *in vivo* is $\leq 37°C$ due to room-temperature insufflation.

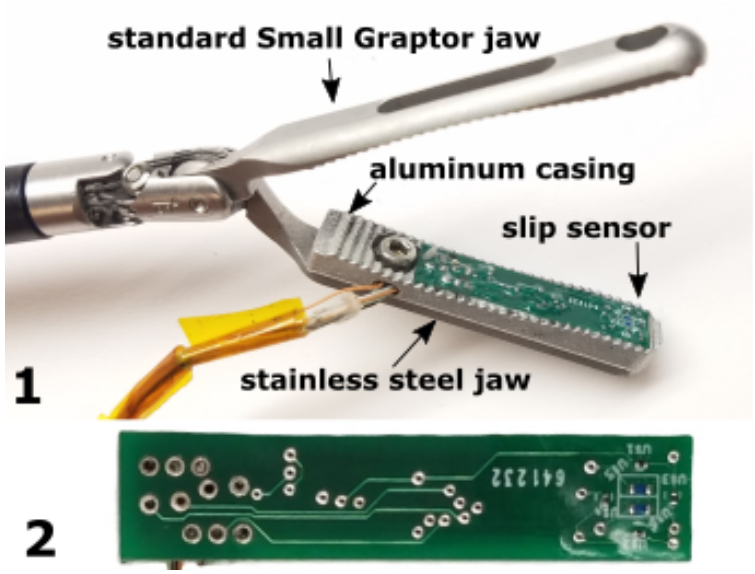

Figure 5.7 – Robot-mounted slip sensor. **1**: Slip sensor board mounted on a modified EndoWrist® instrument. **2**: Detail photo of populated sensor PCB. Adapted from [10].

Cooler objects have steeper thermal gradients and therefore sharper changes in slip signals associated with slip; therefore, some reduced sensitivity is expected *in vivo* with more realistic and safe temperature differences.

5.3 Round 2 of Prototypes: Robot-mounted version

5.3.1 Description

The following is based largely on [10], which describes the robot-mounted version of the slip sensor, integrated into an Intuitive Surgical EndoWrist instrument, and a method that uses sensor fusion with a *da Vinci* ® Surgical System to identify slip only once a reliable grasp is established and maintained for 1 s. The major goals of this round of prototyping were to demonstrate the feasibility of implementing the slip sensor onto a tool of relatively the correct dimensions and use it to sense slip during unconstrained tissue manipulation. The tests involving such freeform grasping guided implementation of the sensor in the user study presented in Chapter 6, where it was crucial to present users only with the information they wanted to avoid information saturation and consequent annoyance.

Experiments involved a custom *da Vinci* ® 8 mm instrument with the sensor integrated

and interacting with *ex vivo* porcine tissue. Results demonstrated slip detection within 2.1 mm average motion across five tissue types. During freeform tissue manipulation experiments, slip was detected with a 92% true positive rate and 94% positive predictive value. Experiments were performed using the da Vinci robot and ex vivo tissue (rather than homogeneous processed meat as in Section 5.2). See Figure 5.7 for the new slip sensing instrument (*1*) and the updated slip sensor PCB (*2*) used in the experiments described in this section.

Advances made over the prior work (see Section 5.2) include the following contributions:

- Miniaturization and integration of the slip sensor and signal conditioning hardware into a da Vinci EndoWrist® instrument (see Fig. 5.7)
- Implementation of closed-loop temperature control to ensure safe heating and improve thermal sensitivity
- Validated sensor performance with a realistic grasper on ex vivo porcine esophagus, fallopian tube, intestine, lung, and ovary (Fig. 5.15–5.17)
- Implementation of sensor fusion with the *da Vinci*® Surgical System to implement grasp state detection
- Validated method to detect slip during unrestricted grasping, traction, and release of excised tissue

5.3.2 Integrated sensor development

Updates to the sensor presented in Section 5.2 include reducing the PCB size slightly, moving first-stage signal conditioning components onto the PCB to reduce noise, reducing copper near the sensing region, and integrating the PCB into a standard RAS grasper to enable testing on the *da Vinci*® Xi. The sensor has four thermistors surrounding a heater and a reduced surface area of $3 \times 3\,\mathrm{mm}^2$; the overall PCB is $6 \times 24\,\mathrm{mm}^2$. These dimensions were driven by off-the-shelf availability of components, ease of manufacture, and the grasper jaws' size constraints as well as results from the numerical thermal simulation. The trace widths were also reduced from 8 mil down to 4 mil to reduce the amount of copper near the slip sensor. The slip sensor and its substrate were designed to minimize internal conduction because, ideally, the thermistors would sense temperature changes at the grasping contact interface and not through the substrate (see Section 4.3.3 for more information).

The PCB's underside is sprayed with a conformal coating, press-fit into a prototype aluminum housing filled with silver epoxy to increase thermal conductivity on the underside

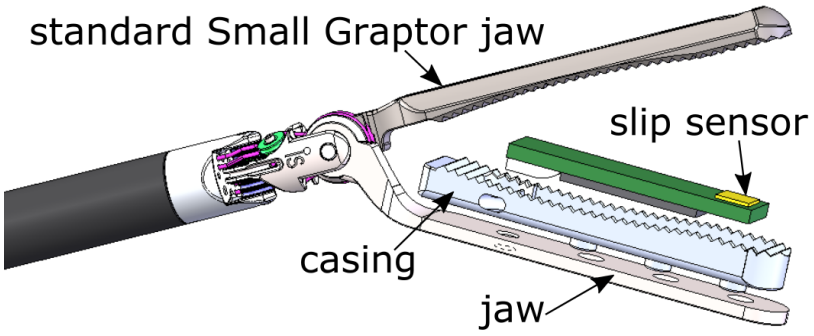

Figure 5.8 – Robot-mounted slip sensor represented in CAD.

of the sensor board, and waterproofed with a thin coat of UV cure adhesive. Aluminum was chosen for its high thermal conductivity, which would help wick away heat from the underside of the slip sensing PCB and thus avoid heat saturation within the sensor substrate. The reader should note that aluminum is an unacceptable long-term solution in a MIS environment due to corrosion issues. This packaged sensor is then fit onto a prototype steel jaw adapted from the *da Vinci*® 8 mm Small Graptor (Figure 5.8).

See Figure 5.9 for final board design in EAGLE. The signal conditioning components shown in Figures 5.10 and 5.11 were both moved onboard the slip sensor PCB to reduce noise and enable sensing output voltages rather than resistances through the (necessarily) long cables.

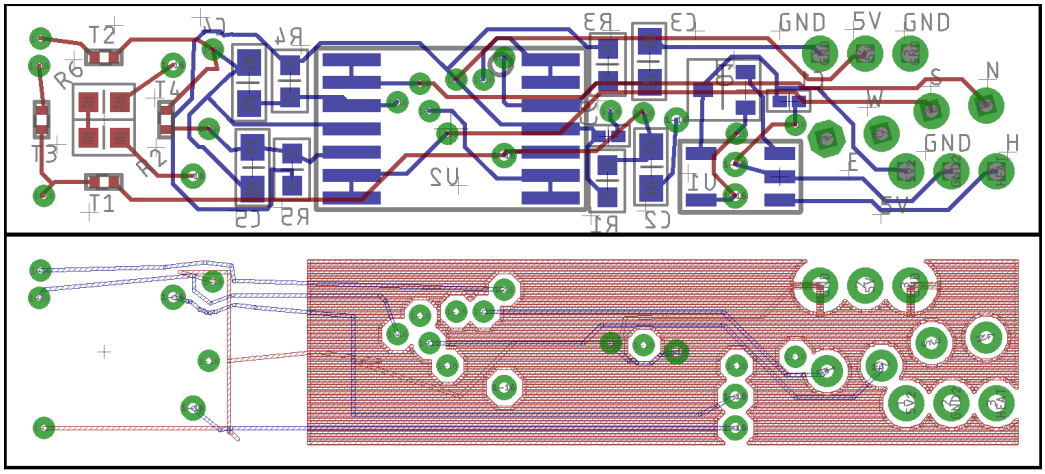

Figure 5.9 – Slip sensor PCB in EAGLE. Top shows top and bottom layers of the PCB. Bottom image shows internal layers 2 and 3. Traces are 4 mil. Spaces are 6 mil for different signals, 2 mil for same signals. See Appendix A for slip sensor schematic and bill of materials.

5.3.3 Software

In Section 5.2, tests were run with a $> 10^\circ$ C temperature difference (between the heater and grasped object) that would be unsafe *in vivo*. Here, the heater (a pair of 47Ω thin film 0402 size resistors in series) resistively heats to 30° C, or 5° C over the tested tissue's temperature with PID temperature control (>1 kHz). For *in vivo* use, it would be set to 41°C, which is below the 43°C safe limit for extended direct tissue contact [58]. The control temperature is the maximum of the four thermistors. From Table 4.3, there is an expected 1.7° C difference between the heater and thermistors during prolonged liver tissue contact.

A 2kΩ NTC thermistor was selected for its low cost, fast response, and compact 0201 size. Their resistances are converted to voltages using on-board buffered, filtered voltage divider circuits. Resistance is related to temperature:

$$R = R_0 \exp\left[B\left(\frac{1}{T} - \frac{1}{T_0}\right)\right] \tag{5.2}$$

where $T_0 = 298.2\,\text{K}$, $R_0 = 2.0\,\text{k}\Omega$, and $B = 4450.5\,\text{K}$. A DAQ reads the voltage across each thermistor, and opposing thermistor pairs (N-S, W-E) are differenced, differentiated (to remove offsets), and digitally filtered (rather than in hardware, as in Section 5.2) with an active 2-pole lowpass filter ($f_c = 10\,\text{Hz}$) to produce the directional slip signals in Equation 3.5. $\dot{S}_x$ and $\dot{S}_y$ are combined to form the slip signal $\dot{S}_{mag^2}$ used for slip detection from Equation 3.6.

This signal may be considered as slip magnitude squared. $\dot{S}_{mag^2}$ is more responsive than the separate signals used in Section 5.2; a change necessary due to the reduced temperature difference between the grasped tissue and the heater. This sensing strategy is not robust to uneven contact or release of tissue, which causes unpredictable changes in the sensed temperatures and can mimic slip (see Section 5.3.5 for the mitigation approach).

5.3.4 Heater control

In these trials, the heater (a pair of 47Ω thin film resistors in series) was maintained at 28° C to maintain a 6° C temperature difference with the room temperature tissue. Gain scheduling is used to achieve the steepest thermal gradient as quickly as possible without allowing overshoot to occur. The maximum current is supplied to the heating resistors until the sensed temperature is within 3° C of the temperature setpoint, then the control scheme switches to proportional-integral-derivative (PID) control. The amount of voltage supplied

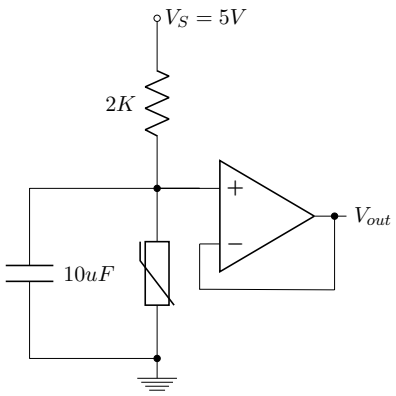

Figure 5.10 – Thermistor signal conditioning circuit.

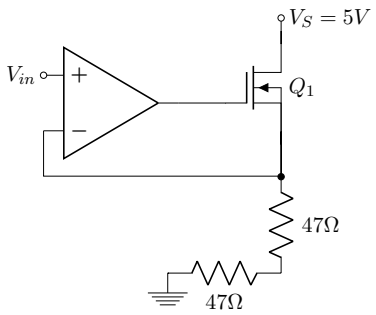

Figure 5.11 – Heater signal conditioning circuit.

to the heating circuit is controlled based on the temperature the thermistors sense.

This strategy used far less heating power than in the experiments discussed in Section 5.2, 45 mW as compared to 110 mW. The control temperature is the maximum of the four thermistors, which is safer than using the average of the four, yet noisier. PID control is used to aid performance: it is desirable to have the heater as hot as possible to enable generation of the steepest thermal gradient possible yet not so hot that it causes irreversible tissue damage.

The circuit shown in Figure 5.11 controlled current with a PWM signal or a DAC analog voltage. V_{in} was varied from 0-4.5 V to control a proportional amount of current through the 47Ω heating resistors in series. Because the DAQ was an Arduino Due that uses 3.3 V logic, its output was converted to 5 V logic levels using external components. See Appendix A for slip sensor schematic and bill of materials.

5.3.5 Slip detection state machine

Identifying when slip detection is important would help cognitively overloading the surgeon; unnecessary or irrelevant information can hinder rather than facilitate a procedure [59]. As described previously, the sensor is unable to reject asymmetric changes in contact, which can mimic slip (and are slips, but not the kind we wish to sense). First identifying a grasp may help reject false positives. Thus, a classifier that can identify whether a surgeon has stably grasped tissue with the intent to tension it will improve sensor performance and only provide relevant slip information.

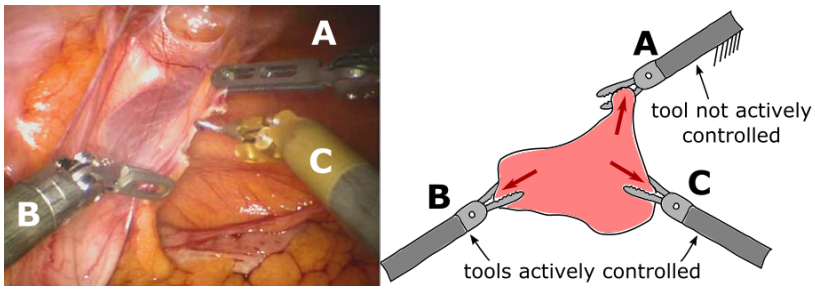

Figure 5.12 – Slip can occur in active and non-active tools. Although **A**, **B**, and **C** may tension the tissue, the user only actively controls tools **B** and **C**. This situation is not unusual; a surgeon may use tools A and B to initially tension the tissue, release control of tool **A** while it holds the tissue conveniently, and resume work using tools **B** and **C**.

Three surgeons well-versed in RAS and MIS and two CDEs (see Section 2.1 for description) from Intuitive Surgical, Inc. were interviewed and 15 RAS endoscope videos from relevant procedures (splenectomies, cholecystectomies, Nissen fundoplications, colectomies, etc.) were studied to characterize RAS tissue grasping. Two main situations where a surgeon would benefit from slip detection were identified (see figure 5.12). The first is *dynamic retraction*: the surgeon has grasped the tissue and is applying a load to it, either to manipulate the tissue using that tool or to counteract tension applied with another. The second is *passive retraction*: this occurs following active retraction, when the surgeon stops actively controlling the tool (to switch to another) but is still using it to hold tissue in place.

Detecting when a surgeon is likely to apply tension to tissue requires sensor fusion. The *da Vinci*® Surgical System is equipped with many sensors that monitor its state, several of which were hypothesized to be useful in identifying a stable grasp. Ultimately, the following variables were used: the identity of the tool (only sense slip for grasping tools; i.e. no needle drivers, etc.) and jaw angle. This information was obtained through a custom Matlab program that interfaces with the *da Vinci Xi* and queries the robot for state variables. Of the available information from the *Xi*, this is the preferred, appropriate set of values to judge when the tool is in a reliable, maintained grasp. As is discussed in Section 6.4, additional information that would be advantageous (but is currently unavailable) include an estimate of how much of the grasper jaws are covered with tissue and/or a sense of the speed of tissue slip.

The slip detection algorithm applied in this section's experiments is depicted in figure 5.13. The state machine is initialized in an idle state: the tool is not yet contacting

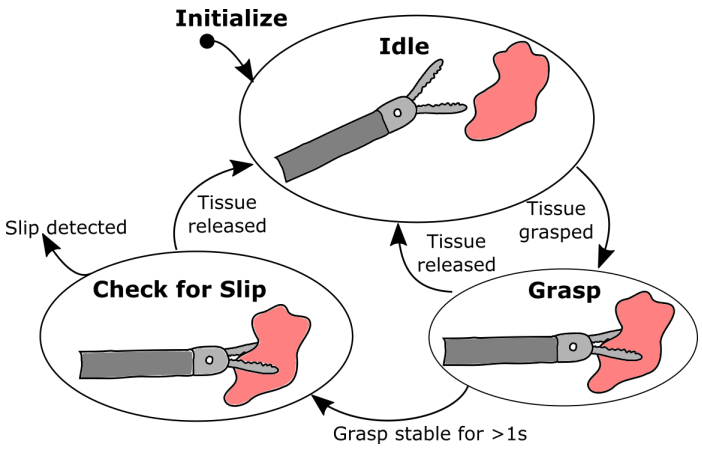

Figure 5.13 – State machine describing transitions between slip detection states. The sensor initializes in the idle state, where it stay until the tool grasps tissue. It then waits until the grasp is maintained for 1 s, then checks for slip unless tissue release is detected. If slip is detected, then the sensor responds. Section 6.2 has an updated version of this algorithm that provides slip notifications only when the slip sensing tool is nonactive (Fig. 6.2).

tissue on its grasping surface, and the goal is to identify when this occurs and monitor whether that grasp changes substantially. To detect a grasp or release of tissue, a combination of jaw angle and its time derivative are used. A fixed time delay is used to allow these signals to settle; if they do, it signifies a reliable grasp with a possible intent to retract tissue. What this evaluates is most closely related to 'ability to hold,' as defined in [61]. Experimentally, a waiting period of 1 s is a practical compromise that allows the thermal gradient to develop without adding a noticeable wait. If the grasp is modulated appreciably during this period, the wait timer is restarted. If a release is detected, the system is idle until a grasp is detected. Once this grasp is maintained, the system checks for slip by determining whether $\dot{S}_{mag^2}$ crosses a threshold. Loss of grasp is monitored as well and results in a state change back to Idle. For the user study discussed in Section 6, this state machine was updated to improve false positive rejection.

5.3.6 Validation experiments

Ex vivo tissue slip

Purpose: These tests sought to validate the sensor's $\dot{S}_{mag^2}$ response to slip with 30-40 slip trials each on porcine esophagus, fallopian tube, intestine, lung, and ovary. These

tissues were selected because they are commonly manipulated and each present grasping challenges. Esophagus, lung, and intestine are all quite delicate. Ovaries are bulky with large radii of curvature, making them difficult to grasp atraumatically. These tests were also used to determine a slip threshold for use in the freeform grasping tests.

Setup: Drawing from the experiments described in Section 5.2.2, this setup (see figure 5.14, top) enforces controlled slip displacement, velocity, and acceleration. A clamp attached to a linear guide and motorized ballscrew are used to generate movement. Accuracy of the this linear positioning system was validated using a laser displacement sensor (LK-H082, Keyence) [11]. The slip sensor is mounted on a RAS tool on the *da Vinci*® Surgical System. A DAQ records the output from the linear ballscrew's encoder and the analog output from 4 thermistors (N,S,W,E) at 4 kHz and outputs a heat modulation signal. Digital signal processing is used to differentiate the thermistor pair differences and apply a lowpass filter in real time, an advancement over the previous experiments.

Video was recorded at 60 fps with 1280x720 pixels resolution and used as a ground truth for motion. All motion tracking was done using the DLTdv5 software [62], an open source Matlab tool. Data is time-synced with video by tracking motion of the DC motor-driven carriage and comparing it with encoder counts. Next, tissue travel is estimated by tracking the displacement of ink dots on the grasped tissue. Because the tissue is pulled in tension and relaxed back to start, it is possible to track relaxation due to stretch, and $slip = travel - stretch$. Stretch is removed from the overall tissue trajectory by linearly scaling travel to the maximum slip amount. Finally, only the component of slip in the sensor's plane is kept; the 2D slip vectors are dotted with a unit vector along the grasper jaw's long axis.

Description: These tests had controlled amounts of slip enforced on one clamped end of the tissue; few restraints were imposed on the grasped end. In each trial, the slip sensing instrument grasped the tissue such that it covered the sensing surface and the jaw's long axis was generally aligned with the direction of slip. The tissue was immersed in a room temperature saline solution bath to maintain its properties, avoid dessication, and mimic a moist *in vivo* environment. Specific alignment of the instrument, amount of tissue between the jaws, grasp force, the length of time the tissue was grasped before testing, or how long the heater was on prior to testing were not controlled. Humans need approximately 150 ms to process and begin to respond to visual stimuli [63], notably slower than responses to haptic or auditory stimuli [34], [64]. Tests were run with a range of slip onset velocities that

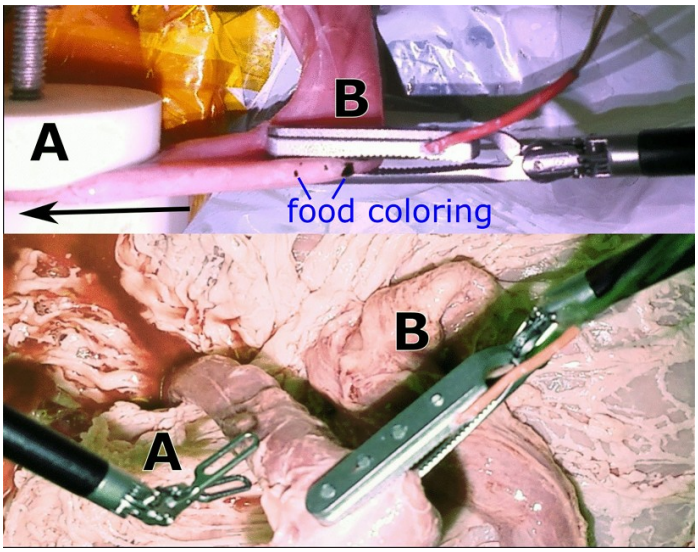

Figure 5.14 – *Top*: Slip experiment. **A** clamps the intestine and enforces slip trajectory. **B** is the slip sensor tool grasping the intestine, marked with food coloring for offline point tracking. *Bottom*: Freeform grasping experiment with a porcine esophagus. **A** is a ProGrasp®. **B** is the slip sensor tool (the standard Small Graptor® is the same size).

CDEs deemed appropriate and realistic in RAS.

Freeform grasping

Purpose: Freeform grasping tests involved a *da Vinci* ® ProGrasp and the slip sensor tool manipulating a set of porcine tissues. The goal was to (offline) identify grasping and release of tissue, identify reliable grasps, and then look for and detect tissue slip within 3 mm. Thresholds for detection of events were maintained across all trials. Tissue manipulation bore no restrictions and involved the slip sensing instrument grasping tissue and the ProGrasp® pulling the tissue out of its grasp. These tests focused on application of tension and counter-tension on tissue, which occurs in almost every procedure and is often used to set up the surgical critical view or enable the main task.

Setup: The sensor was mounted on a RAS instrument and integrated with the *da Vinci*® Surgical System (see figure 5.14, bottom). A ProGrasp® was also mounted on the system. The same video setup was used here as in Section 5.3.6. A proprietary software interface from Intuitive Surgical streamed the aforementioned robot variables at ≥ 1 kHz while reading the slip sensor data as in the prior experiment. Data was time-synced and

post-processed offline.

Description: In each 30-40 s trial, tissue was manipulated using the slip sensing tool and the ProGrasp®, chosen for its strong grasping capability, which could be used to force slips in the opposing tool. Thresholding the robot jaw angle input variable and its derivative enabled identification of grasp and release events. The jaw angle is first read in radians and converted to degrees, then lowpass filtered to 15 Hz. Next, its time derivative is calculated using digital signal processing and filtered to 10 Hz. Then, a grasp was identified if the last recorded event was a release and either the angular velocity of the jaw was $< 1.5^\circ$ /s, or the jaw angle was $< -15^\circ$. Jaw angle is represented as a negative number when the jaws are already fully closed but more torque is applied. A release is identified when the last recorded event was a grasp and the jaw's angular velocity is $> 0.2^\circ$ /s or the jaw angle is $> 20^\circ$. A *reliable* grasp is identified if the grasp continues to meet the grasp conditions for one second after the initial grasp was detected and no release has occurred (see Figure 5.13). The ground truth for grasp and release events was found manually in the collected videos. Time of slip onset was confirmed with point tracking. Slip was detected when a stable grasp was confirmed and the sensor signal crossed the slip threshold found in the performance validation experiments. The same thresholds were used for all five tissue types.

5.3.7 Results and Conclusions

Figures 5.15-5.17 show results from the $\dot{S}_{mag^2}$ vs. slip validation tests. These tests sought to characterize the sensor's performance under realistic RAS conditions with few restrictions on how the grasper interacted with the tissue.

Results are highly dependent on the selected slip threshold. Here, it was set at 5.1×10^{-4} $(^oC/s)^2$, or >5 standard deviations over the mean baseline noise for ovary tissue, which had (by a factor of 5) the most noise in baseline $\dot{S}_{mag^2}$. This was likely due to the ovary's large curvature which caused inconsistent contact on the sensing surface. The choice of threshold was confirmed after ensuring it allowed slip detection beneath the 3 mm specification for all five tissues. Figure 5.15 shows the median slip signals generated by tissue slip for each tested tissue. Figure 5.16 shows the mean and 95% confidence interval for detectable slip in each tested tissue.

Although variance is high (as is expected with more realistic, less controlled tests than in Section 5.2.2), the mean slip that occurred before detection lies below the desired threshold. No correlation or trend was found between detectable slip and initial temperature (range:

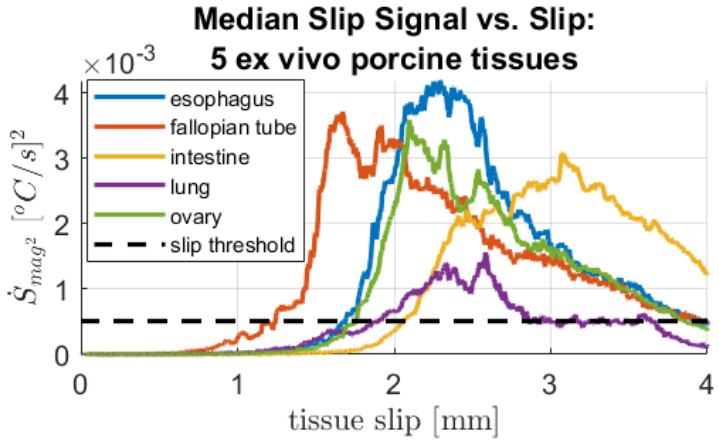

Figure 5.15 – Median signal vs slip for 5 tissues, 30-50 trials each. Note that all tissue types were readily detectable within the 3 mm target.

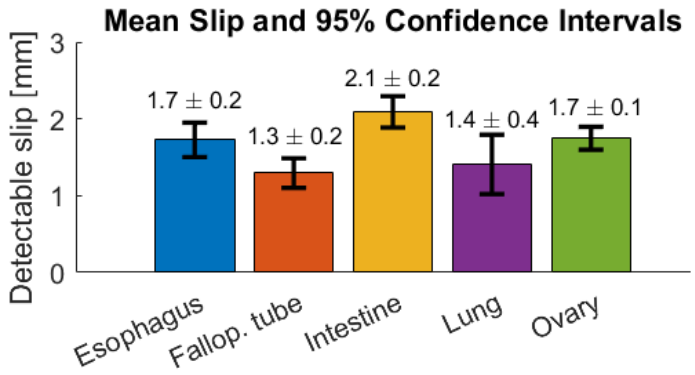

Figure 5.16 – Mean detectable slips and 95% confidence intervals (calculated with standard error and t-score) for 5 types of *ex vivo* porcine tissue.

20-24° C) or amount of stretch that occurred during testing. Fig. 5.17 relates onset slip velocity to detectable slip. Region **C** denotes the 3 mm specification for slip detection; most of our test points fall in this desirable region. Rarely, points fall in region **B**, which although outside our established specification indicates a state where the tissue may not have fully slipped from the jaw.

Table 5.1 summarizes the results from the freeform grasping experiments. Over 21 trials, 84 slips, 145 grasps, and 138 releases were performed using the slip sensing instrument (the ProGrasp® was not tracked). See Fig. 5.18 for a representative trial. Two plots are shown: the top shows $\dot{S}_{mag^2}$ vs. time with dashed pink regions of reliable grasp overlaid, which

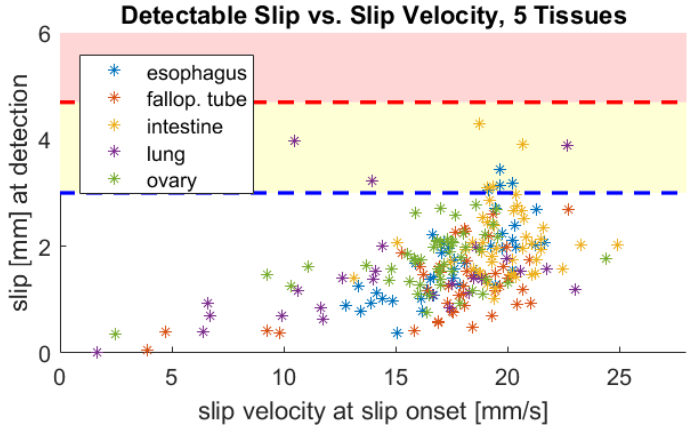

Figure 5.17 – Onset slip velocity vs. the detectable slip. Catching slip in the red region is undesirable because tissue has slipped the width of a da Vinci grasper jaw. In the yellow region, tissue has slipped > 3 mm but not yet a jaw width. The white region is desirable: slip is detected before our 3 mm specification. The bulk of our data lies here.

	TPR			**PPV**		
	Slip	*Grasp*	*Release*	*Slip*	*Grasp*	*Release*
Fallop. tube	100%	100%	100%	83%	100%	100%
Ovary	80%	100%	100%	94%	98%	95%
Lung	94%	100%	100%	94%	100%	97%
Intestine	100%	100%	100%	94%	100%	91%
Esophagus	90%	100%	100%	95%	95%	90%
Overall	92%	100%	100%	94%	98%	94%

Table 5.1 – True positive rate (TPR) and Positive predictive value (PPV) for Freeform grasping events

denote when the algorithm checks for slip. Green asterisks denote slip detection, and green circles denote observed slip in the video (ground truth). The same slip threshold was used for all tissues. The bottom plot shows the data used to identify reliable grasp regions: jaw angle is in heavy black and its derivative in yellow. Predicted grasps and releases are asterisked in red and blue, respectively, with their ground truths denoted with same-colored circles. In this trial, all slips, grasps, or release events are correctly identified.

The slip detection threshold used here was selected to ensure a safe margin between the mean slip detection and the design target of 3 mm. At the selected threshold, the mean detectable slip for intestine was highest (2.1 mm). In the user study presented in Chapter 6,

tuning the detection threshold was found to be advantageous because it allowed participants to determine the sensor's sensitivity.

Some of the variance in the results was due to the use of *ex vivo* tissue. Excised porcine tissue samples exhibit non-uniformity in thickness, compliance, moisture content, thermal mass, etc. Trials were also intended to mimic actual use, so many test aspects were intentionally uncontrolled, as described in Section 5.3.6. In particular, the lung was grasped far more gently for fear of tearing. To reduce some variability, samples were sprayed with saline solution prior to testing. Further work is required to understand the effects of the uncontrolled experimental aspects of grasping. Regardless, there were only minor differences in performance amongst the different tissues, and the same slip detection threshold was applicable for all five tissues. These promising results prompted the experiments presented in Section 5.4.

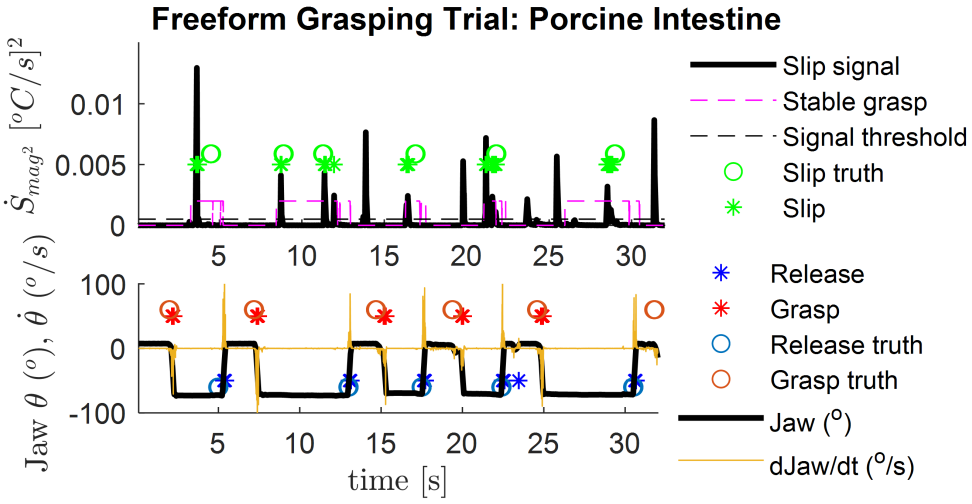

Figure 5.18 – Representative freeform grasping trial on excised porcine intestine.

The proposed thermal-based sensing method is suitable for the proposed application. The presented sensing package has been integrated into a RAS instrument and can be inserted through a standard cannula for use in a *da Vinci* ® system. Although small motions are detectable (mean detectable slip of <2.1 mm), there is considerable variability in precisely how small, depending on the tissue type, (historical) thermal conditions, moisture content, etc.

For ground truth comparison of tissue motion, the slip detection sensor was compared with tissue motion measured by optical tracking of tissue markers and features. There is

unavoidably some uncertainty regarding what motions precisely constitute slip (as opposed to stretch, dilation, etc.) in a variable, stretchy, wet, viscoelastic medium. These factors prevent the detection of slips less than 2 mm. Nevertheless, the current sensor provided robust and actionable data about clinically relevant slip.

5.4 In vivo testing

This first pass of *in vivo* tests (see Fig. 5.19) were conducted to address the shortcomings of working predominantly with *ex vivo* tissue. The tissues that were anticipated to be most problematic were either fatty or perfused tissue. Fat posed potential issues for this slip sensor due to its friability. As discussed in Section 4, thermal conductivity of grasped objects affects sensor performance because it contributes to the local thermal gradient that forms local to the heater through the grasped object. Steeper local thermal gradients are desired and are produced when grasping objects with lower thermal conductivity. Perfused tissue was hypothesized to pose issues because bloodflow introduces convection, which mimics the effect of slip.

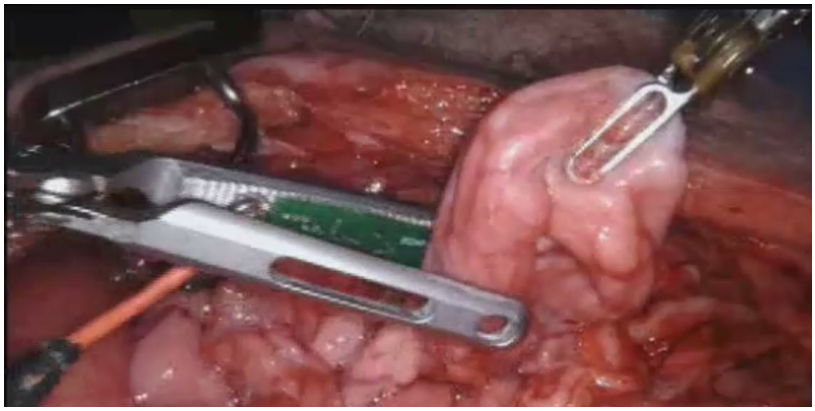

Figure 5.19 – *In vivo* porcine testing via laparotomy and da Vinci Xi Surgical System with prototype grasper (left hand) and Fenestrated Bipolar Forceps (right hand).

5.4.1 Purpose and Methods

This study sought to validate the tissue slip sensor on living, perfused porcine tissues. We anticipated that the convective effects of blood flow (either in highly perfused tissue like mesentery or in a blood vessel with strong flow) may affect the performance of the device. In addition, we tested fat because its thermal conductivity is quite low compared to other

biological tissues (approximately 0.2 W/(m K) vs. 0.5 W/(m K) [56]), although the thermal model presented in Chapter 4 did not indicate that this would negatively impact the slip sensor's performance. Lastly, we wished to compare the new data with our earlier *ex vivo* results (see Section 5.3.7) to determine whether the device under *in vivo* conditions has comparable sensitivity. With these considerations in mind, we tested mesentery, an artery, fat, and bowel.

Animal studies at Intuitive Surgical are covered by Intuitive Surgical's ACUP Protocol 005 (IACUC). All measurements were taken using the sensor mounted on the modified Small Graptor™ da Vinci instrument and the software described in Section 5.3 to obtain a slip signal:

$$\dot{S}_{mag^2} = \dot{S}_{EW}^2 + \dot{S}_{NS}^2 \tag{5.3}$$

where $\dot{S}_{EW}$ and $\dot{S}_{NS}$ are time derivatives of the differences in signals between thermistors on opposite sides of a miniature heating element. The software was modified to increase sensitivity to slips at low speed by reducing the low-pass filter frequency from 5 to 1 Hz.

Repeated measurements of slip were taken on *in vivo* tissues from a single porcine model. Video recording using the da Vinci endoscope (30 fps, 736x486 pixels resolution) was used as the ground truth measurement for timing and speed of slips. Digital image correlation (as described in Section 5.2.2) was used to calculate the amount of slip that occurred in each video. All motion tracking was done using the DLTdv5 software [62], an open source Matlab tool.

5.4.2 Results

Figures 5.20 and 5.21 show results from the $\dot{S}_{mag^2}$ vs. slip validation tests on *in vivo* tissue. Figure 5.20 shows how the tissue slip and resultant signal vary over time, and Figure 5.21 compares $\dot{S}_{mag^2}$ to our *ex vivo* results from Section 5.3.7. While the past slip threshold was 5 standard deviations above the mean, the presented slip threshold was set at that which participants chose most often during the user study (Chapter 6). The threshold for slip detection, $0.0013\,(^\circ\mathrm{C/s})^2$, was maintained for all tissues.

There was little difference in the results among the 4 tested *in vivo* tissues, as expected from the results reported in Section 4.3.3. There were no adverse effects due to tissue perfusion, even when grasping mesentery (which contains small, very superficial vessels) and a large, strongly pulsating artery (the mesenteric artery). Surgeons tend to avoid grasping strong, superficial arteries because the risk of bleeding is too high. However, should they

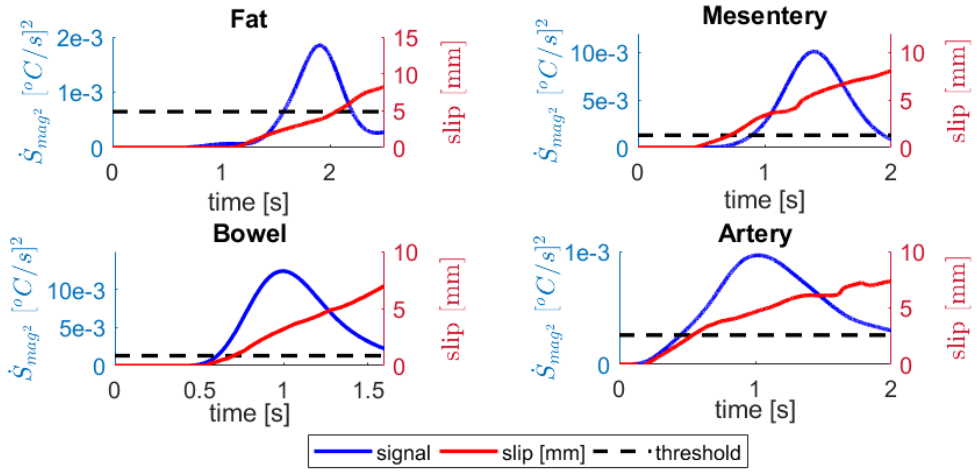

Figure 5.20 – Slip signal $\dot{S}_{mag^2}$ and tissue slip vs. time for each of the four tested *in vivo* tissues. Representative trial shown. Importantly, these plots qualitatively all look very similar. There are no altered frequency components due to perfusion in mesentery or artery.

elect to grab near one, the sensor has demonstrated robustness to the effects of bloodflow.

The $\dot{S}_{mag^2}$ signal produced in response to slip on *in vivo* tissue is not as large as that produced on *ex vivo* tissue. This is because the tested slip speeds were predominantly lower than those tested in Section 5.3.6 to ensure safety of the porcine model (see Fig. 5.22). In previous testing, we observed that speed had a similar limiting effect on the peak slip signal obtained. Therefore, we feel confident in stating that the differences seen in Fig. 5.21 are due primarily to speed rather than perfusion or starting temperature. Far fewer trials (3-7 vs. 30-50) were taken due to the porcine model being a shared resource. However, with the same slip detection threshold used throughout, slip was detectable on all *in vivo* tissues well within our 3 mm specification as developed in [10], which allows provision of timely information to surgeons.

Figure 5.22 relates onset slip velocity to detectable slip of the *in vivo* tissues; the *ex vivo* data is shown for comparison. Although more slip occurred at detection for the slower slip velocities tested, all *in vivo* slips were detectable within the 3 mm specification.

Having demonstrated that the slip sensor works as well on tissue *in vivo* as *ex vivo*, the next steps seek to demonstrate the utility of providing slip feedback to users in a surgically-inspired setting.

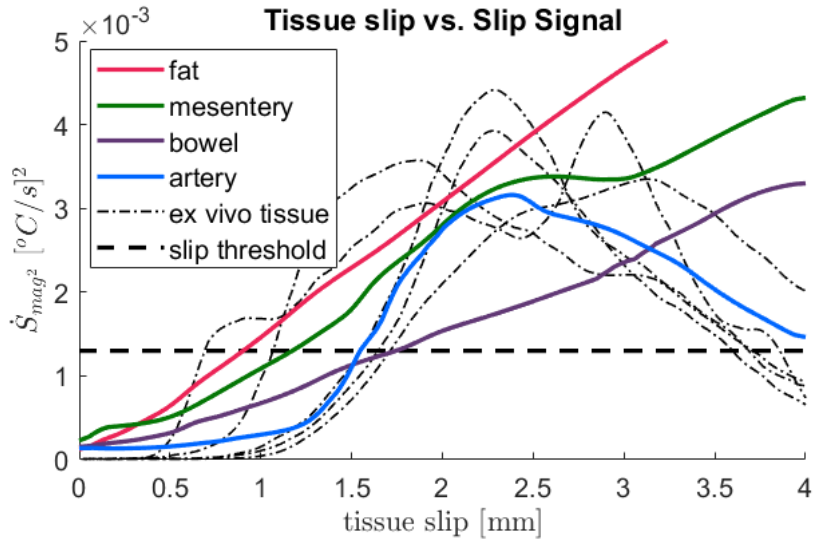

Figure 5.21 – *In vivo* data vs. *ex vivo* data (dashed in black) from [10]. The *in vivo* data shown are the mean signals produced from 3-7 trials per tissue type. The *ex vivo* tissues shown are esophagus, bowel, fallopian tube, lung, and ovary and are the mean signals produced over 30-50 trials per tissue type. Slip of all tissues are detectable well within the 3 mm specification to provide timely information to surgeons. The detectable slips ranged from 0.32-2.99 mm.

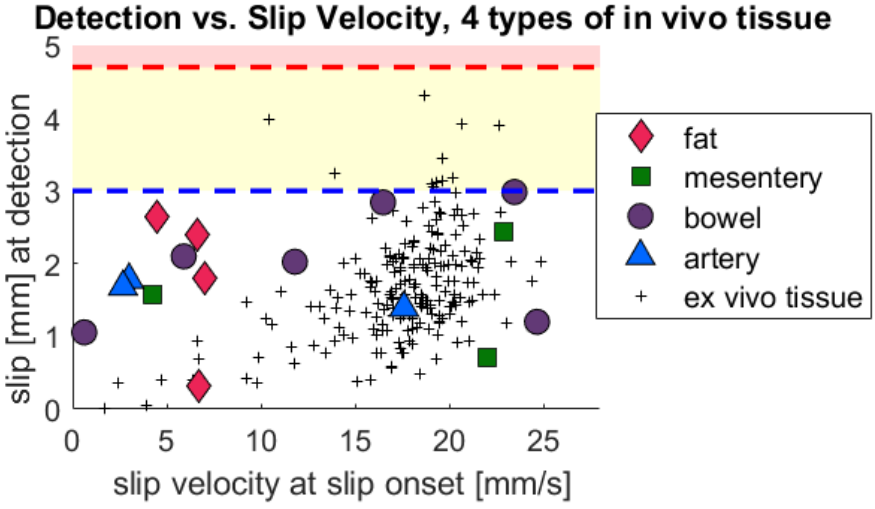

Figure 5.22 – Onset slip velocity vs. detectable slip for 4 *in vivo* tissues (*s) and 5 *ex vivo* porcine tissues (*ex vivo* data reproduced from [10]). Catching slip in the white region is desirable; slip is detected within 3 mm. The yellow region denotes that tissue has slipped > 3 mm but not yet a jaw width. The red region is undesirable as the tissue would have slipped entirely from the jaw.

Chapter 6

User Study

6.1 Purpose

The purpose of this user study was to explore whether users would find feedback helpful if it provided information regarding tissue slip from the non-active tool. The choice to focus on non-active rather than active tools was motivated by the reasoning that there is likely a ceiling on the performance of simple tasks so that adding sensory feedback (or any other kind of assistance) will not result in an improvement in performance metrics. Experts in particular are highly skilled at using all available information channels to complete their task. Thus, when an additional channel of information (e.g. slip feedback) is provided to the expert surgeons, it is difficult to see the effect. In RAS, surgeons typically focus on their active tools, so one would expect them to detect slip visually. However, on the non-active tool, the slip sensor has the opportunity to provide otherwise unobservable information. Other practical reasons for our choice of study design concern the user experience. The prototype slip sensing tool has a large lower jaw that makes manipulation difficult, which can be frustrating to the study participant.

In the future, robotic surgery may incorporate shared autonomy or automation of low-level surgical tasks. This will require more information regarding the robot's interaction with biological materials and a heightened ability to communicate that information with the human user. To that end, testing the utility of supplying feedback to a tool that is not controlled by the human user can provide important insights.

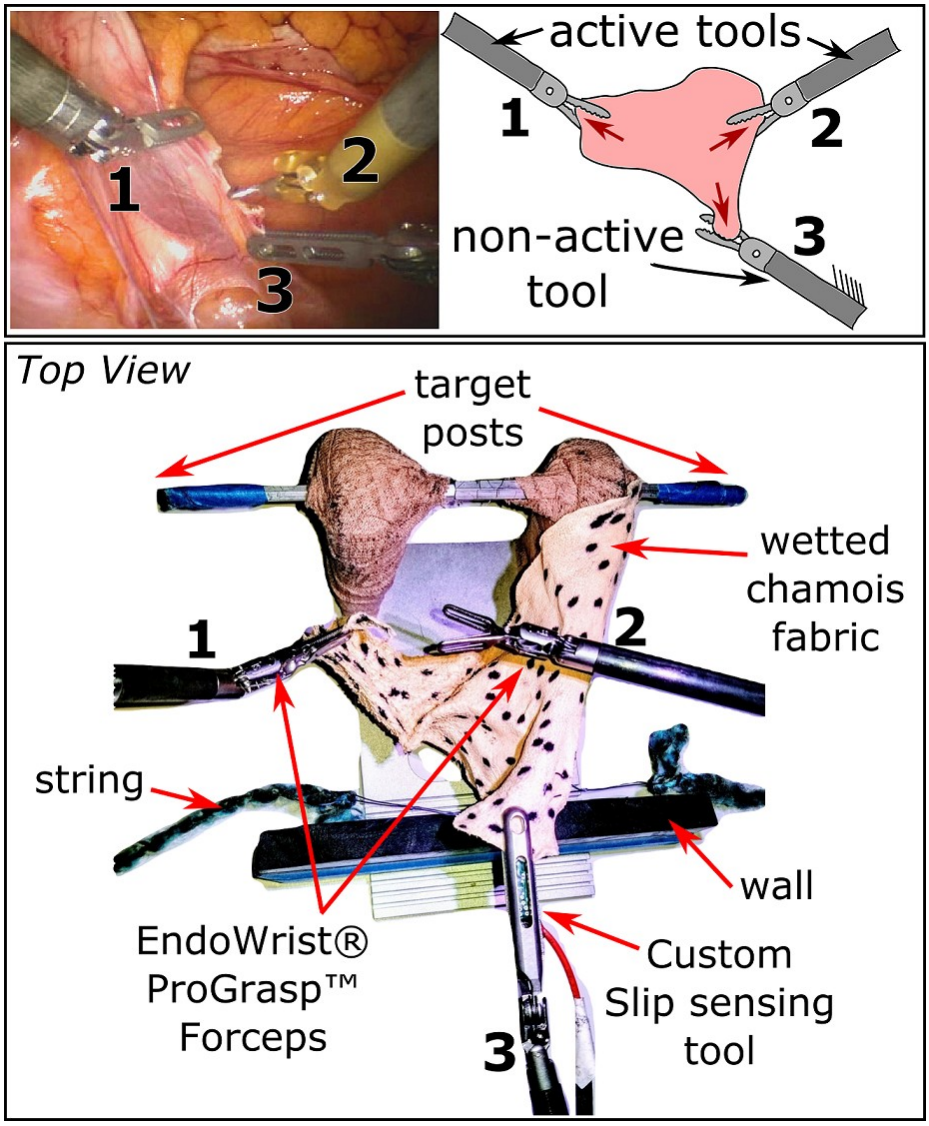

Figure 6.1 – *Top: Motivation.* Tools **1**, **2**, and **3** may be used to tension the tissue, but only tools **1** and **2** are actively controlled. A surgeon may use tools **1** and **3** to initially tension the tissue, release control of tool **3** while it retracts the tissue, and resume work using **1** and **2**. Slip at **3** can go unnoticed and result in loss of traction and exposure. *Bottom: Study setup.* Study participants must use the slip sensing tool **3** to retract the 'tissue' (chamois) behind the wall. Then, the participant releases control of **3** and uses the *da Vinci*® ProGrasps **1** and **2** to hook the chamois over the target posts. Meanwhile, external slips applied to the control strings may cause slip to occur in **3**.

6.2 Methods and Materials

The hardware and software presented in Section 5.3 were used in this study with a minor modification to the algorithm to detect slip only when the tool jaws were closed *and* the tool was inactive (Fig. 6.2). This helped reject false positives (due to uneven tissue contact) and unwanted slip alerts from an actively used tool.

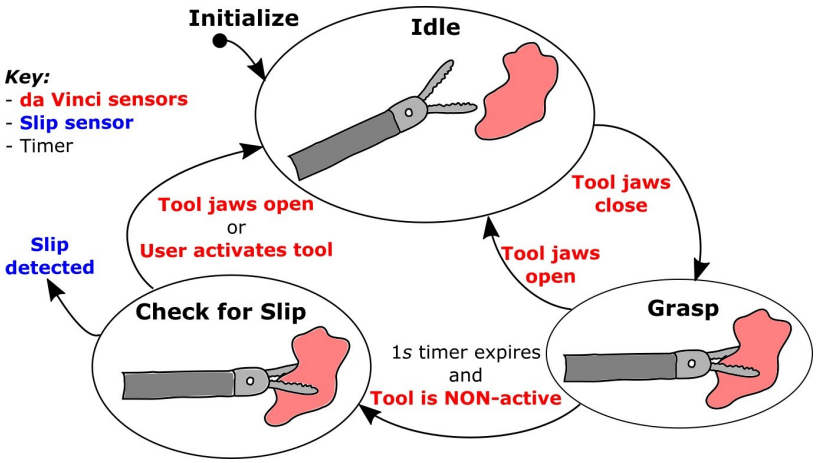

Figure 6.2 – State machine describing transitions between slip detection states. We start in the idle state until the slip sensing tool grasps tissue. When the grasp is maintained for 1 s and the tool is non-active, we transition to Checking for Slip unless we detect tissue release or activation of the tool. The 1 s wait time helps avoid false positives generated during grasping, as contact can be uneven.

After obtaining approval from the institutional review board of Stanford University (Protocol #46474), we began recruiting for our user study. Informed consent was received for all participants included in the study. Participation requests outlining the requirements for eligibility were sent electronically within Intuitive to potential subjects with expert-level experience, including familiarity with swapping between tools, clutching[1], and moving the camera. No honoraria were provided. 24 subjects gave their informed consent to participate in the study; see Fig. 6.4 for demographics. Many participants were CDEs (see Section 2.1 for description).

Many iterations of the task were tested in pilot studies before selecting the final construct

[1]Clutching means acquiring and releasing a tool to re-center it in the workspace. It is similar to lifting and replacing a computer mouse on a mousepad.

(Section 6.3). Important aspects of the task include required skilled user precision, dexterity, manipulation, and grasping while forcing the user to divide their attention between competing goals. Here, users had to complete a dexterous manipulation task as quickly as possible while also maintaining situational awareness and attending to the periphery for unusual or unexpected events. Finding a balance in difficulty that allowed study subjects to use the slip feedback to perform the task better while ensuring appropriate difficulty of the task was a delicate compromise. If the task was too difficult, participants would not respond to the feedback because they felt frustrated with a seemingly impossible task. However, if the task was too easy, they would ignore the feedback because they believed they could finish before slip at the non-active tool would matter.

6.3 Task Construct

The user study was run as follows. Each subject received instruction on the study task (see Fig. 6.3), which was designed to mimic the situation in surgery where the surgeon is using their third arm to provide traction on tissue and thus exposure so they can perform some intervention with their other two (active) arms (see Fig. 6.1). Here, the subject was required to use the slip sensing tool to retract the tissue (chamois, dotted with black ink to provide visual cues, and wetted) behind a wall, then use two graspers to loop the tissue over two target posts. Synthetic chamois was chosen for its tissue-like properties – it retains moisture, is slightly stretchable and has similar friction to skin [65]. As noted in Section 5.4, the ability to detect slip was not substantially different for live tissue; however, synthetic tissue is logistically easier to use in a series of tests.

During half of the trials, subjects received auditory slip feedback as an audible chirp when slip onset occurred in the slip tool. Auditory feedback was selected based on the survey results (Section 2.2.2). During training, subjects explored the feedback's responsiveness and tuned the threshold to suit their preferences. During testing, they could request further changes to the slip sensitivity. The vast majority of users chose a slip threshold of $0.0013\,(^{\circ}\mathrm{C/s})^2$, which was used as the threshold in the *in vivo* testing in Section 5.4. The other half of the trials had no auditory feedback. All trials were recorded for data collection purposes.

Subjects were instructed to keep the endoscope 200-400 mm from their active workspace. This requirement combined with the setup dimensions forced subjects to have their third

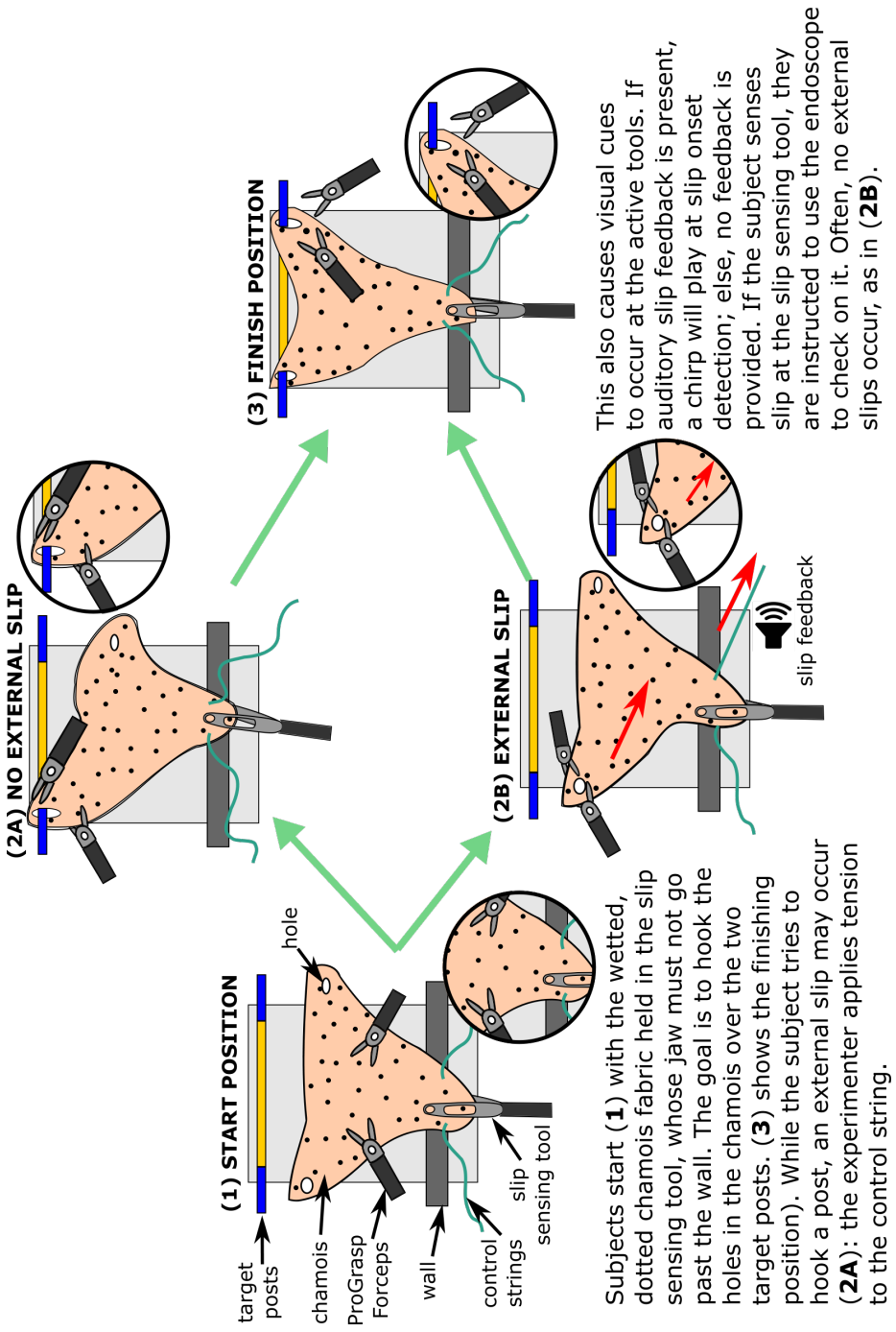

Figure 6.3 – User study task. The circled insets show what the subject sees through the endoscope at each stage of the task.

arm off-screen often (see Fig. 6.3, bottom row). This forced subjects to rely on subtle visual cues (the movement of the chamois's dots, or exogenous tension in the material) in the absence of slip feedback.

Over each subject's 12 test trials, 7 external slips occurred. External slips involved the protocol director applying tension from out of view to the chamois via control strings, slowly enough that it would take 3-10 s for tissue loss to occur from the third arm. Tension was applied at 0.5-0.7 N/s up to a maximum pull force of 2.5 N. Subjects were instructed to respond to slip by moving the endoscope to check on the third arm. The external slip would stop as soon as they began responding, and subjects were *not* penalized for slips unless it resulted in grasp loss from the 3rd arm. This likely makes it easier to arrest slip than in a true surgical procedure. The external slips were designed to replicate observed or described RAS slips that may be outside the surgeon's control, including those arising from breathing, organs shifting, poor coordination with an assistant, etc. Externally generated slips were deemed necessary for this study because slip occurs in RAS only 2-3 times over a multi-hour case (see Section 2.2.2).

Artificially increasing the frequency of slips while maintaining their apparent randomness and preventability was required for an efficient study. The number and timing of occurrence of external slips were predetermined and randomized prior to testing, and external slips were present during training.

Subjects were informed that their task score was dictated by their time to complete it (1 penalty point per second) and if loss of tissue ever occurred at the slip tool (100 penalty points, plus re-start the task). This penalty for catastrophic slip from the retracting arm combined with the time constraint was intended to recreate the division of attention present in surgery. Although surgeons' main focus is on using their two active tools to complete an intervention, they must also maintain awareness of their surroundings. Although the incidence of slips was higher than in typical RAS procedures and the assigned penalty for loss of tissue was high, subjects did not report a high mental demand or stress (Section 6.4).

After 4 training trials, 12 test trials were conducted: 6 with auditory slip feedback and 6 without in randomized order. Midway through testing, the protocol director asked participants questions about their experience completing the task with and without feedback: did they like or dislike slip feedback; did they feel more, less, or similarly confident with slip feedback; what feedback modality might they prefer during a real surgery. If the subject

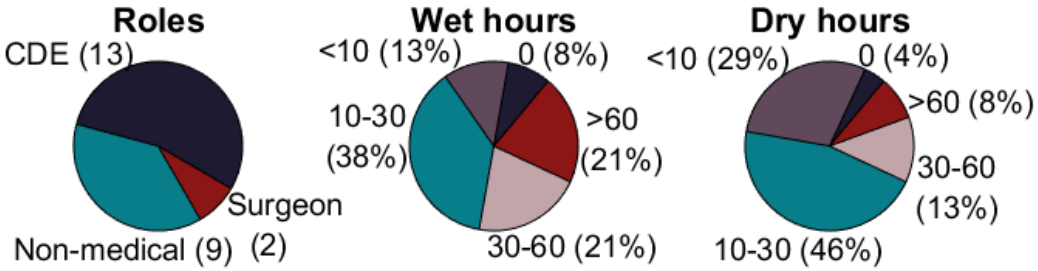

Figure 6.4 – Demographics and experience levels of participants.

was a CDE or a surgeon, they were also asked to name any surgical processes during which they would anticipate wanting to receive slip feedback. After testing, subjects completed the Surgery Task Load Index (SURG-TLX) [66] to self-assess the surgical workload for tasks with and without auditory slip feedback. Video data of test trials were used to evaluate users' responses to external slips with and without feedback.

Learning effects were minimized by observing the following considerations. Only expert users of the da Vinci robot were solicited for participation in the study to ensure that participants did not become more skilled at using the robot throughout the user study. Even so, subjects each were required to complete four training trials prior to testing with the option to do more training if they wished. The order of feedback and no feedback task trials were randomized for each subject, as were the occurrence of the 14 slip events.

6.4 Results

Figure 6.4 shows the demographics and experience levels of the 24 study participants. Of the two surgeons who were tested, one was a general surgeon and one was thoracic. All users were highly familiar with using the da Vinci Xi but had differing experience levels, which were classified into 'wet' and 'dry' hours. 'Wet hours' refer to RAS experience with biological materials, such as human, porcine, canine, or cadaveric models. 'Dry hours' refer to RAS experience with non-biological materials, like rubber bands, etc. CDEs tended to have more wet hours than non-medical participants.

Each subject experienced 7 slip events with auditory slip feedback and 7 without. Their responses to each slip event fell into one of three categories: (1) they **caught slip** before it resulted in grasp loss, (2) they **dropped** the tissue because they did not respond in time, or (3) the slip went **unnoticed or ignored**, meaning the slip did not result in tissue loss

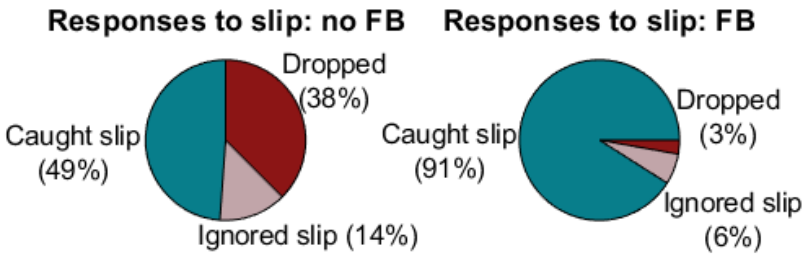

Figure 6.5 – Participant responses to slip during user study, without and with auditory slip feedback (FB). In the no FB case, unnoticed/ignored slip indicates that the user either never noticed slip occurring or chose to not respond to it. In the FB case, users were notified of every slip, so having slip go unnoticed was not possible.

but did not cause a response from the subject. In the case where subjects received auditory feedback, no slips were unnoticed because they received an audible cue each time. Figure 6.5 shows how participants responded to slips in the feedback and no feedback cases. Without auditory feedback, subjects dropped the tissue or did not respond to slip far more often than with feedback.

Table 6.1 shows some additional test metrics. The following metrics give the mean and one standard deviation, if applicable. The time to complete the task was significantly lower (79.4 ± 41.3 s compared with 93.8 ± 52.6 s, p value < 0.0008) during trials with feedback, and subjects responded to slip significantly faster as well (2.8 ± 1.1 s compared with 3.3 ± 1.8 s, p value < 0.002). This faster response could be further improved by tuning the sensor to respond faster to slips. Subjects' response to slip during feedback trials had two components - their own response to the auditory beep, and the slip sensor's response to the slip event which they themselves tuned. The takeaway is that given an auditory signal, subjects can respond in 1.3 s on average, whereas without it they require nearly three times that amount of time.

When subjects responded to slips with and without feedback, there was no significant difference (p value > 0.6) in how long it took them to recover from the event. Typical responses involved moving the endoscope back to visualize the third arm, then using one or two other tools to help the third arm re-grasp.

When auditory feedback was on, there were times when the sensor would alert subjects to a very minor slip (1.2 ± 1.3 times per trial), and subjects spent 1.9 ± 2.3 s responding to each non-critical event. Subjects disliked receiving these alerts and reported finding them disruptive. Classifying these as false positives is incorrect because slip in the jaws

did occur, but these alerts frustrated subjects instead of helping them perform well on the task. Subjects sometimes requested elevated sensor thresholds after experiencing these non-critical alerts to reduce their occurrence. However, without feedback, subjects felt compelled to check on the third arm far more often, a total of 74 times as compared with only 10 total for the trials with feedback, and they reported disliking this as well. Subjects spent approximately the same amount of time glancing back with or without feedback (2.8 vs. 2.7 s), but spent less time checking on the third arm when feedback was present. This may help explain subjects' reported preference for feedback vs. none.

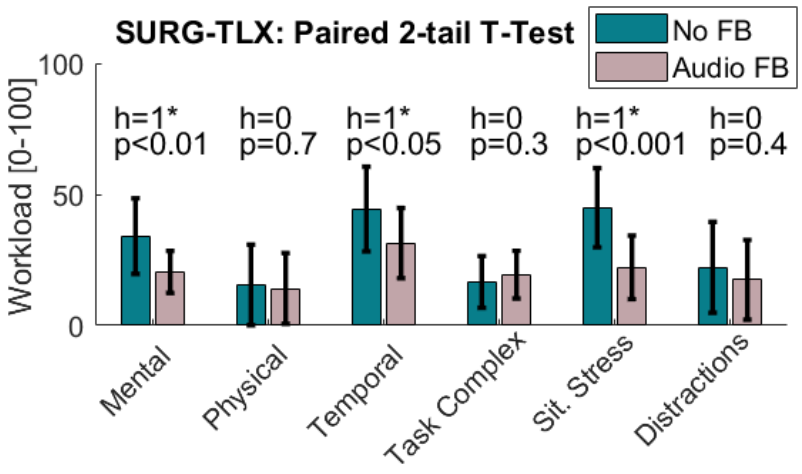

Figure 6.6 – Perceived workload results as measured by the SURG-TLX [66]. The six rating scales are Mental demands, Physical demands, Temporal demands, Task complexity, Situational stress, and Distractions. The only significant differences (*) were decreased mental and temporal demands and situational stress in the presence of auditory slip feedback.

After the robotic manipulation portion of the study was done, subjects were asked to score their perceived workload during the trials with and without feedback using the SURG-TLX (see Fig. 6.6 for description). The subjects' perceived mental demands, temporal demands, and situational stress all decreased significantly when they had auditory feedback; the other three workload ratings did not change significantly.

Halfway through testing, subjects were informally interviewed. All 24 subjects reported liking the slip feedback because they felt they could focus more on their active tools and accomplishing the task. They also felt they could ignore the periphery and enjoy a heightened ease of mind, relying on being told when they needed to respond to slip rather than glancing back to check. The vast majority of subjects reported feeling more confident in their ability

Table 6.1 – User study metrics for No Feedback (No FB) and Feedback (FB) cases. Averages and 1 std dev shown.

Metric	**No FB**	**FB**	***p* value**
Duration: task [s]	93.8 ± 52.6	79.3 ± 41.3	0.0008
Response: subject to slip [s]	3.3 ± 1.8	2.8 ± 1.1	0.002
Response: beep to slip [s]	-	1.5 ± 0.6	-
Response: subject to beep [s]	-	1.3 ± 0.8	-
Response duration: subject to slip [s]	11.9 ± 8.6	12.5 ± 8.6	0.60

to perform the task when feedback was present; only two subjects felt no change in their confidence, and none felt it diminish with feedback. Subjects generally agreed on what how they wanted to see slip feedback implemented. They wanted to only receive feedback when slip would be catastrophic. However, their perception of what indicates impending catastrophe differed; subjects cited either high slip speed or small contact area as their desired metric.

When asked whether they liked the feedback modality, subjects had mixed responses. While most were content with auditory feedback, they felt that a more distinctive noise would be needed in an operating room because many other machines are constantly beeping as well. A third of subjects reported preference for a visual indication of slip over auditory, with several describing a display similar to the current da Vinci Xi off-screen indicator (a feature that provides an overlay on the UI when an instrument exits the endoscope's field of view). No subjects reported preferring any form of haptic feedback, and most stated explicitly that receiving haptic feedback for a non-active tool would be confusing and detrimental.

Lastly, CDEs and surgeons were asked to reflect on the surgical procedures during which they would find slip feedback useful. Several procedures were recommended because important retraction can occur off-screen, e.g. cholecystectomies or any large intestine work, particularly in lower anterior resections. If additional traction is required, surgeons report applying it to the rectum without visualizing the (already off-screen) tool. Both surgeons reported that they may elect to retract with a wide field of view then zoom in to focus on a small region, which forces the third arm off-screen; loss of grasp is only known once they have already lost exposure. Other procedures were recommended because the retracted anatomy or object posed grasping challenges due to low surface friction (e.g., a lubricated Foley catheter) or requiring very high traction (e.g., stomach fundus manipulation during

a Nissen fundoplication).

6.5 Discussion

This user study sought to determine the benefits of slip feedback in a 3-tool RAS procedure where off-screen tissue retraction was required. The task provides insight into future scenarios which may involve shared autonomy or automation of low-level surgical tasks. These scenarios will require more information regarding the system's interaction with biological materials and a heightened ability to communicate that information with the human user. To that end, testing the utility of supplying feedback to a tool that is not controlled by the human user can provide important insights.

In the case where users position instruments outside their field of view, feedback regarding the state of that tool's grasp is advantageous to users. It permits them time to respond, and one could imagine scenarios where perhaps although the surgeon does not have adequate time to respond, they would at least know to turn off electrocautery or close their scissors, etc. We believe that the presented results provide a solid incentive to continue this line of work toward producing a production-level tool with integrated slip sensing.

One interesting and unexpected result is that study participants performed the task more quickly when given slip feedback. This is partly because participants spent less time checking the third tool at arbitrary times, but it is also due to the task construct. Because participants were required to restart the task if loss of grasp occurred at the third arm, this added time to the task. Although this penalty was contrived to ensure participants valued preventing slip, it is not unreasonable to imagine that similar consequences may occur in surgery. If slip results in tissue damage or loss of critical view, the surgeon will need to spend time fixing these consequences, which will add time to the case. This finding thus may have potential, unanticipated importance for MIS.

This study had several limitations. Clearly, the setup was contrived: surgeons rarely (if ever) experience tissue being retracted against their will. Rather, slips tend to happen gradually rather than due to some exogenous tension. In addition, the external slips had artificially higher repercussions than in a true surgical situation. The choice to implement this into the user study task was made in order to elicit stronger, more measurable responses from participants. Caution must be observed when interpreting the results of this study; it is not anticipated that the results of a true use case would show such a large difference

in performance metrics during a surgery. The results would certainly better reflect surgical realities if the study was conducted during a surgical task. However, because slips happen only once every hour or so, the amount of time and resources required to make this happen was deemed unreasonable.

A possible application of providing slip feedback on a non-active tool is during MIS training. The feedback would help surgical novices remember to keep track of all of their tools, even those they are not actively controlling. Studies that examine the repercussions of providing such feedback should be conducted to ensure that possible negative side effects do not occur. For example, because the feedback allowed study participants to focus more on their active tools, many reported feeling as though they could then completely ignore the periphery, which can have negative repercussion in MIS.

Chapter 7

Conclusions and Future Work

7.1 Conclusions

This dissertation presents the first comprehensive look at slip of grasped biological tissue in MIS with applications across all surgical disciplines. Due to the nature of the project, the focus here was on RAS. Loss of grasped tissue can result in a drastic, unplanned reorientation of tissue, which can put vital structures at risk and cause tearing or bleeding. The consequences are more serious if the surgeon is using electrocautery. At the very least, having tissue slip from a grasper adds significant length to a case and adds to overall surgeon frustration and workflow disruption. Through the first survey on this topic, 112 RAS surgeons reported tissue slip as equal in clinical importance to tissue crushing or tearing and indicated a desire to prevent slip's occurrence during surgery.

The presented slip sensor's working principle takes inspiration from hot-wire anemometry, which is used in fluid mechanics. A heater keeps the sensor and its local environment above the environmental temperature. When the environment is stationary, the temperature at all four thermistors changes approximately equally. When slip occurs, thermistors on opposite sides of the heater experience different temperature changes. Taking the derivatives of these temperature differences amplifies the sensitivity to slip.

Transient thermal simulations were used to explore the underlying concept and governing principles of the sensor. The first round of prototypes provided a useful proof-of-concept; validation experiments demonstrated the sensor's feasibility. Further prototyping realized a RAS instrument-mounted sensor driveable by the da Vinci Xi, enabling a user study and further performance validation on *ex vivo* tissue. An *in vivo* study on a porcine model

confirmed the slip sensor's robustness to perfused, living tissue. Finally, a user study established that participants found slip feedback helpful and felt more confident with it than without. They also experienced significantly decreased mental and temporal demands as well as lowered situational stress. Consequently, user study participants also completed the task more quickly. We believe this category of sensor has potential to contribute positively to MIS.

7.2 Future Work

7.2.1 General improvements

Before deployment of this sensing method in a commercial RAS product, the sensor implemented in Section 5.3 must be improved to demonstrate several crucial abilities, including the ability to withstand autoclaving and immunity to electrocautery. The theoretical solution for this is to enclose the sensor and signal conditioning circuitry in a conductive (Faraday cage) enclosure but with thin walls in appropriate regions around the sensor for low thermal resistance. This is not straightforward and still has challenges to overcome due to the size restrictions and need for the slip sensor to have good thermal conductivity between the heater and the tissue and between the thermistors and tissue, while isolating the heater from the thermistors. An alternate approach may involve use of fiber bragg gratings (FBG) in optical fibers as temperature sensors, as these would be immune to this type of noise. An investigation into sensor fusion to provide more useful information to users (e.g., frequent study participant requests included slip speed and/or grasped tissue surface area) may prove fruitful as well. Possibly providing an estimate of the grasped object's thermal conductivity [67], [68] could provide useful information as well. In any event, an exploration of alternate feedback modalities for presenting slip information would be required for final implementation.

In any implementation, cabling will be an obstacle to implementation. Routing through the distal wrist joint of a RAS tool might be possible, but the space constrictions and the need to withstand bending through a tortuous path may preclude this route. Bundling the shielded cable in a loose 'sock'-like contraption around the wrist may be the more robust solution but would then run the risk of getting caught on other tools, etc., and may be more difficult to clean. For all of these options, reduction of the number of signal lines from 7 (10 are used in the current design, but 3 are redundant; only 7 are needed) to 2 or 3 is

possible by including a small microcontroller on the slip sensor circuit so digitization could occur locally. Having three lines for power, ground, and data is feasible; having two could be possible if the data can be overlaid on the power line.

Having multiple sensing sites on a grasping surface provides various interesting avenues of future research. First, three or more sensors would provide sufficient information to fully describe the movement of the tissue in a plane, as each provides a 2D vector of tissue motion. This would help distinguish rotation, stretching, etc. from the tissue's net displacement. Other interesting information may also be inferred. In Section 6.4, participants indicated that receiving information related to the amount of grasping surface area or the tissue's slip speed would be useful for their decision-making. An array of multiple sensors would enable an estimation of both of these quantities. Furthermore, there may be a useful relationship between stretching and slipping of biological tissue that may help inform incipient, rather than total, tissue slip. The usefulness of supplying any of these quantities to users would require evaluation.

Scaling the sensor to a smaller package may or may not have advantages. For instance, if the sensor were scaled to 1/10 the size it is now, this would make the sensor very sensitive to very small and clinically insignificant slips, which is a disadvantage. Scaling the sensor to be smaller yet still sensitive to slips on the scale that surgeons care about is important. A smaller sensor area would make it more robust to different tissue types and surface irregularities.

Many additional design and implementation choices for integrating the sensor are required before further advancement; these are outlined below.

7.2.2 Instrument considerations

Any further sensor design must be motivated by its target instrument. The following discussion is restricted to Intuitive EndoWrist instruments because they are the leading purveyor of robotic instruments (and are similar by design to their laparoscopic predecessors). The slip sensor's intended purpose is to improve grasping in RAS, so the field can be narrowed to a reduced number of instruments; some commonly purchased and used tools from Intuitive are discussed below and shown in Fig. 7.1. Although each of these tools is intended for grasping, they have different surgical applications and user expectations. An evaluation of the design considerations for implementing the sensor into each tool's footprint is presented. In all tools, ideal sensor location is near the tip because surgeons tend to grasp there as

opposed to deep in the jaw.

A surprising result from the user study (described in Section 6) is that participants with medical training (e.g., CDEs and surgeons) reported that their expectations for tissue slip in traumatic and atraumatic tools differed greatly. Traumatic tools have more aggressive grasping abilities than atraumatic tools, stemming mainly from higher grasping torque limits but also from the shape of the jaws and the tooth profile. Some tools with nearly identical jaws have atraumatic and traumatic versions, distinguished mainly by their torque limit (e.g., *da Vinci*® Cadiere and ProGrasp). Therefore, if any slip occurs in a traumatic tool, it would not only be highly surprising and likely indicative of impending grasp loss, it would also likely be accompanied by tearing. In general, the amount of slip that users find permissible in traumatic tools is less than that of atraumatic ones. This difference in the desired detectable amount of slip should influence the layout of the slip sensor's components.

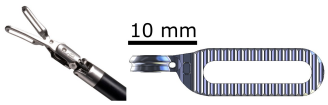

(a) ProGrasp® Forceps

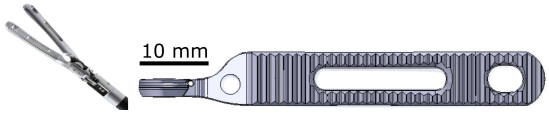

(b) Small Graptor® (Grasping Retractor)

(c) Maryland Bipolar Forceps

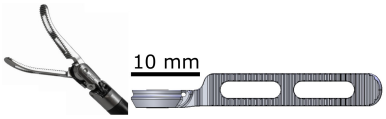

(d) Tip-Up Fenestrated Grasper

Figure 7.1 – Common EndoWrist instruments. The *da Vinci*® ProGrasp, Small Graptor, and Tip-Up Fenestrated Grasper are all grasping instruments. The Maryland is for dissecting and cautery but also grasps and manipulates tissue. Both the ProGrasp® and Maryland are traumatic instruments; the Tip-Up and Graptor are atraumatic.

The ProGrasp® forceps, shown in Fig. 7.1a, is a traumatic tool – its maximum grasp force is the highest of all the graspers. The expectation surgeons have with traumatic tools is that slip should never occur. This means that surgeons will likely want to receive slip feedback for smaller slips than in atraumatic tools, say 1 mm or so. Accordingly, the thermistor and heater should be placed closer together. From the simulation in Section 4, the thermistor and heater should lie approximately 1 mm apart or even closer if the heater is small. Currently, the latest prototype's heater is 1x1 mm^2, so the thermistors must lie at least 1.5 mm away to limit internal heat conduction effects. However, the ProGrasp®has a large

central fenestration that prevents this layout without some modification. Implementation into this jaw would require one of the following workarounds:

1. Space the thermistors much further away from the heater than recommended, and implement a system that can lower the noise floor enough to be sensitive to changes in the shallow thermal gradient. This system is not likely to work well with the heater working at safe levels.
2. Fill in the last 3-4 mm of the fenestration to fit the sensor in, decreasing the window size. If surgeons deem this unacceptable, consider a depressed inset like a shallow fenestration.

The Cadiere and the Fenestrated Bipolar Forceps (FBF) are both quite similar in appearance to the ProGrasp® (and are thus not shown in Fig. 7.1). However, the Cadiere is an atraumatic tool because its grasping torque limit is far lower than that of the ProGrasp®. Surgeons expect tissue to slide some between the grasper jaws and are more forgiving and expectant of tissue movement. Here, the thermistors and heater should be placed further apart (1.5-2 mm from the heater should work) than in the ProGrasp® for sensitivity to 2-3 mm slips. The other design considerations for the ProGrasp® apply here. The expectations for the FBF, as an electrocautery tool, lay between the Cadiere and ProGrasp®.

The Grasping Retractor, or the Small Graptor® (see Fig. 7.1b), is the atraumatic tool I modified for the prototypes described in Section 5.3. Its jaws are very large, providing ample space for a slip sensor, but maintaining the grasping surface is important to surgeons, and either the fenestration or teeth will be compromised to some extent. There are several implementation options. If the sensor covers some teeth, that may adversely affect grasping and thus surgeon acceptance. However, if the tip fenestration is filled in with a deep inset or similar (as in the proposed ProGrasp® implementation), this would avoid that problem. Surgeon preferences would require assessment to inform this decision. The Tip-Up Fenestrated Grasper is a similarly atraumatic tool with many of the same design considerations.

The Maryland Bipolar Forceps (Fig. 7.1c) is a bipolar cautery tool that is used for dissection and electrocautery as well as grasping. This tool is not typically used to grasp and retract as one might with a ProGrasp® or Small Graptor® but would be a good candidate for autonomous grasp modulation using slip as a control signal. The jaws have a large grasping surface near the tip obstructed only by teeth. Possibly the sensor components could be vapor deposited between the teeth, or small flats are made to accommodate the

components.

With all of these instruments, participants from the user study reported wishing they could receive feedback related to remaining grasp surface area and/or tissue slip speed because they think these are the best indications of when catastrophic slip is imminent. For traumatic tools, this may not be very important because all slips are important. However, for an atraumatic grasper or retractor, this information could be very helpful to reduce the number of alerts the surgeon receives.

In summary, when integrating the sensor into an EndoWrist instrument, it is important to consider what the tool's intended use is, for this determines whether additional sensors to provide surface area or speed information are useful. It also determines the recommended spacing of the components.

7.2.3 Packaging considerations

Successfully packaging the sensor into any of the above instruments additionally requires meeting or addressing the following considerations:

- Space the thermistors and heater according to the size of slip you wish to sense most often. For the heating resistors and power used, between 1.5-2 mm is optimal, but this will change with component and powering choices.
- Ensure good thermal contact (high thermal conductivity) with the grasping surface. This means a thin coat of protective and electrically insulating material with a thermal conductivity of $0.3\,\mathrm{W/(m\,K)}$ or higher.
- Thermally sink the underside of the sensor to avoid thermal saturation. The prototype used silver epoxy and an aluminum case to achieve this, but these materials are, respectively, not bio-compatible and susceptible to corrosion.
- Maximize thermal isolation between the heater and thermistors to improve the sensor sensitivity. Silica aerogels would be the ideal candidate as a filler between components, but ceramics, polyurethane, glass fibers, or polystyrene would be more realistic material choices.

Determining what sensor package (e.g., an ASIC) is best for packaging and survival of sterilization and autoclaving is critical to implementation of the slip sensor. The prototypes discussed in Chapter 5 are all implemented on PCBs. Although beyond the scope of the presented work, other sensor packages will be better suited to address the size constraints

of the smaller graspers for production-level implementation.

Improved PCB

Improvements over the presented PCB design exist but were not pursued due to pricing and manufacturing time constraints. Due to space constraints on RAS grasper jaws, pursuing an improved FR4 PCB design that will fit most graspers given fenestrations etc. is likely unwise and unfeasible. Furthermore, FR4 boards do not conduct heat well (thermal conductivity of FR4 is approximately 0.2-0.3 $\mathrm{W/(m\,K)}$), and heat dissipation from the sensor's underside (not in contact with tissue) is important for performance. To be clear, the preferred thermal conditions are thermal isolation between the heater and the thermistors, high thermal conductivity between the board and its environment to prevent thermal saturation, and excellent thermal conduction between the sensor and the grasped material. The current slip sensor requires an elaborate potting method to help heat sink the board. Moreover, PCBs have rigid layouts, which is somewhat limiting when considering the 3-dimensional contours of grasper jaws. Overall, pursuing this route is not recommended.

Flex circuit

A flexible circuit platform is likely to work well for the slip sensor because it maintains or improves thermal isolation between the thermistors and heater (as compared with what the current design permits). In addition, the flexible substrate allows greater ease of fit into the various RAS tool jaw geometries. The lack of bulky FR4 implies easier heat dissipation from the signal conditioning geometry, and the flex circuit can be wrapped around thermally conducting materials. This design route would likely meet our space requirements.

Integrated circuit

The general expectation with IC packages is that they produce chip-scale packaging, save board space, are more durable, and reduce assembly costs by reducing the overall number of discrete components. Such a package is likely to be thermally efficient as well; a large solder ground pad can be used for good sensor underside heat dissipation. However, thermally isolating the thermistors from the heating element within the IC may prove challenging, as achieving this in an IC is often difficult and expensive. However, if an ASIC with exposed and potted parts is possible, this packaging method would fare better than the PCB and

perhaps be on par with the flex circuit version.

Physical vapor deposition

Physical vapor deposition (PVD) is a method of thin film deposition that involves ejecting material from a target source onto a substrate and is extensively used in the semiconductor industry during integrated circuit manufacturing. To create the thermistors and resistors that form the slip sensor, a metallic alloy layer would be deposited onto a ceramic, silicon, or glass base, and laser etching/ablation would follow PVD to remove extra material. This method seems like the best for thermal conductivity because the components are put directly on metal but are still exposed. If this method was viable, it would be the most compact and able to fit in the most EndoWrist instruments (see Section 7.2.2).

7.2.4 Further user studies

The results from the presented user study (Section 6) prompt several further investigations. A study that compares, in an operating room setting, how participants respond to different feedback modalities would be useful to better understand how slip information could most effectively be displayed. Perhaps a more advanced implementation would have an adaptive slip feedback that modulates the slip threshold based on how often users respond to it, thereby learning what users care about.

Another interesting avenue of exploration would examine the utility of slip feedback on an active tool. There are several interesting questions here: do surgeons dislike having grasp force modulated for them, using slip as a control signal? Would they notice it happening, and would they incur less tissue damage than if they modulated the grasper themselves? A comparison of autonomous grasp modulation with simply providing feedback for the user to respond to would be interesting as well and would likely prompt an comparative study of feedback modalities, as in the non-active tool case.

7.3 Final thoughts

This thesis has presented the design, model, and validation of a novel anemometric sensor for detecting the onset of biological tissue slip from a MIS grasper. The next thesis in this line of research would seek to more firmly establish the utility of providing slip feedback on a nonactive tool and, in parallel, seek to understand the utility of feedback on an active

tool, either for autonomous grasp modulation or simply slip onset notification. Determining the worth of this tool to surgeons is best pursued before lengthy development towards a properly packaged grasper.

Appendix A

Slip sensor

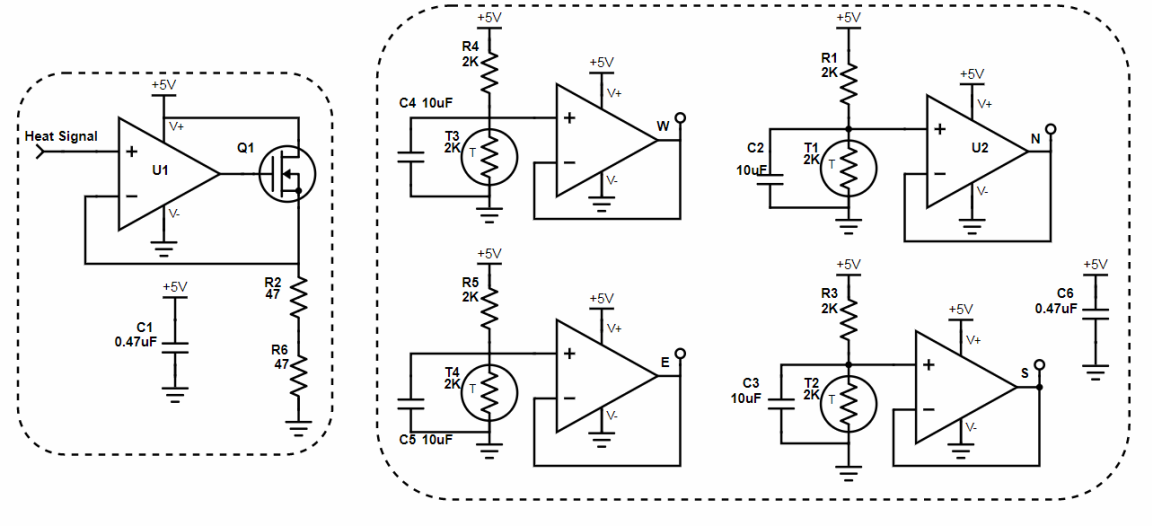

Figure A.1 – Slip sensor PCB schematic. See Table A.1 for bill of materials.

Table A.1 – Bill of Materials for slip sensor board

#	Value	Package	Parts	Description	Digikey PN
2	0.47uF	01005 (0402)	C1, C6	±20% 6.3V Ceramic Capacitor	490-13217-1-ND
4	10uF	0402 (1005)	C2, C3, C4, C5	±20% 6.3V Ceramic Capacitor	445-8920-1-ND
4	2kΩ	0201 (0603)	T1, T2, T3, T4	NTC Thermistor	P12020CT-ND
4	2kΩ	0402 (1005)	R1, R3, R4, R5	±0.5% 0.2W Resistor Thin Film	749-1513-1-ND
2	47Ω	0402 (1005)	R2, R6	± 0.5% 0.2W Resistor Thin Film	749-1508-1-ND
1	-	SOT-523	Q1	N-Channel MOSFET 20V 630mA 280mW	DMG1012T-7DICT-ND
1	-	SOT-353	U1	Amplifier 1 Circuit Rail-to-Rail 10MHz	296-36890-1-ND
1	-	14-TSSOP	U2	Amplifier 4 Circuit Rail-to-Rail 20MHz	296-21237-1-ND

Bibliography

[1] M. Mabrouk, M. Frumovitz, M. Greer, S. Sharma, K. M. Schmeler, P. T. Soliman, and P. T. Ramirez, "Trends in laparoscopic and robotic surgery among gynecologic oncologists: A survey update," *Gynecologic Oncology*, vol. 112, no. 3, pp. 501–505, 2009.

[2] J. Rosen, B. Hannaford, and R. M. Satava, *Surgical robotics: Systems, applications, and visions*. Springer Science & Business Media, 2011.

[3] N. Hubert, M. Gilles, K. Desbrosses, J. Meyer, J. Felblinger, and J. Hubert, "Ergonomic assessment of the surgeon's physical workload during standard and robotic assisted laparoscopic procedures," *The International Journal of Medical Robotics and Computer Assisted Surgery*, vol. 9, no. 2, pp. 142–147, 2013.

[4] R. VanDerSchatteOlivier, C. van't Hullenaar, J. Ruurda, and I. Broeders, "Ergonomics, user comfort, and performance in standard and robot-assisted laparoscopic surgery," *Surgical Endoscopy*, vol. 23, no. 6, 2009.

[5] K. Ahmed, M. Khan, A. Vats, K. Nagpal, O. Priest, V. Patel, J. Vecht, H. Ashrafian, G.-Z. Yang, and T. Athanasiou, "Current status of robotic assisted pelvic surgery and future developments," *International Journal of Surgery*, vol. 7, no. 5, pp. 431–440, 2009.

[6] J. Cartmill, A. Shakeshaft, W. Walsh, and C. Martin, "High pressures are generated at the tip of laparoscopic graspers," *Australian and New Zealand Journal of Surgery*, vol. 69, no. 2, pp. 127–130, 1999.

[7] S. De, "The Grasper-Tissue Interface in Minimally Invasive Surgery: Stress and Acute Indicators of Injury," Doctor of Philosophy, University of Washington, 2008.

[8] E. A. M. Heijnsdijk, "Tissue manipulation in laparoscopic surgery," Doctor of Philosophy, Delft University of Technology, 2004. [Online]. Available: `https://repository.tudelft.nl/`.

[9] *The da Vinci Xi Surgical System*, 2018. [Online]. Available: `https://intuitivesurgical.com/company/media/videos/systems/xi-overview.html`.

[10] N. T. Burkhard, M. R. Cutkosky, and J. R. Steger, "Slip sensing for intelligent, improved grasping and retraction in robot-assisted surgery," *IEEE Robotics and Automation Letters*, vol. 3, no. 4, pp. 4148–4155, 2018.

[11] N. T. Burkhard, R. Steger, and M. R. Cutkosky, "Sensing slip of grasped wet, conformable objects," *2017 IEEE/RSJ International Conference on Intelligent Robots and Systems (IROS)*, pp. 5744–5749, Sep. 2017.

[12] S. De, J. Rosen, A. Dagan, B. Hannaford, P. Swanson, and M. Sinanan, "Assessment of tissue damage due to mechanical stresses," 11-12, vol. 26, Sage Publications Sage UK: London, England, 2007, pp. 1159–1171.

[13] C. P. Childers and M. Maggard-Gibbons, "Understanding costs of care in the operating room," *JAMA surgery*, vol. 153, no. 4, e176233–e176233, 2018.

[14] D. D. Marucci, A. J. Shakeshaft, J. A. Cartmill, M. R. Cox, S. G. Adams, and C. J. Martin, "Grasper trauma during laparoscopic cholecystectomy," *Australian and New Zealand Journal of Surgery*, vol. 70, no. 8, pp. 578–581, 2000.

[15] M. T. Edgerton, *The Art of Surgical Technique*, 1st ed. Baltimore: Lippincott Williams & Wilkins, 1988.

[16] J. Stoll and P. Dupont, "Force control for grasping soft tissue," in *Proceedings of the IEEE International Conference on Robotics and Automation (ICRA)*, 2006, pp. 15–19.

[17] T. D'Alessio and R. Steindler, "Slip sensors for the control of the grasp in functional neuromuscular stimulation," *Medical engineering & physics*, vol. 17, no. 6, pp. 466–470, 1995.

[18] L. Russell, "The Design and Development of an Intelligent Atraumatic Laparoscopic Grasper," Doctor of Philosophy, The University of Leeds, Institute of Functional Surfaces, 2015. [Online]. Available: `http://etheses.whiterose.ac.uk/`.

[19] G. S. Fischer, T. Akinbiyi, S. Saha, J. Zand, M. Talamini, M. Marohn, and R. Taylor, "Ischemia and force sensing surgical instruments for augmenting available surgeon information," *IEEE/RAS-EMBS International Conference on Biomedical Robotics and Biomechatronics, (BioRob) 2006.*, pp. 1030–1035, 2006.

[20] T. Kimura, H. Goto, Y. Takeuchi, M. Yoshida, T. Kobayashi, S. Sakuramachi, and Y. Harada, "Intraabdominal contamination after gallbladder perforation during laparoscopic cholecystectomy and its complications," *Surgical endoscopy*, vol. 10, no. 9, pp. 888–891, 1996.

[21] J. Peters, G. Gibbons, J. Innes, K. Nichols, M. Front, S. Roby, and E. Ellison, "Complications of laparoscopic cholecystectomy.," *Surgery*, vol. 110, no. 4, pp. 769–777, 1991.

[22] E. Heijnsdijk, J. Dankelman, and D. Gouma, "Effectiveness of grasping and duration of clamping using laparoscopic graspers," *Surgical Endoscopy and other Interventional Techniques*, vol. 16, no. 9, pp. 1329–1331, 2002.

[23] R. Anup and K. Balasubramanian, "Surgical stress and the gastrointestinal tract," *Journal of Surgical Research*, vol. 92, no. 2, pp. 291–300, 2000.

[24] H. Ceylan, M. Karakok, E. Guldur, B. Cengiz, C. Bagci, and E. Mir, "Temporary stretch of the testicular pedicle may damage the vas deferens and the testis," *Journal of pediatric surgery*, vol. 38, no. 10, pp. 1530–1533, 2003.

[25] R. Shi and J. D. Pryor, "Pathological changes of isolated spinal cord axons in response to mechanical stretch," *Neuroscience*, vol. 110, no. 4, pp. 765–777, 2002.

[26] T. Sammour, A. Kahokehr, S. Srinivasa, I. P. Bissett, and A. G. Hill, "Laparoscopic colorectal surgery is associated with a higher intraoperative complication rate than open surgery," *Annals of Surgery*, vol. 253, no. 1, pp. 35–43, 2011.

[27] J. C. Kalff, W. H. Schraut, R. L. Simmons, and A. J. Bauer, "Surgical manipulation of the gut elicits an intestinal muscularis inflammatory response resulting in postsurgical ileus," *Annals Surgery*, vol. 228, no. 5, pp. 652–663, 1998.

[28] M. Van Der Voort, E. A. M. Heijnsdijk, and D. J. Gouma, "Bowel injury as a complication of laparoscopy," *British Journal of Surgery*, vol. 91, no. 10, pp. 1253–1258, 2004.

[29] B. F. Levy, J. De Guara, P. D. Willson, Y. Soon, A. Kent, and T. A. Rockall, "Bladder injuries in emergency/expedited laparoscopic surgery in the absence of previous surgery: A case series," *The Annals of The Royal College of Surgeons of England*, vol. 94, no. 3, pp. 118–120, 2012.

[30] S. W. Suh, J. M. Park, S. E. Lee, and Y. S. Choi, "Accidental Gallbladder Perforation During Laparoscopic Cholecystectomy: Does It Have an Effect on the Clinical Outcomes?" *Journal of Laparoendoscopic & Advanced Surgical Techniques*, vol. 22, no. 1, pp. 40–45, 2012.

[31] B. I. Chung, M. M. Desai, and I. S. Gill, "Management of intraoperative splenic injury during laparoscopic urological surgery," *BJU International*, vol. 108, no. 4, pp. 572–576, 2011.

[32] M. Down, L. Brozowski, H. Younis, D. Benedict, J. Feghali, M. Schubert, R. Brender, G. Gruska, G. Vallance, M. Krasich, and W. Haughey, *Potential Failure Mode and Effects Analysis (FMEA) Reference Manual*. Chrysler LLC, Ford Motor Company, General Motors Corporation, 2008, pp. 1–77.

[33] R. D. Howe, "Tactile sensing and control of robotic manipulation," *Advanced Robotics*, vol. 8, no. 3, pp. 245–261, 1993.

[34] R. S. Johansson and J. R. Flanagan, "Coding and use of tactile signals from the fingertips in object manipulation tasks.," *Nat. Rev. Neurosci.*, vol. 10, no. 5, pp. 345–59, May 2009.

[35] H.-C. Wu, *Continuum Mechanics and Plasticity*. CRC Press, 2004.

[36] B. McGinty, *Continuum Mechanics*. [Online]. Available: `http://www.continuummechanics.org/`.

[37] R. W. Ogden, *Non-linear Elastic Deformations*. Courier Corporation, 1997.

[38] M. T. Francomano, D. Accoto, and E. Guglielmelli, "Artificial sense of slip – a review," *IEEE Sensors Journal*, vol. 13, no. 7, pp. 2489–2498, 2013.

[39] M. R. Cutkosky and J. Ulmen, "Dynamic Tactile Sensing," in *The Human Hand as an Inspiration for Robot Hand Development*, ser. Springer Tracts in Advanced Robotics, 1st ed., vol. 95, Springer International Publishing, 2014, ch. 18, pp. 389–403.

[40] M. Ueda, "Tactile sensors for industrial robot to detect a slip," in *Procedings of the 2nd Intelligent Systems and Robotics (ISIR)*, 1972, pp. 63–76.

[41] E. Donlon, S. Dong, M. Liu, J. Li, E. Adelson, and A. Rodriguez, "GelSlim: A High-Resolution, Compact, Robust, and Calibrated Tactile-sensing Finger," 2018. arXiv: 1803.00628. [Online]. Available: http://arxiv.org/abs/1803.00628.

[42] K. Hosoda, Y. Tada, and M. Asada, "Internal representation of slip for a soft finger with vision and tactile sensors," *2002 IEEE/RSJ International Conference on Intelligent Robots and Systems (IROS)*, pp. 111–115, 2002.

[43] M. R. Tremblay and M. R. Cutkosky, "Estimating friction using incipient slip sensing during a manipulation task," in *Proceedings of the 1993 IEEE International Conference on Robotics and Automation (ICRA)*, IEEE, 1993, pp. 429–434.

[44] R. D. Howe and M. R. Cutkosky, "Sensing skin acceleration for slip and texture perception," in *Proceedings of the 1989 IEEE International Conference on Robotics and Automation (ICRA)*, 1989, pp. 145–150.

[45] X. Wu, N. T. Burkhard, B. Heyneman, R. Valen, and M. R. Cutkosky, "Contact Event Detection for Robotic Oil Drilling," in *Proceedings of the 2014 IEEE International Conference on Robotics and Automation (ICRA)*, IEEE, 2014, pp. 2255–2261.

[46] A. W. Brown, S. I. Brown, Z. Wang, D. Maclean, and A. Cuschieri, "Development Of An Autonomous Smart Graspers To Prevent Tissue Slip During Laparoscopic Surgery," in *Soc. Am. Gastrointest. Endosc. Surg.*, 2013.

[47] S. J. Kim, D. Y. Hwang, H. Moon, H. R. Choi, and J. C. Koo, "Development of a resistive compact slip sensor using dielectric elastomer," *Microsyst. Technol.*, vol. 23, no. 11, pp. 5163–5169, 2017.

[48] B. L. Hutchings, A. R. Grahn, and R. J. Petersen, "Multiple-layer cross-field ultrasonic tactile sensor," in *Proceedings of the 1994 IEEE International Conference on Robotics and Automation (ICRA)*, IEEE, 1994, pp. 2522–2528.

[49] S. K. Prasad, M. Kitagawa, G. S. Fischer, J. Zand, M. A. Talamini, R. H. Taylor, and A. M. Okamura, "A modular 2-dof force-sensing instrument for laparoscopic surgery," in *International Conference on Medical Image Computing and Computer-Assisted Intervention*, Springer, 2003, pp. 279–286.

[50] T. Horeman, E. J. Meijer, J. J. Harlaar, J. F. Lange, J. J. Van Den Dobbelsteen, and J. Dankelman, "Force sensing in surgical sutures," *PloS one*, vol. 8, no. 12, e84466, 2013.

[51] M. Perri, A. Trejos, M. Naish, R. Patel, and R. Malthaner, "New tactile sensing system for minimally invasive surgical tumour localization," *The international journal of medical robotics and computer assisted surgery*, vol. 6, no. 2, pp. 211–220, 2010.

[52] D. Accoto, F. Damiani, R. Sahai, D. Campolo, E. Guglielmelli, and P. Dario, "A thermal slip sensor for biorobotic applications," in *Proceedings of the 2007 IEEE International Conference on Robotics and Automation (ICRA)*, IEEE, 2007, pp. 1523–1528.

[53] D. Accoto, R. Sahai, F. Damiani, D. Campolo, E. Guglielmelli, and P. Dario, "A slip sensor for biorobotic applications using a hot wire anemometry approach," *Sensors and Actuators A: Physical*, vol. 187, pp. 201–208, 2012.

[54] H. W. Huang and T. L. Horng, *Bioheat Transfer and Thermal Heating for Tumor Treatment*. Elsevier Inc., 2015, pp. 1–42.

[55] P. Hasgall, F. Di Gennaro, C. Baumgartner, E. Neufeld, M. Gosselin, D. Payne, A. Klingenbock, and N. Kuster, *IT'IS Database for thermal and electromagnetic parameters of biological tissues*, 2015. [Online]. Available: `www.itis.ethz.ch/database` (visited on 11/15/2017).

[56] *Database: Thermal Conductivity*, 2017. [Online]. Available: `https://www.itis.ethz.ch/virtual-population/tissue-properties/database/thermal-conductivity/` (visited on 11/16/2017).

[57] *Thermal Conductivity of Metals*, 2009. [Online]. Available: `https://www.engineeringtoolbox.com` (visited on 2009).

[58] International Electrotechnical Commission, *IEC 60601-2-2: 2009: medical electrical equipment–Part 2-2: particular requirements for the basic safety and essential performance of high frequency surgical equipment and high frequency surgical accessories.* Geneva, 2009.

[59] C. G. L. Cao, M. Zhou, D. B. Jones, and S. D. Schwaitzberg, "Can surgeons think and operate with haptics at the same time?" *Journal of Gastrointestinal Surgery*, vol. 11, no. 11, pp. 1564–1569, 2007.

[60] J. Blaber, B. Adair, and A. Antoniou, "Ncorr: Open-Source 2D Digital Image Correlation Matlab Software," *Experimental Mechanics*, vol. 55, no. 6, pp. 1105–1122, 2015.

[61] G. A. Kragten and J. L. Herder, "The ability of underactuated hands to grasp and hold objects," *Mechanism and Machine Theory*, vol. 45, no. 3, pp. 408–425, 2010.

[62] T. L. Hedrick, "Software techniques for two- and three-dimensional kinematic measurements of biological and biomimetic systems," *Bioinspiration and Biomimetics*, vol. 3, 2008.

[63] S. Thorpe, D. Fize, and C. Marlot, "Speed of processing in the human visual system.," *Nature*, vol. 381, no. 6582, pp. 520–522, 1996.

[64] M. Dimitriou, D. M. Wolpert, and D. W. Franklin, "The Temporal Evolution of Feedback Gains Rapidly Update to Task Demands," *Journal of Neuroscience*, vol. 33, no. 26, pp. 10 898–10 909, 2013.

[65] A. Dabrowska, G.-M. Rotaru, S. Derler, F. Spano, M. Camenzind, S. Annaheim, R. Stampfli, M. Schmid, and R. Rossi, "Materials used to simulate physical properties of human skin," *Skin Research and Technology*, vol. 22, no. 1, pp. 3–14, 2016.

[66] M. R. Wilson, J. M. Poolton, N. Malhotra, K. Ngo, E. Bright, and R. S. Masters, "Development and validation of a surgical workload measure: The surgery task load index (SURG-TLX)," *World Journal of Surgery*, vol. 35, no. 9, pp. 1961–1969, 2011.

[67] R. A. Russell, "A thermal sensor array to provide tactile feedback for robots," *The International Journal of Robotics Research*, vol. 5, no. 3, pp. 35–39, 1985.

[68] G. J. Monkman, P. M. Taylor, F. Miyazaki, R. K. Kankaanranta, H. N. Koivo, S. Francisco, H. Mcclamroch, N. H. Mcclamroch, D. Wang, K. Mills, A. A. Goldenberg, M. Takegaki, D. E. Whitney, T. Wen, M. Vidyasagar, E. Cliffs, and I. Introduction, "Thermal tactile sensing," in *IEEE Transactions on Robotics and Automation (ICRA)*, vol. 9, 1993, pp. 313–318.